Year : 2022

Mapping the fate of CD8+ T cells during acute and chronic viral infection

Gomes Da Silva Joana

Gomes Da Silva Joana, 2022, Mapping the fate of CD8+ T cells during acute and chronic viral infection

Originally published at : Thesis, University of Lausanne

Posted at the University of Lausanne Open Archive http://serval.unil.ch
Document URN : urn:nbn:ch:serval-BIB_134EA7DCB3784

UNIL | Université de Lausanne
Faculté de biologie et de médecine

Département d'Oncologie

Mapping the fate of CD8$^+$ T cells during acute and chronic viral infection

Thèse de doctorat ès sciences de la vie (PhD)

présentée à la

Faculté de biologie et de médecine
de l'Université de Lausanne

par

Joana GOMES DA SILVA

Master de Biologie Humaine et Environnement
de l'Université de Lisbonne, Portugal.

Jury

Prof. Fabienne Tacchini-Cottier, Présidente
Prof. Werner Held, Directeur de thèse
Prof. Grégory Verdeil, Expert
Prof. Manfred Kopf, Expert

Lausanne
(2022)

UNIL | Université de Lausanne
Faculté de biologie et de médecine

Ecole Doctorale
Doctorat ès sciences de la vie

Imprimatur

Vu le rapport présenté par le jury d'examen, composé de

Président·e	Madame	Prof.	Fabienne	**Tacchini-Cottier**
Directeur·trice de thèse	Monsieur	Prof.	Werner	**Held**
Expert·e·s	Monsieur	Dr	Grégory	**Verdeil**
	Monsieur	Prof.	Manfred	**Kopf**

le Conseil de Faculté autorise l'impression de la thèse de

Joana Gomes da Silva

Master in human biology and environment, Université de Lisbonne, Portugal

intitulée

Mapping the fate of CD8$^+$ T cells during acute and chronic viral infection

Lausanne, le 25 février 2022

pour le Doyen
de la Faculté de biologie et de médecine

F. Tacchini-Cottier

Prof. Fabienne Tacchini-Cottier

Acknowledgements

I am deeply thankful to everyone who have supported me during my PhD studies.

First of all, I would like to express my gratitude to my thesis director Prof. Werner Held for giving me the opportunity to develop my research in his group. His constant support, mentorship and guidance throughout my PhD were essential not only for this work but to grow as a scientist. I also appreciate for being always available, for all the discussions and for the critical thinking and strategic input brought into this work. Thanks for all the scientific and non-scientific support along these years.

I would also like to thank my current and past thesis committee Prof. Fabienne Tacchini-Cottier, Prof. Grégory Verdeil, Prof. Manfred Kopf and Prof. Sanjiv Luther for their advice and critical insights while evaluating this thesis.

A very special thank you to all current and past members of the Held lab: Maxime, Daniela, Tania, Mel, Julia, Romain, Yannis, Alex, Catherine, Imran and Vijay for their constant support and help with experiments as well as all the discussions over a cup of coffee. Thank you to Maxime to introduce me to the in vitro experiments. Thank you to Mel for helping with big experiments and for all the help of organization in the lab. Thanks to Daniela, for bringing a bit of the Portuguese culture to my life and for all the help. A special thanks to Mel and Romain for correcting the French abstract. I would also like to thank Aline and Catherine Fumey for caring and maintaining our mouse colony.

A special thanks to all collaborators that made this thesis possible. Thanks to Anne Wilson for the FACS training, all the technical advice, tips and for believing on my skills as teaching assistant. The FACS facility, especially Romain, Francisco and Kevin, for their technical support. Thanks to Leonardo and Roeltje for the help with the histology and microscopy experiments.

Thanks to the fellow research neighbours on Biopole3 for the good moments, the help and the company during the night-shifts at the FACS. Thanks to my “PhD friends”, for the many great times together and for all the brunches. We make a great team and I feel so lucky to have you as close friends! Thank you to my friends from Lausanne with whom I shared many happy moments and help me to “recharge” my energies. Thank you to my friends and previous colleagues from before Switzerland, for the skype calls during FACS acquisition and for the constant texts

Thanks to Elsa for her laboratory support, and always for her kind words. Thank you to Leonor for “adopting” me and treating me as her family.

I would like to thank my family, my parents, my siblings and nephews for the help, support and patience. Thanks to my parents for giving me the best education, the strength to follow my dreams and for standing by my side on all my life’s decision. For my sister, for her support and her example that anything is possible.

Thank you to my “Belle famillie” for their care and their support.

My deepest gratitude I owe to Damien for his total support, love and optimism. For making laugh and cheering me up when I needed. For the understanding and for the patience whenever I made him listen to my presentations. For standing by me through late nights and weekends, for baking surprise cakes after my long days, for being the first to celebrate my successes and to provide me comfort in the failures. I owe you half of my PhD diploma.

Résumé large public **Joana Gomes da Silva** **Département d'Oncologie**

Traçage du devenir des lymphocytes T CD8$^+$ au cours d'une infection virale aiguë et chronique

Lorsque l'hôte rencontre un agent pathogène (virus, bactéries et vers), une réponse immunitaire complexe se met en place afin de le détecter et de l'éliminer efficacement. Suite à la détection de l'agent infectieux, deux types de réponses se produisent : une réponse rapide et non spécifique à l'agent pathogène (appelée réponse immunitaire innée), et une tardive plus complexe qui peut générer une réponse spécifique à l'agent pathogène, avec pour caractéristique la formation de cellules mémoires (réponse immunitaire adaptative). La réponse immunitaire adaptative a la capacité de générer des lymphocytes avec différentes fonctions : les lymphocytes B qui sécrètent des anticorps, les lymphocytes T CD4$^+$ qui sécrètent des cytokines et agissent comme des cellules auxiliaires, et les lymphocytes T CD8$^+$ qui sont cytotoxiques et peuvent tuer les cellules infectées par des agents pathogènes.

Les cellules T CD8$^+$ spécifiques du pathogène sont les médiateurs majeurs de la protection contre les agents infectieux intracellulaires, tels que les virus. Lors d'une infection virale, les cellules T CD8$^+$ sont activées, s'expandent et se différencient en populations hétérogènes de cellules effectrices et mémoires. Ces cellules visent à éliminer l'infection et à renforcer la protection contre la réinfection. Toutes les cellules CD8$^+$ naïves expriment le facteur 1 des cellules T (Tcf1, codé par le gène *Tcf7*). Tcf1 n'est pas nécessaire pour la génération des cellules effectrices, mais est requis pour la génération d'un type de cellules mémoire avec des propriétés de cellule souche. Une question longuement débattue en immunologie a été de savoir quand ces cellules sont générées et quelle est l'origine développementale des cellules effectrices et mémoires au cours d'une infection aiguë. Ici, nous avons abordé le devenir des lymphocytes T CD8$^+$, en suivant les cellules exprimant *Tcf7* au cours de la réponse immunitaire.

Nous avons pu déterminer que certains types de cellules mémoire étaient générés beaucoup plus tôt au cours de la réponse immunitaire qu'on ne le pensait auparavant. De plus, nous avons montré que les cellules effectrices (à courte durée de vie) étaient générées seulement au cours des 2 premiers jours de l'infection. Déterminer la chronologie détaillée de la différenciation au cours de la réponse des lymphocytes T CD8$^+$ pourrait contribuer à l'amélioration du développement futur de vaccins et de la réponse vaccin-hôte, visant à protéger contre une réinfection.

Alors que dans une infection aiguë, le pathogène est efficacement éliminé, lors d'une infection chronique, les cellules T CD8$^+$ sont incapables d'éliminer le virus et sa persistance conduit à un affaiblissement progressif de la réponse des cellules T CD8$^+$ (épuisement). Cependant, un type rare de cellules exprimant Tcf1 est toujours capable de maintenir la réponse au cours de l'infection chronique. Nous avons déterminé que dans leur environnement naturel, les cellules Tcf1$^+$ se renouvellent et se différencient continuellement en cellules T CD8$^+$ épuisées. L'élucidation de ces événements peut aider à comprendre et à optimiser les futures immunothérapies pour revigorer les cellules T CD8$^+$ épuisées.

Résumé **Joana Gomes da Silva** **Département d'Oncologie**

Traçage du devenir des lymphocytes T CD8$^+$ au cours d'une infection virale aiguë et chronique

Au cours d'une réponse immunitaire à un agent pathogène intracellulaire, de rares cellules T CD8$^+$ naïves (T_N) sont activées, s'expandent et se différencient en cellules effectrices (T_{EF}) qui éliminent les cellules infectées. Une fois l'infection éliminée, la plupart des T_{EF} meurent, mais une population hétérogène de cellules mémoires subsiste. Ce sont elles qui protègent de la réinfection par le même agent pathogène. Le facteur de transcription Tcf1 (codé par le gène *Tcf7*), qui est exprimé par les cellules T_N, n'est pas nécessaire à la génération de cellules T_{EF} mais est essentiel à la formation d'une population de cellules mémoires présentant des caractéristiques de cellules souches, appelées cellules centrales-mémoires (T_{CM}). L'origine développementale de ces dernières reste controversée. Afin d'aborder cette question, nous avons établi un système de traçage en vue de déterminer le devenir des cellules T CD8$^+$ exprimant Tcf1 lors d'une infection virale.

Nous avons identifié de rares lymphocytes T *Tcf7*$^+$ CD8$^+$ à tous les stades de la réponse primaire à une infection virale. Le traçage du devenir cellulaire a montré que ces cellules ont généré quantitativement des cellules T_{CM}, représentant ainsi les précurseurs non identifiés des T_{CM}. Contrairement aux cellules T_{CM}, qui sont générées à tous les stades de l'infection, les cellules T_{EF} ont été générées à partir de cellules *Tcf7*$^+$ de manière transitoire et seulement jusqu'au jour 2 de l'infection virale. A ce stade les cellules ne s'étaient pas encore divisées et Tcf1 était encore exprimé de manière homogène à des niveaux élevés. Par la suite, Tcf1 reste fortement exprimé au cours des 3-4 premières divisions cellulaires, avant que certaines cellules le régule négativement, ce qui est associé à la différenciation en cellules effectrices. La régulation négative de Tcf1 a été induite par des cytokines inflammatoires. Ces données ont soutenu un modèle, dans lequel les cellules T CD8$^+$ naïves génèrent des cellules dotées de propriétés de cellules centrales-mémoires, tandis que les signaux inflammatoires conduisent à la différenciation de certaines de ces cellules en cellules effectrices cytotoxiques.

Lorsqu'une réponse immunitaire primaire est incapable d'éliminer le pathogène, les cellules T CD8$^+$ réduisent leur fonctionnalité afin de limiter les dommages tissulaires. Cela conduit à une réplication virale persistante en regard d'une réponse des lymphocytes T CD8$^+$ affaiblie, qui maintient néanmoins un contrôle viral constant. Cette réponse des lymphocytes T CD8$^+$ est soutenue à long terme par une population de lymphocyte T CD8$^+$ de type mémoire (T_{ML}) exprimant Tcf1. Ici nous avons suivi le traçage du devenir pour montrer que les cellules T_{ML}, maintenues dans leur environnement naturel, se renouvellent et produisent en permanence des cellules T CD8$^+$ plus différenciées. Nos résultats ont confirmé et étendu les expériences de transfert de cellules et de re-stimulation qui ont suggéré que les T_{ML} ont des propriétés des cellules souches.

Dans cette thèse, le traçage du devenir des cellules a révélé la relation développementale des cellules T CD8$^+$ effectrices et mémoires au cours d'une infection aiguë et a montré qu'au cours d'une infection chronique une population de cellules T CD8$^+$ a des propriétés similaires à celles des cellules souches.

Summary **Joana Gomes da Silva** **Department of Oncology**

Mapping the fate of CD8$^+$ T cells during acute and chronic viral infection

During an immune response to an intracellular pathogen, rare naive CD8$^+$ T cells (T_N) are activated, expand and differentiate into effector cells (T_{EF}) that eliminate pathogen-infected cells. Most T_{EF} die once the infection has been cleared, leaving behind a heterogeneous population of memory cells that protect from re-infection with the same pathogen. The transcription factor Tcf1 (encoded by *Tcf7*), which is expressed by T_N cells, is not needed for the generation of T_{EF} cells but is essential for the formation of a subset of memory cells with stem cell-like properties, so-called central memory cells (T_{CM}). The developmental origin of T_{CM} cells has been controversial. To address this issue, we established a lineage tracing system to determine the fate of Tcf1-expressing CD8$^+$ T cells during a viral infection.

We identified rare *Tcf7*$^+$ CD8$^+$ T cells at all stages of the primary response to viral infection. Fate mapping showed that these cells gave quantitatively rise to T_{CM} cells and thus represented the elusive T_{CM} precursor. In contrast to T_{CM} cells, which derived from all time-points, T_{EF} cells were generated from *Tcf7*$^+$ cells only transiently and until day 2 of the viral infection. At this stage, the cells had not yet divided and Tcf1 was still expressed at homogeneously high levels. Subsequently, Tcf1 remained highly expressed during the first 3-4 cell divisions before some cells downregulated Tcf1, which was associated with effector differentiation. Tcf1 downregulation was induced by inflammatory cytokines. These data supported a model, in which naive CD8$^+$ T cells gave rise to cells with central memory properties and inflammatory signals lead to the differentiation of some of these cells into cytotoxic effector cells.

When a primary immune response is unable to clear a pathogen, CD8$^+$ T cells reduce their functionality to limit tissue damage. This leads to persistent viral replication in the face of a weakened CD8$^+$ T cell response that nonetheless limits viral infection. This CD8$^+$ T cell response is sustained long-term by a subset of Tcf1-expressing memory-like CD8$^+$ T cells (T_{ML}). Here we used fate mapping to show that T_{ML} cells, which were left in their natural environment, continuously yielded more differentiated CD8$^+$ T cells, while the T_{ML} cell pool was maintained. These data confirmed and extended cell transfer and restimulation experiments that suggested that T_{ML} have stem cell-like properties.

Overall, Tcf1-guided cell fate mapping revealed the developmental relationship of effector and memory CD8$^+$ T cells during acute resolved infection and showed that the immune response to chronic infection harbours a CD8$^+$ T cell subset that had stem cell-like properties.

List of Abbreviations

4-OHT: 4-hydroxytamoxifen
ACK: Ammonium-Chloride-Potassium buffer
ACT: Adoptive T cell transfer
AP1: Activator protein 1
APC: Antigen-presenting cell
Arm: LCMV Armstrong
ATACseq: Assay for Transposase Accessible Chromatin with high-throughput sequencing
B6: C57BL/6
BAC: Bacterial artificial chromosome
Bcl2: B-cell lymphoma 2 protein
Bcl6: B-cell lymphoma 6 protein
Blimp1: B lymphocyte-induced maturation protein-1
BM: Bone marrow
BZ: B cell zone
CCL: Chemokine (C-C motif) ligand
CCR: C-C chemokine receptor
CD: Cluster of Differentiation
CFSE: Carboxyfluorescein succinimidyl ester
ChIPseq: Chromatin immunoprecipitation sequencing
CpG: Cytosine-phosphate-Guanine dinucleotides
Cl13: LCMV Clone 13
Ctrl: Control
CTV: Cell Trace Violet
CX3CR1: C-X3-C Motif Chemokine Receptor 1
Cxcr: C-X-C Motif Chemokine Receptor
DC: Dendritic cells
DT: Diphtheria Toxin
DTR: Diphtheria toxin receptor
Eomes: Eomesodermin
FoxO1: Forkhead box O1
FoxP3: Forkhead box P3
Gata3: GATA binding protein 3
GFP: Green Fluorescent Protein
GRG/TLE: Groucho-related gene / transducin-like enhancer
GSEA: Gene set enrichment analysis
GzmA/B: Granzyme A/B
H3K4me3: Trimethylation of lysine 4 of histone 3
H3K27me3: Trimethylation of lysine 27 of histone 3
HBV: Hepatitis B virus
HCV: Hepatitis C virus
HDAC: Histone deacetylase
HIV: Human immunodeficiency virus
HMG: High-mobility group
HSC: Hematopoietic stem cell
HSV: Herpes simplex virus
i.p.: intraperitoneally
i.v.: intravenously
ID2/3: Inhibitor of DNA Binding 2/3
IEL: Intraepithelial Lymphocyte
IFN: Interferon
IL: Interleukin
IL12rβ2: IL12 receptor β2 chain
IL2rα: IL2 receptor α chain
IL7rα: IL7 receptor α chain
KLRG1: Killer cell lectin-like receptor G1
KO: Knock out
Lag3: Lymphocyte Activation gene-3
LCMV: Lymphocytic choriomeningitis virus
Lef1: Lymphoid Enhancer Binding Factor 1
LM: Listeria monocytogenes
LN: Lymph node
MHC: Major Histocompatibility Complex
MFI: Mean Fluorescence Intensity
MPEC: Memory precursor effector cell
mTORC: Mammalian target of rapamycin Complex
NFAT: Nuclear Factor of activated T-cells
NK: Natural killer cell
NLR: NOD-like Receptor
Ova: Ovalbumin
p.i.: post-infection
PAMP: Pathogen-associated molecular patterns
PBMC: Peripheral blood mononuclear cell
PD1: Programmed cell death protein 1
PFU: Plaque forming units
PRR: Pattern Recognition Receptors
PY: Proximity of T and B cell zone within Red pulp
RLR: RIG-I-like receptor
ROI: Region of interest
RP: Red pulp
RT: Room Temperature
Sca-1: Stem cell antigen-1
ScRNAseq: Single cell RNA sequencing
SD: Standard deviation

SLAM: Signalling Lymphocyte Activation Molecule
SLEC: Short-lived effector cells
STAT: Signal Transducer and Activator of Transcription
Suv39h1: Suppressor of Variegation 3-9 Homolog 1
T-Bet: T-box transcription factor 21
TAM: tamoxifen
Tcf7: gene coding for T cell factor 1
Tcf1: T cell factor 1
T_{CM}: Central memory $CD8^+$ T cell
TCR: T cell receptor
T_{EF}: Terminal effector $CD8^+$ T cell
T_{EM}: Effector memory $CD8^+$ T cell
T_{EX}: Exhausted cell $CD8^+$ T cell
TF: Transcription factor
T_{FH}: Follicular helper T cell
ThPOK: T-helper-inducing POZ/Krueppel like factor
TIL: Tumour infiltrating lymphocyte
TLR: Toll-like receptor
T_{ML}: Memory-like $CD8^+$ T cell
T_N: Naive $CD8^+$ T cell
TNF: Tumor necrosis factor
TOX: Thymocyte selection-associated high mobility group box protein
t-SNE: t-distributed stochastic neighbour embedding projection
T_{RM}: Tissue-resident memory $CD8^+$ T cell
T_{TEX}: Terminally exhausted cell
T_{trans}: Transitory exhausted cell
TZ: T cell zone
VV: Vaccinia Virus
VSV: Vesicular Stomatitis Virus
Wnt: Wingless/Integration 1
WT: Wild type
βBD: β-catenin binding domain

Table of Contents

List of Figures

List of Tables

1.Introduction

1. The immune response to infection

The immune system comprises different branches that act sequentially and synergistically to protect the host from an infection. A functional immune system enables the host to detect and eliminate a diversity of pathogens (virus, bacteria, and worms) that are themselves constantly evolving. The immune system may additionally help the host to eliminate tumour cells. In response to pathogens, the host immune system mounts a rapid and organized response characterized by a fast innate inflammatory response that is followed by the generation of a pathogen-specific adaptive immune response (Samji and Khanna, 2017; Zhou et al., 2012). In the next chapters I will briefly present the innate and the adaptive immune components, addressing in particular the role of adaptive $CD8^+$ T lymphocytes to control infection.

1.1 Innate immune response

Innate immunity refers to the immediate response of the body to infection. It comprises predominantly Neutrophils, Macrophages and antigen-presenting cells (APC) dendritic cells (DCs). The innate immune response is fast and directed against tissue damage and microbial threats but poorly adapted to specific pathogens (Samji and Khanna, 2017). Innate immune cells can sense certain components of pathogens (pathogen-associated molecular patterns, PAMP) and tissue damage, through a variety of innate immune receptors (pattern recognition receptors, PRR). These receptors include the Toll-like receptors (TLR), NOD-like receptors (NLR) and RIG-I-like receptors (RLR) (Janeway and Medzhitov, 2002). Engagement of such receptors leads to the production of inflammatory cytokines that trigger an inflammatory response. Nucleic acid sensing mainly induces the production of type I interferon (IFN), which induces an anti-viral state and orchestrate the immune response. Inflammation recruits additional myeloid cells to the site of infection, where these cells use phagocytosis to ingest and kill microbes. In addition, DCs can take up microbial material, migrate to the local lymph node, where they present antigens complexed to Major Histocompatibility Complex (MHC) I and II molecules to naive T cells. DC activated by TLR ligands or by $CD4^+$ T cells can then provide all the signals required for a full activation of naive $CD8^+$ T cells: antigen, co-stimulation and interleukin (IL) 12 or IFN-I signals (Mescher et al., 2006). These interactions between DCs and cells from the adaptive immune system are crucial, not only because they activate naive lymphocytes but also guide the differentiation of antigen-specific T cells (Kaech and Cui, 2012).

1.2 Adaptive immune response

Unlike the innate immune system, the adaptive immune system has the capacity to recognize pathogens in a specific fashion, based on the expression of antigen-specific receptors. The adaptive immune system can protect the host from re-infection with the same pathogen based on three features. First, the adaptive immune system generates effector lymphocytes, such as plasma cells (derived from B lymphocytes) that secrete antibodies,

helper cells ($CD4^+$ T lymphocytes) that secrete cytokines and stimulate other immune cells, and cytotoxic T lymphocytes ($CD8^+$ T lymphocytes) that can kill pathogen-infected host cells (Fearon et al., 2001; Mescher et al., 2006). Second, a hallmark feature of the adaptive immune response is memory, i.e. the ability of the immune system to efficiently recognize and generate a more rapid and robust response to a secondary encounter with the pathogen (Fearon et al., 2001; Samji and Khanna, 2017; Zhou et al., 2012). Thus, memory lymphocytes protect against future re-infection. Third, in case of a chronic infection, such as those caused by hepatitis B virus (HBV), human immunodeficiency virus (HIV), *Mycobacterium tuberculosis*, etc, the adaptive immune system is able to continuously generate effector cells that sustain the immune response over long periods of time, perhaps for the life-time of the host (Fearon et al., 2001; Mescher et al., 2006).

The induction of an adaptive immune response is slower than that of an innate response, and different components cooperate and orchestrate its response. While B cells provide the humoral component of the adaptive immunity and mediate the protective effect of most current vaccines, this thesis will focus on T cells, and specifically, $CD8^+$ T cells, which are key mediators of protection against intracellular pathogens. Upon pathogen invasion, DCs process and present antigenic peptides complexed to MHC-molecules to very rare (only few hundreds) quiescent naive T cells that circulate through secondary lymphoid organs (Masopust and Schenkel, 2013; Obar et al., 2008). The binding to the T cell receptor (TCR) on naive T cells to peptide-MHC complex (signal 1), together with the engagement of costimulatory receptors (such as CD28, CD27) (signal 2) and the exposure to inflammatory cytokines (signal 3) are required for a productive T cell response (Masopust and Schenkel, 2013; Mescher et al., 2006). While the first 2 signals improve $CD8^+$ T cell expansion, survival and persistence, inflammatory cytokines such as IL12 and type I IFN or high levels of IL2 are required for effector T cell differentiation (Kim and Harty, 2014).

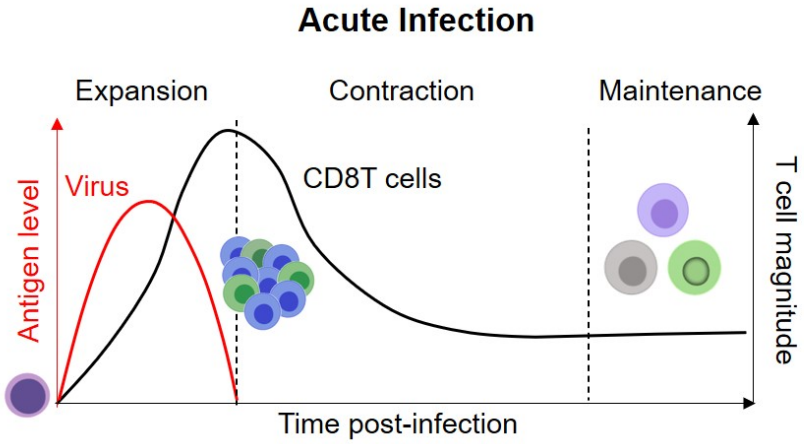

Figure 1 - Kinetics of the $CD8^+$ T cell response during an acute viral infection.
Upon a viral infection, $CD8^+$ T cells are activated and differentiate into a heterogeneous population, during the expansion phase. Upon viral clearance (low viral titer), $CD8^+$ T cells contract and only rare heterogenous population remains, forming the memory compartment. Different cells indicate the cell heterogeneity during infection. Red: Viral titer; black: $CD8^+$ T cell response

Following infection with Lymphocytic choriomeningitis virus (LCMV), the viral titer is maximal around day 3 post-infection (p.i.). By day 8 p.i., the viral load has decreased below detection (Ahmed et al., 1984). Virus control is mediated by a $CD8^+$ T cell response. Viral clearance around day 8 p.i. coincides with the peak in the number of virus-specific $CD8^+$ T cells (**Fig 1**) (Homann et al., 2001; Masopust and Schenkel, 2013; Matloubian et al., 1994). Indeed, a single virus-specific $CD8^+$ T cell can divide more than 14 times during the 1^{st} week post-infection, leading to an enormous expansion of antigen-specific cells (Blattman et al., 2002). The primary $CD8^+$ T cell response to LCMV is not dependent on $CD4^+$ T cells or B cells, although neutralizing antibodies are necessary to prevent viral re-emergence. While a $CD4^+$ T cell response is not required for primary LCMV control, IL2 produced by $CD4^+$ T cells during the primary response, is important for the expansion of memory $CD8^+$ T cells during recall responses (Asano and Ahmed, 1996; Matloubian et al., 1994; Williams et al., 2006).

1.3 $CD8^+$ T cell response to acute infection

Upon an infection, naive T cells bearing a TCR for the specific antigen are activated and undergo extensive clonal expansion and differentiation to antigen-specific effector $CD8^+$ T cells. Following viral clearance, most of these antigen-specific effector $CD8^+$ T cells die, leaving behind a heterogeneous pool of long-lived memory cells (**Fig 2**) (Joshi et al., 2007). *In vivo* studies have shown that the strength of TCR-ligand interaction dictates the magnitude of the cell expansion, the kinetics of T cell migration to the bloodstream and the timing of onset of contraction. The antigen load and the early cytokine milieu may altogether affect the initial events involved in $CD8^+$ T cell differentiation (Joshi et al., 2007; Whitmire et al., 2005; Zehn et al., 2009). During the course of the infection, the combinations and concentrations of cytokines change, and may influence the development of functionally distinct T cell subsets (Kaech and Cui, 2012; Masopust and Schenkel, 2013). Moreover, inflammatory cytokines that act directly on responding $CD8^+$ T cells are greatly pathogen-specific. Infection with LCMV generates a strong type I IFN response (IFNα/β), which is important for early viral control and for the generation of a protective LCMV-specific cytotoxic T cell response (Muller et al., 1994; van den Broek et al., 1995). Type I IFN is less critical for the control of Vaccinia virus (VV) or *Listeria monocytogenes* (LM) infection, where IL12 signalling is essential for $CD8^+$ T cell expansion and differentiation (Kolumam et al., 2005; Murali-Krishna et al., 1998). On the other hand, in the case of LCMV or Vesicular stomatitis virus (VSV), IL12 is not limiting to control infection (Keppler et al., 2009).

Upon activation, primed naive T cells present some heterogeneity on their expression patterns. Although most primed cells upregulate Sca1 early post-infection (DeLong et al., 2018), some downregulate CD62L, a cell adhesion molecule that facilitates lymph node homing (Alon et al., 1994; Carlson et al., 2006; Johnston and Butcher, 2002; Kerdiles et al., 2009). Additionally, other markers reflect the strength of TCR stimulation during acute activation such as Nur77 (Moran et al., 2011) and the IL2 receptor subunit α (IL2Rα) (CD25) (Kalia et al., 2010; Lin et al., 2016). Indeed, weakly stimulated cells express lower CD25 levels

at d4 p.i., while IL2Rβ (CD122), co-stimulatory molecules (CD27, CD28), or other activation markers (PD1 and CD44) are not different (Zehn et al., 2009). IFNαβ signals are also known inducers of the surface marker CD69 (Shiow et al., 2006; Shipkova and Wieland, 2012).

By day 4-5 p.i., a subset of effector cells expressing low levels of CD127 (IL7Rα) and high levels of killer cell lectin-like receptor G1 (KLRG1^{hi} CD127^{-}) are detected, so-called short-lived effector cells or SLEC, which increase in number and frequency until the peak of CD8^{+} T cell response (d8 p.i.) (Joshi et al., 2007). These cells present effector functions such as cytokine production (IFNɣ, TNFα) and cytolytic activity (Granzymes (Gzm) and Perforin production), which restricts viral replication by killing pathogen-infected cells. During the expansion phase, another subset of KLRG1^{lo} CD127^{hi} cells (so-called memory precursor cells or MPEC) is detected (Joshi et al., 2007). The cytotoxic activity, GzmB expression and ability to produce IFNɣ of MPEC is comparable to SLEC, but MPEC produce relatively high levels of IL2 (Joshi et al., 2007; Pais Ferreira et al., 2020; Shin, 2018; Wherry et al., 2003). Upon virus clearance, the majority of SLEC undergo a precipitous contraction phase where approximately 90% of the cells die by apoptosis while MPEC will survive and give rise to memory. However, some SLECs can also survive and become memory cells and not all MPECs survive and become memory cells. Indeed, a significant fraction of MPEC disappears following viral clearance (Herndler-Brandstetter et al., 2018; Joshi et al., 2007; Pais Ferreira et al., 2020; Renkema et al., 2020; Sarkar et al., 2008).

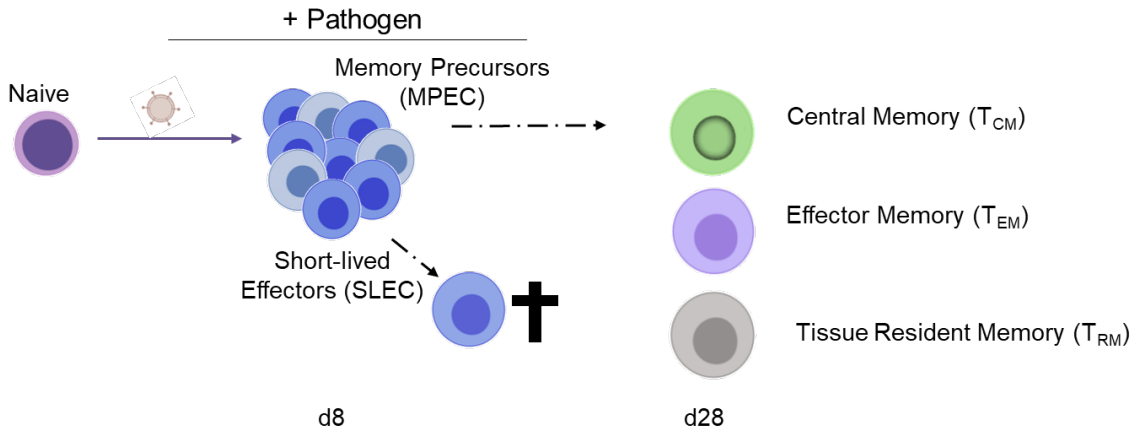

Figure 2 – Heterogeneity of CD8^{+} T cell population.
Naive CD8^{+} T cells are activated and differentiate into a heterogeneous population (MPEC and SLEC) until the peak of the effector phase. Once the virus is cleared, most cells die and only few cells remain in the absence of pathogen and form the memory compartment (T$_{CM}$, T$_{EM}$ and T$_{RM}$).

The duration of functional antigen presentation and the amount of inflammation at the time of priming influences CD8^{+} T cell differentiation. Shortening the duration of antigen presentation caused by infection (i.e. killing *Listeria* using antibiotic treatment starting at d1 p.i.) decreased the number of SLECs formed, but did not impact MPEC and subsequent memory CD8^{+} T cell formation. This may be related to an altered inflammatory environment.

"High-dose" LM inflammation generated an overabundance of SLEC. Therefore, the abundance of SLEC was proportional to the amount or duration of inflammation at the time of priming (Joshi et al., 2007). Together, these data suggest that exposure to antigen in the context of DCs but in the absence of systemic inflammation results in default memory formation (i.e., accelerates the rate at which $CD8^+$ T cells acquire memory characteristics) (Badovinac et al., 2005). Kinetics of T cell migration is dictated by the affinity of the TCR for antigen, meaning that the earliest wave of effector cells released into the blood stream is mostly composed of low affinity T cells (Zehn et al., 2009). Thus, antigen and inflammation determine the cellular heterogeneity in response to an acute infection.

1.4 $CD8^+$ T cell memory compartments

In contrast to naive cells, memory T cells are maintained in the absence of tonic TCR signals but depend on homeostatic IL7 and IL15 signals for self-renewal and survival (Surh and Sprent, 2008). The memory compartment is heterogeneous with regard to their migration capacity, effector functions and recall expansion potential (**Fig 3**) (Shin, 2018; Youngblood et al., 2015; Youngblood et al., 2017). Central memory T cells (T_{CM}) express the lymphoid homing markers chemokine receptor (CCR) 7 and CD62L and primarily circulate through secondary lymphoid organs, while effector memory T cells (T_{EM}) lack expression of lymphoid homing markers and instead express other migratory receptors (CCR1, CCR3 and CCR5), allowing surveillance of non-lymphoid tissues and migration to inflamed tissues (Masopust et al., 2001; Sallusto et al., 1999). T_{EM} have readily available lytic activity and can produce effector cytokines such as IFNɣ. On the other hand T_{CM} lack lytic activity, but can produce IL2 and proliferate extensively upon restimulation (Sallusto et al., 1999).

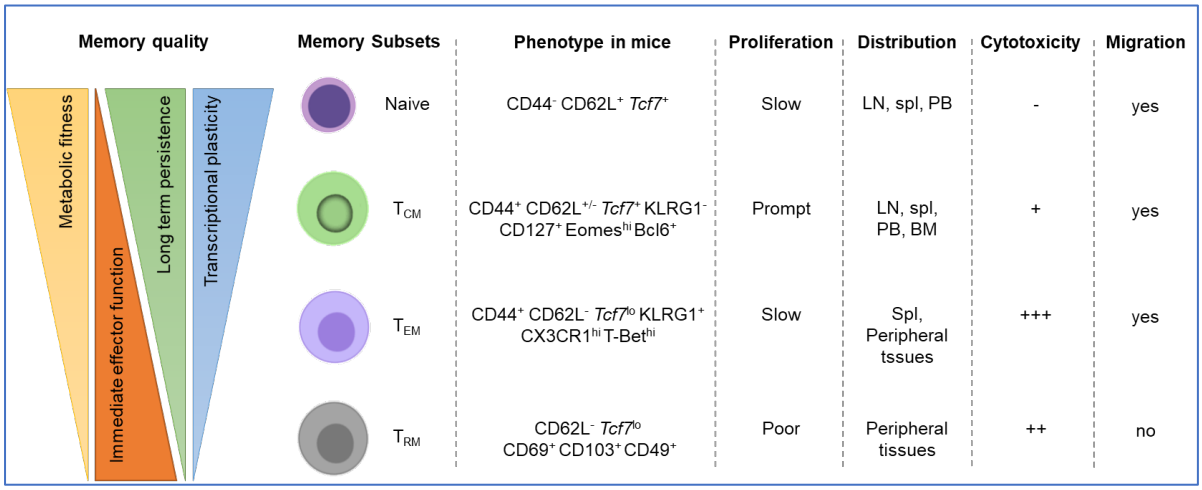

Figure 3 – Naive and memory characteristics, expressed markers, functionality and distribution.
T_{CM}: Central memory T cells; T_{EM}: effector memory T cells; T_{RM}: tissue-resident memory cells; LN: lymph node; spl: spleen; PB: peripheral blood; BM: bone marrow. Adapted from (Jandus et al., 2017).

Recently, CX3CR1 (fractalkine receptor) was used to differentiate memory $CD8^+$ T cells. $CX3CR1^-$ memory cells lacked GzmB, were the main producers of IL2 upon re-stimulation and had high proliferative capacity upon re-transfer and challenge (characteristics of T_{CM}). $CX3CR1^+$ memory cells constitutively expressed GzmB (irrespective of CD62L) and showed cytotoxic effector functions directly *ex vivo* (characteristics of T_{EM}). However, no difference in IFNɣ production was found (Bottcher et al., 2015).

In addition to circulating T_{CM} and T_{EM}, non-hematopoietic tissues harbour a non-circulating memory $CD8^+$ T cell subset with a distinct transcriptional program (**Fig 4**). These tissue-resident memory cells (T_{RM}) express high levels of CD69, an activation marker that is usually transiently upregulated during priming of T cells, and the integrins CD49 and CD103, which binds to collagen and E-cadherin, respectively. These cells have immediate effector functions and can mediate pathogen control within the tissue. Although T_{RM} from a wide range of tissues share a core set of characteristics, it is likely that T_{RM} establishment and function is tissue-dependent, however our understanding of these tissue-specific requirements is incomplete (Shin, 2018; Wu et al., 2018).

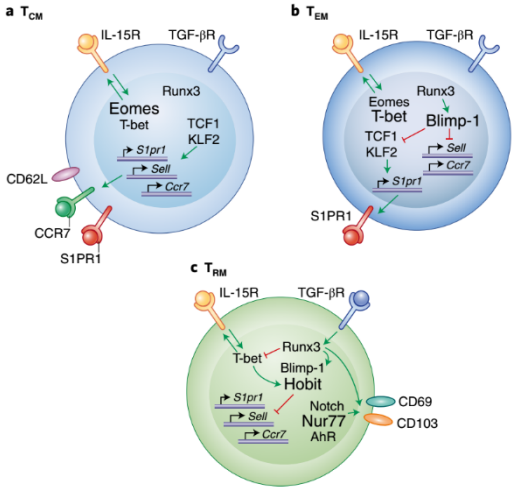

Figure 4 –Transcriptional regulation of memory $CD8^+$ lineages.
T_{CM}: Central memory T cells; T_{EM}: effector memory T cells; T_{RM}: tissue-resident memory cells (Amsen et al., 2018)

Although it is not fully understood from which precursor cells T_{RM} derive, an analysis of TCR sequences revealed overlap between circulating T_{CM} and T_{RM} cells, suggesting that the two memory subsets are related (Gaide et al., 2015). Early effector $CD8^+$ T cells can home to non-hematopoietic tissues between d4.5 to d7 p.i., defining the timeframe during which T_{RM} precursors can seed tissues (Masopust et al., 2010). It has been suggested that the potential T_{RM} precursor derives from cells that have previously expressed KLRG1 or from $KLRG1^-$ cells with higher expression of CXCR3 with preferential migration toward CXCL9 and CXCL10 chemokines (Herndler-Brandstetter et al., 2018; Mackay et al., 2013).

1.5 Signals influencing effector versus memory CD8$^+$ T cell differentiation

The differentiation into effector versus memory cells is a critical step to protect the host against acute infection and for the long-term protection against re-infection. In the first few hours after activation, naive CD8$^+$ T cells initiate a transcriptional program that leads to the formation of memory and effector T cells, but the regulation of this process is poorly understood. Extensive research efforts have led to the identification of various factors affecting the formation of memory CD8$^+$ T cells vs effector differentiation (**Fig 5**).

Besides antigen and co-stimulation, cytokines are key regulators of the coordinated and dynamic expression of multiple transcription factors that control the development of memory and cytotoxic effector T cell (Xin et al., 2016). Cytokines chiefly act via signal transducer and activator of transcription (STAT) factors. IL12 activates STAT4 in CD8$^+$ T cells and this is needed for effector differentiation in response to bacterial infection (Joshi et al., 2007; Li et al., 2006). Type 1 IFNs activates STAT1 and STAT4 to promote effector differentiation in response to certain viral infections, including LCMV (Nguyen et al., 2002). IL21 signals through STAT3 thereby favouring memory differentiation (Croce et al., 2015; Sutherland et al., 2013). IL27 can phosphorylate STAT1, STAT3, STAT4 and STAT5. IL27 is also greatly upregulated in viral infections and promotes effector differentiation (Harker et al., 2018; Morishima et al., 2005; Perona-Wright et al., 2012). IL2, IL7 and IL15 chiefly activate STAT5 and ensure the survival of naive and memory CD8$^+$ T cells (Becker et al., 2002; Hand et al., 2010; Lord et al., 2000; Osborne and Abraham, 2010; Tripathi et al., 2010).

Cytokine signalling regulates the expression of downstream transcription factors, most of which seem to work in pairs in order to balance memory and effector differentiation. T-Bet, Blimp1, ID2 and STAT4 promote the differentiation towards terminally differentiated effector cells, which have reduced proliferative capacity and longevity. On the other hand, Eomes, Tcf1, Bcl6, ID3, Foxo1 and STAT3 prevent terminal differentiation of effector cells and promote memory cell development.

During CD8$^+$ T cell priming, inflammatory signals define a T-Bet-Eomes expression gradient. T-Bet and Eomes collaborate for the production of IFNγ and expression of GzmB and Perforin (effector functions) by antigen-specific CD8$^+$ T cells (Intlekofer et al., 2005; Morishima et al., 2005; Sutherland et al., 2013; Takemoto et al., 2006; Xin et al., 2016). Additionally, they both induce CD122, which is required for the IL15 responsiveness of memory cells, but also for effector cell survival (Banerjee et al., 2010; Becker et al., 2002). However, besides their redundant roles, T-Bet and Eomes have unique roles. The maximum levels of T-bet transcripts are observed in KLRG1^{hi} CD127^{lo} SLEC cells (Intlekofer et al., 2005; Joshi et al., 2007; Rao et al., 2010; Takemoto et al., 2006; Xin et al., 2016). T-Bet suppresses IL2 production by effector and memory cells in a STAT4-independent way (Mollo et al., 2014). In the absence of T-Bet, clearance of viral infection still occurs, but CD8$^+$ T cells express high levels of CD127, CD62L and CD27 and preferentially home to peripheral lymph nodes. However, the observed increase in the frequency and abundance of MPEC at the d8 p.i. of

LCMV infection does not translate into an increased number of memory cells (Intlekofer et al., 2007; Mollo et al., 2014). Additionally, T-Bet$^{-/-}$ cells show increased Eomes expression (Mollo et al., 2014). Eomes is induced later during the response and is highly expressed in memory cells (Intlekofer et al., 2005; Rao et al., 2010; Takemoto et al., 2006). Mice lacking Eomes have normal primary CD8^{+} T cell expansion but defect memory formation (Banerjee et al., 2010). TCR signalling and IL12 have an important role in the regulation of T-Bet versus Eomes: these signals induce T-Bet expression (in a dose-dependent manner) and repress Eomes (Intlekofer et al., 2005; Joshi et al., 2007; Morishima et al., 2005; Rao et al., 2010; Takemoto et al., 2006). Additionally, T-Bet can also be induced by IL27 and IL21 (Morishima et al., 2005; Sutherland et al., 2013) and Eomes can be induced by IL2 and IL4 (Takemoto et al., 2006).

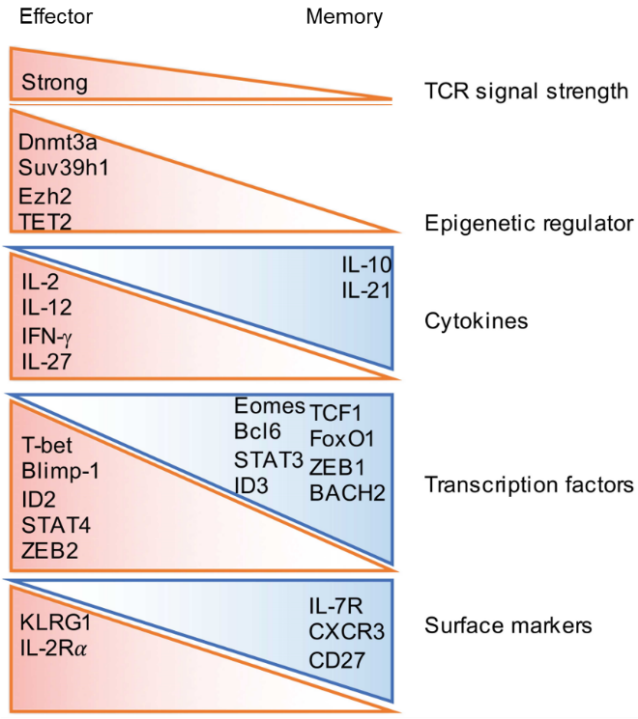

Figure 5 – Factors involved in the balance memory vs effector differentiation during acute viral infection (adapted from (Chen et al., 2018))

Not only T-Bet, but also B lymphocyte-induced maturation protein-1 (Blimp1), a zinc-finger containing repressor, is required for effector differentiation (Xin et al., 2016). Blimp1 induces KLRG1 and GzmB expression and represses the acquisition of central memory T cell properties (inhibition of CD62L, CD127, Eomes and Tcf1, another transcription factor described below) (Kallies et al., 2009; Rutishauser et al., 2009). IL2 is required for optimal Blimp1 induction, although IL12 can also induce Blimp1 in the absence of IL2. Blimp1 is regulated by STAT5 and STAT4-dependent signals (Xin et al., 2016). Mice lacking Blimp1 have no defect in clearing acute LCMV Arm infection (Rutishauser et al., 2009). This may be

due to the fact that T-Bet can partially compensate for the loss of Blimp1 to confer effector differentiation (Intlekofer et al., 2007; Kallies et al., 2009; Rutishauser et al., 2009; Xin et al., 2016). Blimp1 also influences T cell localization in tissues by regulating the expression of several chemokine receptors including CCR5, CCR6 and CCR7. On the other hand, B cell lymphoma 6 (Bcl6) has been shown to suppress GzmB and favour memory T cell generation (Yoshida et al., 2006). The expression of Bcl6 (like Eomes) can be induced by IL21 and IL10, in a STAT3-dependent fashion (Croce et al., 2015; Cui et al., 2011). Bcl6-deficient mice are impaired in their ability to maintain $CD8^+$ T cell memory (especially T_{CM}), while mice overexpressing Bcl6 have increased numbers of memory cells (Ichii et al., 2004).

Another set of transcription factors defining memory versus effector differentiation are the inhibitors of DNA-binding 2 (ID2) and 3 (ID3), which are both expressed in effector $CD8^+$ T cells (Yang et al., 2011). ID2 is involved in the survival of effector $CD8^+$ T cells (Cannarile et al., 2006), whereas ID3 identifies early $CD8^+$ T cells biased for a memory-precursor genetic signature (Ji et al., 2011; Yang et al., 2011). ID2 and ID3 are regulated by IL12, which promotes ID2 and represses ID3 expression (Yang et al., 2011). In addition, ID3 is repressed by Blimp1 (Ji et al., 2011).

FoxO1 induces IL7rα (CD127) and *Tcf7* expression, promoting memory differentiation. Moreover, FoxO1 directly binds to and represses T-Bet expression. Additionally, FoxO1 also controls the expression of CD62L, CCR7 and Klf2, factors crucial for lymphocyte tracking in naive T cells. Some of these functions of FoxO1 are regulated via mammalian target of rapamycin (mTOR) (Delpoux et al., 2017; Hess Michelini et al., 2013; Kerdiles et al., 2009; Kim et al., 2013; Rao et al., 2012).

Finally, T cell factor 1 (Tcf1, encoded by *Tcf7* gene) plays an essential role in $CD8^+$ T cell differentiation. Contrary to previously discussed transcription factors, Tcf1 is constitutively expressed at high levels in naive $CD8^+$ T cells (Boudousquie et al., 2014; Jeannet et al., 2010; Lin et al., 2016). Tcf1 is downregulated at the effector stage of the $CD8^+$ T cell response against infection and highly expressed in memory $CD8^+$ T cells (Boudousquie et al., 2014; Jeannet et al., 2010). Indeed, in LM and LCMV infections, Tcf1 expression is required for the formation of central memory $CD8^+$ T cells but it is not needed for effector differentiation (Boudousquie et al., 2014; Jeannet et al., 2010; Zhou et al., 2010). Tcf1-deficient memory cells have poor survival as well as homeostatic proliferation due to lower expression of Bcl2, IL15Rα and CD122 (probably due to low levels of Eomes) (Zhou et al., 2010).

1.6 T cell factor 1 and the immune system

Tcf1 includes a DNA-binding high mobility group (HMG) domain, a central domain that mediates the interaction with corepressor of the Groucho family, which also has histone deacetylase (HDAC) activity (Xing et al., 2016) and a NH2-terminal β-catenin binding domain (**Fig 6**) (Ioannidis et al., 2001).

Indeed, Tcf1 was initially identified as a nuclear effector of the canonical Wnt/ β-catenin signalling pathway. Tcf1 belongs to the small family of TCF/LEF factors, which included Tcf1, LEF1, Tcf3 and Tcf4 (Boudousquie et al., 2014; Im et al., 2016; Wang et al., 2019; Zhou et al., 2016).

Figure 6 – Schematic representation of the *Tcf7* gene and its structure/domains.
β-cat: β-catenin; HMG: high mobility group

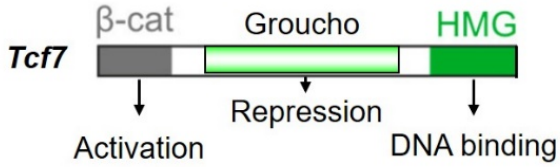

Tcf1 plays a crucial role for the developmental of innate lymphoid cells (Yang et al., 2015) and NK cells (Held et al., 1999). Tcf1 is also expressed in T lymphocytes, but not B lymphocytes (Boudousquie et al., 2014), and is crucial for T cell development (**Fig 7**) (Verbeek et al., 1995). Germline *Tcf7* deletion impairs T cell development, leading to reduced survival of double-positive thymocytes (Ioannidis et al., 2001).

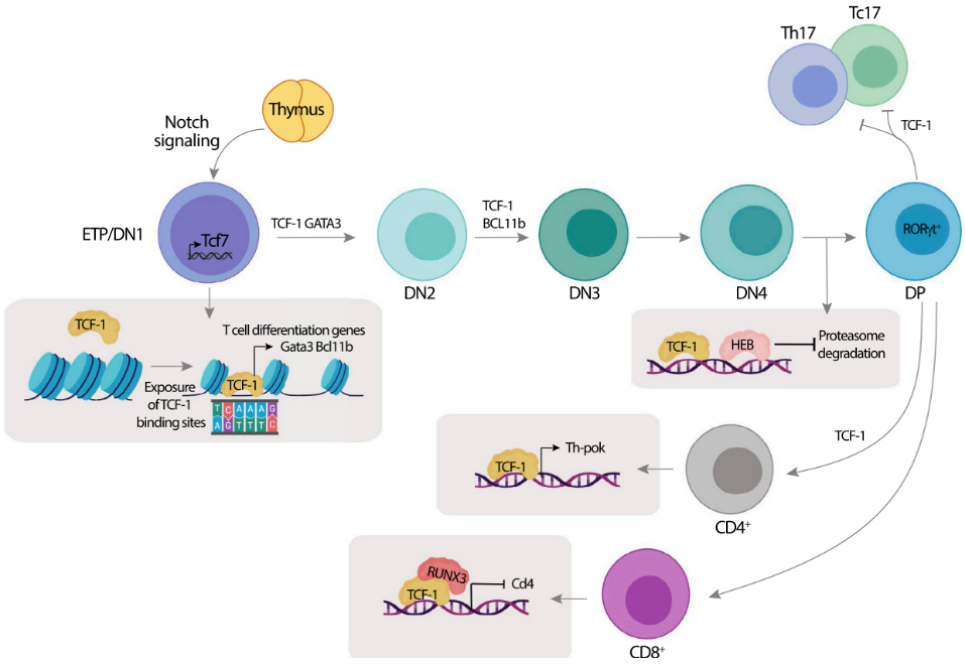

Figure 7 – T cell factor 1 is essential for T cell development.
Notch signalling drives *Tcf7* expression early in thymocyte development. Tcf1 induces the expression of other genes critical for early thymic development including GATA-3 and Bcl11b. Later in thymic development, Tcf1 ensures commitment toward CD4 T cell lineage by promoting Th-inducing POZ-Kruppel factor (Th-POK) expression, or cooperates with Runt-related transcription factor 3 (RUNX3) to limit expression of CD4 and other Th cell lineage associated genes to maintain $CD8^+$ T cell stability (Raghu et al., 2019).

In $CD4^+$ T cells, $Tcf1^+$ cells have less expression of the markers associated with Th1 cell differentiation, T-Bet, CD25 and signalling lymphocyte activation molecule (SLAM), but higher CXCR5, Bcl6 and CD62L expression, which may explain the enrichment in lymphoid sites (Nish et al., 2017). Indeed, Tcf1 initiates Th2 differentiation of activated $CD4^+$ T cells (Yu et

al., 2009) and is essential for T follicular helper (T_{FH}) cell differentiation during acute viral infection (Xu et al., 2015).

In $CD8^+$ T cells, Tcf1 is constitutively expressed in naive T cells, but also expressed in memory cells: high in T_{CM} and detectable in T_{EM} (Boudousquie et al., 2014; Lin et al., 2016). Tcf1 is not essential for the expansion of virus-specific $CD8^+$ T cells in the primary response, for the initial acquisition of effector functions (IFNɣ), viral control and long-term persistence of T_{EM} cells. The emergence of effector and effector memory cells is thus independent of Tcf1 (Danilo et al., 2018; Jeannet et al., 2010). However, Tcf1 is critical for the secondary expansion of virus-specific $CD8^+$ T cells upon re-infection and the generation of T_{CM} cells (Boudousquie et al., 2014; Jeannet et al., 2010; Zhou et al., 2010).

Little information had been available regarding the extrinsic signals regulating Tcf1 expression. This lab has shown that systemic inflammation supressed Tcf1 in primed T cells and that this correlated with effector differentiation. $CD8^+$ T cells lacking Tcf1 underwent effector differentiation, even in the absence of systemic inflammation (Danilo et al., 2018). Here, we established an *in vitro* system to test whether selected cytokines regulated Tcf1 expression (**Chapter 3.4**).

1.7 Epigenetic changes associated with memory and effector $CD8^+$ T cell differentiation

$CD8^+$ T cell differentiation is associated with epigenetic changes (Henning et al., 2018; Kakaradov et al., 2017; Pace et al., 2018; Youngblood et al., 2017). For example, histone modifications lead to changes, which influence positively or negatively the gene expression. During effector differentiation, the *Tcf7* and Eomes loci are associated with histones that are trimethylated on lysine 27 (H3K27me3) and this correlates with repressed expression of these gene during effector differentiation (Kakaradov et al., 2017). The histone-lysine N-methyltransferase Suv39h1 is required for effector differentiation. In mice lacking Suv39h1, the proportion of memory T cells was increased as a result of increased H3K4me1 (enhancer priming) and H3K4me3 (increased transcription) and decreased H3K9me3 (transcriptional repression) deposition in memory associated genes (such as CD127, CD62L, CCR7 and Cxcr4) in effector cells (Pace et al., 2018). Transcription can also be reduced based on the acquisition of cytosine methylation in CpG (cytosine-phosphate-guanine) dinucleotides. Changes in CpG methylation were observed proximal to the *Sell* (CD62L), *Perforin*, *GzmB* and *IFNɣ* promoters during memory/effector differentiation (Youngblood et al., 2017). Multiple studies thus suggest that effector T cell differentiation requires the progressive epigenetic silencing of memory-associated genes (Henning et al., 2018; Kakaradov et al., 2017; Pace et al., 2018). Others suggest that memory differentiation during the effector-to-memory $CD8^+$ T cell transition depends on re-expression of memory-associated genes (Youngblood et al., 2017). These aspects will be discussed in more detail in the next chapter (**Chapter 1.8**). In conclusion, effector versus memory $CD8^+$ T cell differentiation is regulated by signalling

pathways, which control the expression of specific transcription factors that promote or suppress cell fates.

1.8 Models explaining the developmental origin of effector and memory CD8$^+$ T cells

The developmental origin of T cell memory has remained as one of the big open questions in immunology. Some studies suggested that naive CD8$^+$ T cells are programmed during thymic development to adopt different fates upon activation in the periphery (Kaech and Cui, 2012). However, elegant studies using cellular barcoding as well as transfer of single cells have shown that both effector and memory cells can arise from a single naive CD8$^+$ T cell (Buchholz et al., 2013; Gerlach et al., 2013; Stemberger et al., 2007), although individual naive CD8$^+$ T cells display heterogeneous differentiation patterns and differ in their clonal expansion capacity (Buchholz et al., 2013; Gerlach et al., 2013). These results argue against the hypothesis that during the immune response memory and effector CD8$^+$ T cell lineage originate from different cells.

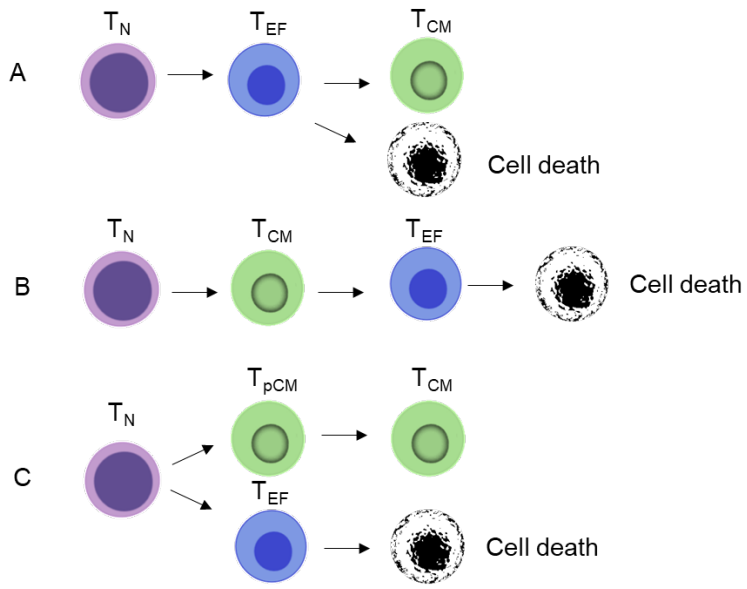

Figure 8 –Schematic of simplified models of the developmental origin of CD8$^+$ T cell memory.
A- Linear differentiation model; B- decreasing potential model; C- asymmetric cell division model
T_N: Naive T cells; T_{CM}: Central Memory T cells; T_{EF}: effector T cells

Several differentiation models have been proposed to explain the relationship between effector and memory CD8$^+$ T cell generation (**Fig 8**) (Henning et al., 2018). According to a **linear differentiation model**, naive cells give rise to effector cells and memory precursor cells, which both have lytic function. The latter dedifferentiate (lose lytic activity) following viral clearance to become memory T cells (T_N>T_{EF}>T_{CM}) (Kalia et al., 2010; Youngblood et al., 2017). This is supported by evidence that cells that previously expressed GzmB (and thus

presumably had lytic activity) can generate central memory cells i.e. cells that have recall expansion capacity (Bannard et al., 2009). A caveat of this study is that it does not completely take into account the existing heterogeneity amongst effector cells (Herndler-Brandstetter et al., 2018). Indeed, certain $CD8^+$ T cells arising during the effector phase show a bias towards a memory cell fate (Chang et al., 2007; Joshi et al., 2007; Kakaradov et al., 2017). However, in support of a linear differentiation, genes associated with central memory cells (such as *Sell* – CD62L) are methylated in memory precursor cells (present at day 8 post-acute LCMV infection) but are unmethylated in central memory cells (Bannard et al., 2009; Youngblood et al., 2017). A caveat of this model is that memory precursors do not quantitatively give rise to (central) memory, and most cells die during the contraction phase. Thus, it remained possible that MPEC include a rare non-lytic subset that gives quantitatively rise to memory.

The **decreasing potential model** proposes that activated $CD8^+$ T cells progressively lose proliferative capacity and multipotency and differentiate into effector cells (T_N>T_{CM}>T_{EF}). This is supported by evidence that memory T cells are more closely related to naive cells in terms of their gene expression profile than to effector cells. Further, epigenetic repression of stemness-associated genes is required for effector differentiation (Holmes et al., 2005; Pace et al., 2018). During T cell priming, repetitive stimulation of a $CD8^+$ T cell through the TCR, co-stimulatory molecules and cytokines is thought to progressively drive effector T cell differentiation with concomitant loss of memory cell potential (Ahmed and Gray, 1996; D'Souza and Hedrick, 2006; Kaech and Cui, 2012). This model is consistent with the observation that high pathogen burden and associated inflammation promote effector differentiation, while blunting an infection with antibiotics promotes rapid formation of memory (Mercado et al., 2000; Obar et al., 2011). Alternatively, effector cell differentiation may depend on the strength of the combination of the 3 signals. Higher signal strength enhances clonal expansion and leads to effector differentiation (Kaech and Cui, 2012). Independently, a central caveat of the decreasing potential model is that the primary response should harbour cells that have all the functions of central memory cells. However, such cells had not been identified.

Lastly, the **asymmetric cell division model** suggests that a single naive $CD8^+$ T cell gives rise to a memory and an effector precursor cell during the first cell division (T_N>T_{CM} or T_{EF}) (Chang et al., 2007; Kaech and Cui, 2012). According to this model, during the first T cell division, the daughter cell proximal to the APC receives stronger signalling input and differentiates into an effector precursor, while the distal daughter receives less signal and differentiates into a memory precursor cell (Chang et al., 2007; Kaech and Cui, 2012). This model is supported by observations that, during the first cell division, certain proteins (such as CD25, T-Bet, Numb and others) are distributed asymmetrically to the two daughter cells (Borsa et al., 2019; Chang et al., 2007; Oliaro et al., 2010). The last 2 models differed regarding the timing when the decision is made, ie that the fate decision is made early during the response rather than progressively (Kaech and Cui, 2012) .

Recent work by this lab has identified a small population of virus-specific $CD8^+$ T cells that expresses *Tcf7* and that is present at the peak of the primary response to infection. These cells lack lytic capacity and have all the functional properties of central memory cells (Pais Ferreira et al., 2020). These findings are not compatible with the linear differentiation model. To gain further insights into the developmental origin of effector and memory cells, the central aim of this thesis was to address the fate of the virus-specific *Tcf7*$^+$ $CD8^+$ T cells in their natural environment *in vivo* during an immune response to acute resolved viral infection.

1.9 The CD8$^+$ T cell response to chronic infection

Approximately a third of the world's population harbours a persistent infection (Krishnamurty and Pepper, 2014). Viruses, such as human immunodeficiency virus (HIV), hepatitis B virus (HBV) and hepatitis C virus (HCV), evolved multiple strategies to escape the surveillance by the immune system (Virgin et al., 2009). A high viral load leads to sustained antigen exposure, and this induces eventually T cell dysfunction (**Fig 9**) (Wang et al., 2019).

In chronic infections, virus-specific CD8$^+$ T cells show a progressive decreased proliferation, reduced ability to secrete effector cytokines (TNFα and IFNɣ) and reduced killing capacity due to the upregulation of expression of inhibitory receptors, such as programmed cell death-1 (PD1) and Lymphocyte Activation gene-3 (Lag3) (Barber et al., 2006; Cornberg et al., 2013; Wherry et al., 2007). This is globally referred as T cell exhaustion (**Fig 10**). Despite the reduced effector functions, exhausted CD8$^+$ T cells have an important role in sustaining viral control (Wang et al., 2019).

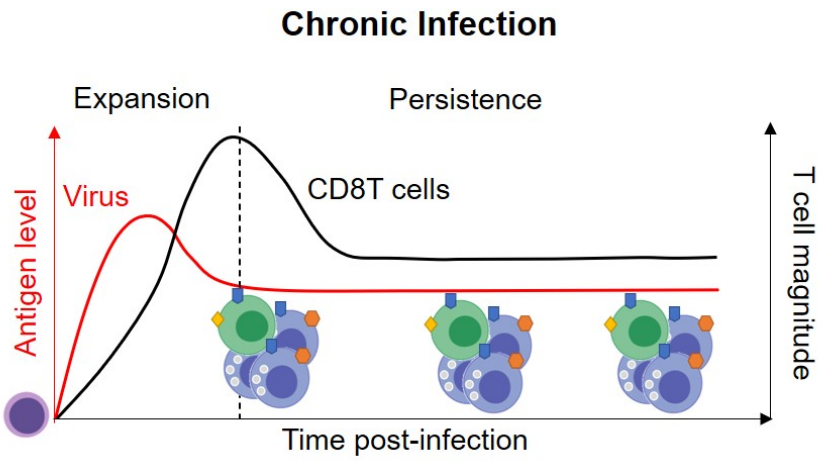

Figure 9 - Kinetics of CD8$^+$ T cell response during a chronic viral infection.
Viral titer (red) and kinetics of CD8$^+$ T cell response (black) during a chronic viral infection. Different cells indicate the cell heterogeneity and cell persistence during infection.

Induction of the exhaustion program upon persistent stimulation is considered a feedback mechanism, which imposes a balance between an attenuated but sustained antiviral response and restriction of excessive pathologic immune activation, which could be detrimental to the host (Cornberg et al., 2013; Pereira et al., 2017). In line with this, PD1 is only transiently expressed by CD8$^+$ T cells upon acute infection, while PD1 is constitutively expressed during chronic infection. Indeed, PDL1$^{-/-}$ mice that are chronically-infected die due to immunopathologic damage (Barber et al., 2006).

Disrupting the PD1:PDL1 interaction (using blocking antibodies) in chronically-infected mice resulted in an improved proliferative response and effector functions of virus-specific CD8$^+$ T cells and reduced viral load (Barber et al., 2006). However, the effects of this so-called

T cell reinvigoration are transient and cells adopt their initial state once PD1:PDL1 blocking is discontinued (Pauken et al., 2016).

Lack of $CD4^+$ T cell help, immunosuppressive cytokines and instructive signals from inhibitory receptors also contribute to T cell exhaustion (Battegay et al., 1994; Blackburn et al., 2009). Mice lacking B cells are also unable to resolve LCMV cl13 infections (Bergthaler et al., 2009; Thomsen et al., 1996). Thus, infection with LCMV cl13 results in generation of B and T ($CD4^+$ and $CD8^+$) cell responses, all of which are needed to eventually control systemic infection (Matloubian et al., 1994; Thomsen et al., 1996).

1.10 Mechanisms underlying T cell exhaustion

The level of antigen at early time points of the infection determines the fate of $CD8^+$ T cells and consequently whether an infection will be resolved or persist. In LCMV infection, low virus and antigen levels result in an acute resolved infection, whereas a high antigen level may result in chronic infection (Utzschneider et al., 2016a). Rather than the TCR stimulation strength, the duration of TCR engagement leads to T cell exhaustion (Utzschneider et al., 2016a).

TCR engagement activates NFAT (Nuclear factor of activated T-cells), AP1 (Activator protein 1) and NFkB transcription factors. Mechanistically, exhaustion seems to be driven by NFATs in the absence of AP1 cooperation. $CD8^+$ T cells expressing a mutant form of NFAT1 unable to interact with AP1, fail to elicit an effector response. Rather they upregulate the expression of several markers of T cell exhaustion. (Martinez et al., 2015; Pereira et al., 2017). CHIP-seq showed that NFAT1 binds directly to Lag3, Tim3, PD1 and GITR, as well as Prdm1 and Tox (see below) in $CD8^+$ T cells. In line with this, chronically-infected mice lacking both NFAT1/2 show dramatic decreases of $CD8^+$ T cells co-expressing PD1, Tim3 and Lag3 (Martinez et al., 2015).

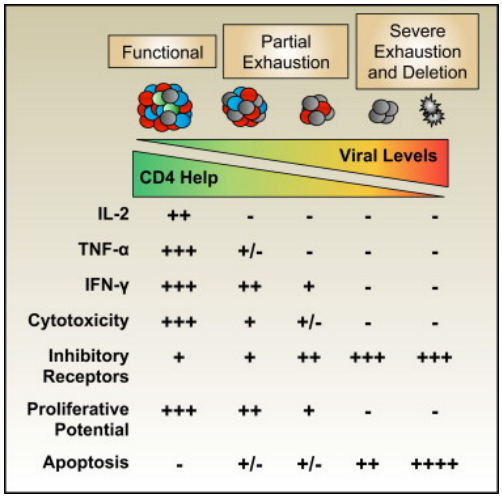

Figure 10 – $CD8^+$ T cells adopt an exhausted phenotype during a chronic viral infection
(Kahan et al., 2015)

Chronically-infected mice show significantly higher levels of Type I IFN in the serum compared to acute-infected mice very early post-infection. At the chronic phase, type I IFN

has been shown to promote immunosuppression (PDL1 and IL10), lymphoid disorganization and viral persistent. Blockade of IFN-I signalling during the chronic phase restores multiple effector functions and increases viral control (Teijaro et al., 2013; Wilson et al., 2013)

IL10 is an immunosuppressive cytokine produced by DCs, CD4 T cells and B cells during LCMV clone 13 infections (Brooks et al., 2006; Frohlich et al., 2009). In mice deficient for IL10 or those receiving IL10 blocking antibodies, abundance and functionality of anti-viral $CD8^+$ T cells are increased leading to a rapid clearance of the virus (Bottcher et al., 2015; Brooks et al., 2006).

IL21, produced mainly by $CD4^+$ T cells, is essential to maintain long-term maintenance, necessary for sustained chronic viral infection control. IL21 is essential as well for sustained effector responses and cytokine production (Frohlich et al., 2009). Moreover, IL21 promotes the differentiation of T_{ML} into exhausted cells (Beltra et al., 2020; Zander et al., 2019).

$CD8^+$ T cell differentiation in chronic LCMV infection is regulated by transcription factors, such as Blimp1, T-Bet and Eomes. Mice lacking these transcription factors show reduced LCMV cl13 control, although viral control during acute LCMV Arm infection still occurs (Banerjee et al., 2010; Intlekofer et al., 2007; Rutishauser et al., 2009). Blimp1 is highly expressed in exhausted $CD8^+$ T cells and promotes expression of inhibitory receptors such as PD1, Lag3, CD160 and 2B4 (Shin et al., 2009). Similarly, Eomes is highly expressed in exhausted $CD8^+$ T cells and its expression correlates with Tim3, PD1, Lag3, CD160 and 2B4 (Paley et al., 2012). T-Bet overexpression increased $CD8^+$ T cell numbers and reduced PD1 expression, and its absence impairs viral control (Kao et al., 2011).

TOX (Thymocyte selection-associated high mobility group box protein) is the first transcription factor found to be selectively expressed in $CD8^+$ T cells responding to chronic infection. TOX is induced via NFAT signalling downstream of constitutive T cell signalling. TOX expression promotes the expression of inhibitory receptors and impairs the cytokine production. TOX mediates in part the epigenetic changes associated with exhaustion. Besides this, TOX also ensures the survival of memory-like cells. (Alfei et al., 2019; Khan et al., 2019; Yao et al., 2019).

1.11 Heterogeneity of exhausted $CD8^+$ T cells responding to chronic infection

As exhausted cells appeared terminally differentiated, which are usually considered to lack of replicative function and to be short-lived, it was unclear how the $CD8^+$ T cell response to chronic infection was maintained long-term. In addition, the cellular basis for T cell reinvigoration in response to checkpoint blockade has been unclear.

Recent studies have shown that exhausted virus-specific $CD8^+$ T cell populations are not homogeneous (Im et al., 2016; Utzschneider et al., 2016b). A subpopulation of antigen-specific $CD8^+$ T cells continually expressing high levels of Tcf1 (also $ICOS^+$ $Bcl6^+$ $Tim3^-$ $PD1^+$) was identified. These so-called memory-like or progenitor exhausted or stem cell-like $CD8^+$ T cells (T_{ML}) maintained an improved proliferative capacity and could self-renew or differentiate into

Tcf1$^-$ (also PD1$^+$ 2B4$^+$ Tim3$^+$ CD39$^+$ Lag3$^+$) CD8$^+$ T cells (exhausted cells or T_{EX}) (Im et al., 2016; Utzschneider et al., 2016b; Wang et al., 2019; Wu et al., 2016). Gene set enrichment analysis (GSEA) showed that T_{ML} were similar to CD4$^+$ T_{FH} and CD8$^+$ memory precursor cells, while T_{EX} were more related to CD4$^+$ Th1 cells and CD8$^+$ effector cells (Im et al., 2016). T_{ML} were predominantly present in lymphoid tissues and mainly localized to the T cell zone of white pulp of the spleen. T_{EX} were present in both lymphoid and non-lymphoid organs and mostly in the red pulp of the spleen (Im et al., 2016).

The finding that Tcf1$^+$ stem cell-like CD8$^+$ T cells maintain the immune response to chronic viral infection is entirely based on cell transfer experiments into infection type-matched secondary recipients or recall responses in naive secondary recipients. It has not been known whether T_{ML} cells that reside in their natural environment actually self-renew or differentiate into T_{EX} during chronic viral infection. Further, it has not been determined at what rate exhausted cells are generated and turnover. These questions were addressed using a *Tcf7*-based lineage tracing model.

Single cell RNA sequencing (scRNA seq) of virus-specific CD8$^+$ T cells from chronic LCMV infection revealed additional heterogeneity among T_{ML} and T_{EX} cells (Beltra et al., 2020; Hudson et al., 2019; Zander et al., 2019). However, the studies differ regarding the markers used to characterize this heterogeneity. Four main subsets have been discriminated: a quiescent progenitor population (Tcf1$^+$ Ly108$^+$ CD69$^+$ PD1$^+$), a proliferating progenitor population (Tcf1$^+$ Ly108$^+$ CD69$^-$ CX3CR1^{int}), transiently exhausted cells (Tcf1$^-$ T-Bet^{hi} CX3CR1$^+$ GzmB^{hi} Tim3$^+$) and terminally exhausted cells (Tcf1$^-$ GzmB^{lo} Tim3$^+$). Other studies suggested a unique transitory population between memory-like and terminally exhausted cells, using transient CX3CR1 expression (Zander et al., 2019) or continuous Tim3 and CD101 expression (Hudson et al., 2019).

However, these studies differed regarding their differentiation trajectories downstream of T_{ML}. A **linear differentiation model** suggested that T_{ML} cells give rise to CX3CR1$^+$ transitory exhausted cells and these then differentiate into terminally exhausted CX3CR1$^-$ cells (Beltra et al., 2020; Hudson et al., 2019). Other papers suggested that T_{ML} give rise separately to CX3CR1$^+$ transitory exhausted or CX3CR1$^-$ terminally exhausted cells in a **bifurcative model** (Chen et al., 2019; Zander et al., 2019). We thus wanted to clarify the differentiation trajectory of T_{ML}.

1.12 Therapeutic advances

Vaccines are arguably the most important advance in modern medicine. Vaccination requires the potent induction of memory responses in order to provide long-term protection against pathogen infection (Shin, 2018). Protection induced by most current vaccines is mediated by antibodies. The failure in designing efficacious vaccines against pathogens such as HIV, herpes simplex virus (HSV) and influenza has increased the interest in the development of T-cell based vaccines (Shin, 2018). Considering T_{CM} cells as a central and

long-term mediator of protection, it is crucial to better understand the developmental origin of T_{CM} in order to improve the development of future preventive vaccines. By identifying and characterising central memory precursors, we believe that this thesis significantly contributes to this quest.

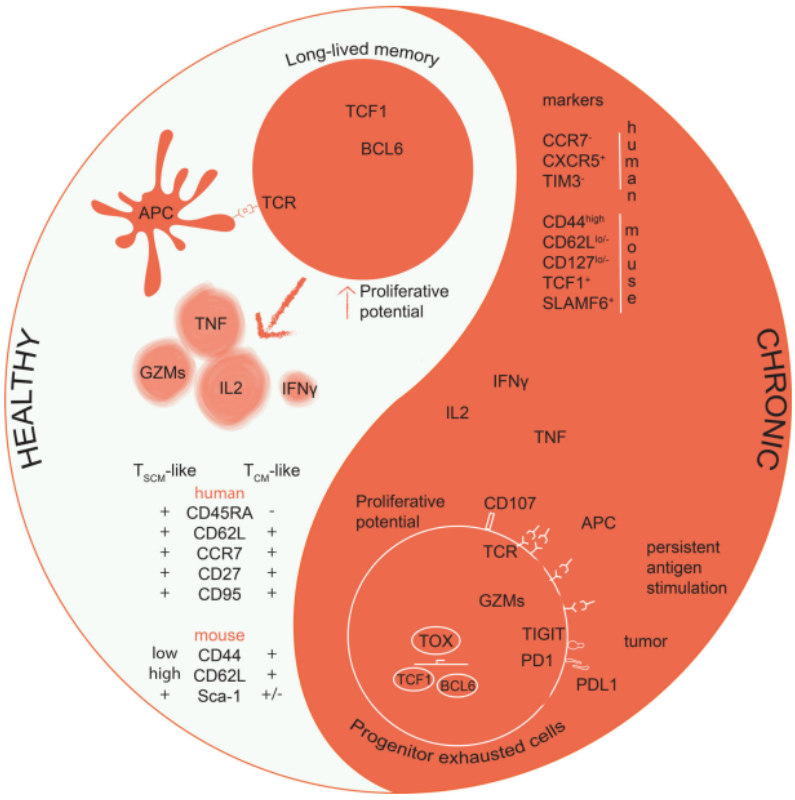

Figure 11 – Phenotype and proliferation potency of long-lived T cells in healthy versus chronic stimulation. Phenotype and proliferation potency of long-lived T cells in healthy homeostatic or upon secondary encounter (left) and under chronic stimulation (right) (Lugli et al., 2020).

T cell vaccines may be equally if not more important in therapeutic settings to treat chronic infection or cancer (**Fig 11**). Immunotherapeutic strategies that boost tumour- and virus-specific $CD8^+$ T cell responses are promising approaches to combat or prevent cancer and chronic viral infections (Henning et al., 2018; Wieland and Thimme, 2016). However, current therapeutic cancer vaccines may amplify relatively terminally exhausted cells or drive the recently identified memory-like cells into terminal differentiation (Klebanoff et al., 2006). Expanding stem cell-like cells in a way that prevents their differentiation may be a potent way to boost tumour- and virus-specific $CD8^+$ T cell responses. Together, a better basic understanding of the underlying immune responses may yield the key information needed to better design vaccines that are tailored to improve immunity (Whitmire, 2014). Along this line, this thesis considerably improves our understanding of the fate of naive $CD8^+$ T cells responding to acute and chronic viral infection.

Aim of the Project

Following encounter with antigen, naive $CD8^+$ T cells can adopt numerous distinct cell fates. During an acute resolved infection, naive $CD8^+$ T cells can differentiate into short-lived effector cells, crucial for viral clearance, or into distinct types of memory cells, which protect from secondary infection with the same pathogen. During chronic infection, naive $CD8^+$ T cells differentiated into memory-like cells that sustain the immune response by continuously producing cells with effector potential. The latter cell types differ profoundly from those observed in acute resolved infections. When and how $CD8^+$ T cells adopt specific fates is still surprisingly poorly understood. In addition, the current knowledge regarding these processes largely derives from cell transfer experiments, during which cells are removed from their natural environment and are asked to perform in a new environment. It is mostly unclear whether these insights truly reflect cell fate changes in their natural environment.

The aim of this thesis has been to develop a lineage tracing approach to map the fate of naive $CD8^+$ T cells in their natural environment during their response to acute resolved or chronic viral infection. We took advantage of the fact that the transcription factor T cell factor1 (Tcf1, encoded by the gene *Tcf7*) is expressed in all naive $CD8^+$ T cells. During acute infection, Tcf1 is downregulated in most but not all $CD8^+$ T cells during the effector phase and is expressed in central memory cells. In chronic viral infection, Tcf1 expression defines memory-like cells that sustain the immune response. Consequently, we generated a *Tcf7* guided fate mapping system that allowed the stable genetic labelling of *Tcf7*-expressing $CD8^+$ T cells in their natural environment and determine the fate of labelled cells.

Based on this system, we sought to obtain insights of the timing of $CD8^+$ T cells fate changes during an acute infection, and the turnover and developmental potential of $CD8^+$ T cells during a chronic infection.

Understanding the events involved in cell fate decision and differentiation trajectories has important implications for the development of T cell vaccines as well as strategies to revert and/or alter T cell function in situations of antigen persistence such as chronic infection or cancer.

2.Materials and Methods

Mouse strain information

C57BL/6 (B6) (CD45.2$^+$) mice were obtained from Charles River (L'Arbresle Cedex, France). CD45.1 congenic B6 mice were bred locally. B6 P14 T cell receptor (TCR) transgenic mice (line 237), which harbours a transgenic TCR (Vα2 Vβ8.1) specific for the LCMV glycoprotein gp33–41 epitope (gp33; KAVYNFATM) present in the context of H-2D^b MHC class I molecules, were provided by H.P. Pircher (Freiburg, Germany) (CD45.2$^+$) (Pircher et al., 1989). *Tcf7*$^{-/-}$ (KO) mice (Verbeek et al., 1995) were provided by H. Clevers (Utrecht, The Netherlands). Vβ5 TCR transgenic mice (Dillon et al., 1994) were provided by P. Fink (Seattle, USA). *STAT4*$^{-/-}$ mice (Kaplan et al., 1996) were provided by M. Löhning (Berlin). Rosa26 lox stop lox Confetti (*R26*^{Confetti}) (Snippert et al., 2010) were provided by J. Joyce (UNIL). Rosa26 lox stop lox TdTomato (*R26*^{Tomato}) (Madisen et al., 2010) were provided by J. Huelsken (EPFL). *Tcf7*^{GFP} and *Tcf7*$^{GFP\text{-}DTR}$ mice have been previously described (Siddiqui et al., 2019; Utzschneider et al., 2016b).

Tcf7$^{GFP\text{-}iCre}$ mice were generated using a bacterial artificial chromosome (BAC) containing the entire *Tcf7* locus plus >60kb of up and down stream sequence (RP23-223A11). An EGFP-T2ACreERT2-polyA fusion gene was inserted into the endogenous translation start codon present in exon Ia' of the *Tcf7* locus. PiggyBAC transgenic *Tcf7*$^{GFP\text{-}iCre}$ mice were generated by pronuclear injection into fertilized B6 oocytes (Cyagen Inc.). Founder mice were identified by PCR and initially characterized by flow cytometry for GFP expression.

P14 *Tcf7*^{GFP}, P14 *Tcf7*$^{GFP\text{-}DTR}$, P14 *Tcf7*$^{-/-}$ *Tcf7*^{GFP}, P14 *STAT4*$^{-/-}$, P14 *Tcf7*$^{GFP\text{-}iCre}$ *R26*^{Confetti}, P14 *Tcf7*$^{GFP\text{-}iCre}$ *R26*^{Tomato} mice were obtained by breeding (all CD45.2$^+$ except indicated otherwise).

Mouse strains were bred and maintained in the SPF animal facility, and experiments with infected mice were performed in the P2 animal facility of the University of Lausanne. Experiments used both male and female mice between 6 and 12 weeks of age, whereby donors and recipients of adoptive T cell transfers were sex matched. Animal experiments were conducted in accordance with protocols approved by the veterinary authorities of the Canton de Vaud.

Lymphocytic choriomeningitis virus (LCMV) infections

The LCMV Arm, WE and Cl13 strains were propagated in baby hamster kidney cells and titrated on Vero African green monkey kidney cells according to an established protocol (Battegay et al., 1991). Frozen stocks were diluted in PBS. Mice were infected intraperitoneally (i.p.) with 2×10^5 plaque forming units (PFU) LCMV 53b Armstrong (Arm) or intravenously (i.v.) with 200 PFU of LCMV WE strain or 2×10^6 PFU of Cl13, one day after cell transfer or on the same day when cells have been sorted (d0).

Tissue preparation and cell suspensions

P14 $CD8^+$ T cells were obtained by mashing total spleen through a 40 µm nylon cell strainer (BD Falcon). Red blood cells were lysed with a hypotonic Ammonium-Chloride-Potassium (ACK) buffer. $CD8^+$ T cells were purified using mouse $CD8^+$ T cell enrichment kit (StemCell Technologies).

Peripheral blood was collected into 1.5mL Eppendorf containing 15 µL of 0.5M EDTA. Peripheral blood mononuclear cells (PBMCs) were obtained by lysing the red blood cells with ACK buffer and subsequent wash with FACS buffer.

For the analysis of Tissue-resident memory cells from the gut, mice were injected i.v. with 3 µg of APC-eF780-labeled anti-CD8α mAb (clone 53-6.7) 4 min prior to sacrifice and organ collection. In the gut, 99% of the cells were $CD8\alpha^-$, which were considered to be resident in nonlymphoid tissues, so i.v. labelling of CD8α was discontinued. For the isolation of Intraepithelial Lymphocytes (IELs), the small intestine was collected. Performed on ice at all times, the intestine was cut in small pieces and flushed with HBSS 2% FCS, before removing all Peyer's patches. Then a longitudinally cut was done to open the intestine, followed by incubation with 1mM of Dithiothreitol (DTT) (Applichem, A3668) in HBSS 10% FCS for 20min at 37°C while stirring. After digestion, the cell suspension (containing the IELs) was filtered using a 100µM strainer (Falcon) and centrifuged to obtain a pellet. The resulting pellet was enriched for CD8 T cells using MACS positive selection (Miltenyi Biotec kit 130-116-478).

Adoptive T cell transfer

Purified P14 cells ($CD45.2^+$ or $CD45.1/2^+$) (usually >95% pure) were adoptively transferred i.v. into naive B6 ($CD45.2^+$, $CD45.1^+$ or $CD45.1/2^+$) or Vβ5 TCR transgenic B6 mice ($CD45.1^+$) one day prior to infection (d-1). In lineage tracing experiments accessed at memory phase, purified P14 *Tcf7*$^{GFP\text{-}iCre}$ ($CD45.1/2^+$) were transferred into *Tcf7*$^{GFP\text{-}iCre}$ recipients ($CD45.2^+$). For primary responses, 10^4 naive P14 cells were usually transferred, except for the early time point analysis: d1-4 p.i. in which mice received ~0.8-2×10^6 P14 cells, and d6 p.i. in which mice received 10^5 naive P14 cells. For all experiments involving flow sorted cells, cell transfer and infection were done on the same day (d0). For secondary transfer experiments, 10^4 flow sorted P14 cells were transferred. The fold expansion of P14 cells in secondary hosts was determined relative to an estimated 10% "take" of transferred input cells (Blattman et al., 2002).

Tamoxifen (TAM) treatment

Tamoxifen (TAM) (T5648, Sigma) was dissolved in 100% ethanol to a concentration of 100mg/ml and then diluted in pre-heated Sunflower seed oil (S5007, Sigma) to a concentration of 10mg/ml. *R26*^{Confetti} and *R26*^{Tomato} mice were injected i.p with 1mg or 0.1mg TAM, respectively, with single or multiple daily injections (ranging from 1-5 consecutive days) at different time-points after infection, according to each experiment's aim. Induction of Cre activity in *R26*$^{Confetti+}$ cells results in the stochastic and mutually exclusive expression of one of

four fluorescent proteins (RFP, CFP, YFP or GFP) (Snippert et al., 2010). Herein irreversible labelling was followed based on RFP expression. TAM treatment also yields GFP^{hi} cells, which could be discriminated from *Tcf7*$^{GFP\text{-}iCre+}$ cells based on the intermediate GFP levels of the latter. The GFP^{hi} cells were excluded from the analysis. Cre activity in *R26*$^{Tomato+}$ cells results in Tomato (RFP) expression exclusively. Control mice were absent of injection or injected with sunflower vehicle.

Diphtheria toxin (DT) treatment

A Diphtheria Toxin (DT) (D0564, Sigma) stock solution (2mg/mL in H_2O) was diluted in PBS to 5µg/mL. Mice were injected i.p with 50µg/kg of body weight (around 1µg of DT in 200µL per mouse of 20g). Control mice were injected with PBS.

EdU treatment

A 10mg/ml EdU (5-ethynyl-2'-deoxyuridine, a thymidine analog) solution was aliquoted and kept at -20ºC. EdU labelling was performed by injecting 2mg (200µl) of nucleoside analogue i.p. 2 hours prior to organ collection. For EdU detection, a Click-it Plus EdU Flow Cytometry Assay Kit (ThermoFisher Scientific, Cat #C10634) was used.

CFSE/CTV labelling

Labelling of cells with Carboxyfluorescein succinimidyl ester (CFSE; 0.5µM) or with CellTrace Violet (CTV; 2.5µM) to track cell division, was performed according to manufacture instructions. Briefly, purified cells were incubated in warm PBS for 8 min at 37ºC and washed 3 times in complete medium before being used.

Cell culture and *in vitro* assay

$CD45.1^+$ total splenocytes were pulsed with gp33-41 peptide (KAVYNFATM) (1µM) for 1h, washed 3 times, and used to stimulate the naive P14 $CD8^+$ T ($CD45.2^+$) cells *in vitro*. Naive P14 cells were purified and labelled with CFSE (0.5µM), as described above. 50 000 naive P14 cells and 50 000 gp33-pulsed splenocytes were plated in tissue-culture-treated flat-bottom 96-well plates and were kept in culture for 3 days *in vitro*, in a total volume of 200µL RPMI supplemented with 10% fetal bovine serum, 100U/ml penicillin, 100U/ml streptomycin, 1mM sodium pyruvate, 1x MEM non-essential amino acids (Gibco), 55µM 2-Mercaptoethanol. Where indicated, cultures were supplemented with 10ng/ml of IL1α, IL1β, IL7, IL12, IL21, IL23, IL33, TNFα and/or LIF (Peprotech), 20ng/ml of IL3, TGFβ or IGF-II (Peprotech), 30ng/ml of IL6 (Peprotech), 50ng/ml of IL2, IL10 or IL15 (Peprotech), 100ng/ml of GM-CSF, mSCF or mFTL3L (Peprotech), 10ng/ml of IL4 (Biolegend), 50ng/ml of IL18 (Biolegend), 25ng/ml of IL27 (ThermoFisher Scientific), 0.25ku IFNα (Chemicon Int Brand, Merk) and/or IFNβ (Biolegend). Cell cycle blockade was performed by using Aphidicolin (1µg/ml; control cells were treated with DMSO) after 48h of stimulation. Transcriptional silencing was address by adding the DNA

methyltransferase inhibitor 5-aza-2-deoxycytidine (Decitabine; 0.5μM; control cells were treated with DMSO) after 48h of stimulation.

Flow cytometry and cell sorting

Surface staining was performed with fluorescent antibodies for 15 min at 4°C in PBS supplemented with 2% FCS (FACS buffer) using the reagents listed in the Key Resource Table. For tetramer staining (D^b Gp33-41 – KAVYNFATC; D^b Np396 – FQPQNGQFI), cell suspensions were incubated with anti-CD16/32 (2.4G2) hybridoma supernatant before staining for 90min at 4°C with APC-conjugated MHC-I tetramers. Zombie Aqua Fixable Viability kit (Biolegend) was used to exclude dead cells.

For intranuclear staining, cells were surface stained extracellularly, then fixed using the Foxp3 transcription factor staining kit (eBioscience: Cat. No. 00-5523), followed by intranuclear staining in Permeabilization buffer 1x (Perm buffer). For the detection of cytokine production, splenocytes were re-stimulated *in vitro* with LCMV gp33-41 (gp33; KAVYNFATM) (1μM) peptide for 5h in the presence of Brefeldin A (5μg/ml) for the last 4.5h. Cells were stained at the surface before fixation and permeabilization (Intracellular Fixation & Permeabilization Buffer Set, eBioscience kit: Cat. No. 88-8824), followed by intracellular staining in 1x Perm buffer. For the detection of GzmB, splenocytes were cultured in the absence of peptide in the presence of 5μg/ml of Brefeldin A for 4.5h, before intracellular staining as described above. For cell cycle analysis, cells were fixed and permeabilized using the Foxp3 kit (eBioscience: Cat. No. 00-5523), followed by intranuclear staining with Ki67-FITC (BD Biosciences 556026) in 1x Perm Buffer. DAPI (2μg/mL) was added for the last 10min of intranuclear staining.

For cell sorting of P14 cells, splenocytes were enriched for $CD8^+$ T cells using the mouse $CD8^+$ T cell enrichment kit (StemCell Technologies), followed by surface staining. Cells were flow sorted on a FACSAria (BD) flow cytometer. The purity of sorted cells was greater than 99%, based on post-sort analysis.

Flow cytometry measurements of cells were performed on an LSR-II or Fortessa flow cytometer (BD). Flow Cytometer data were analysed using FlowJo (TreeStar).

Immunofluorescence labelling and microscopy

For immunohistochemistry analysis, the spleens were fixed in 1% PFA in PBS overnight, infiltrated with 30% sucrose the next day (overnight) and then embedded and frozen in OCT compound. Cryostat sections were collected on Superfrost Plus slides (Fisher Scientific), air dried and preincubated with blocking solution containing BSA, normal mouse serum and normal donkey serum (Sigma). Then, they were labelled for 1 hour using the following primary reagents**:** Rat anti-mCD4 (H129), Mouse anti-CD45.2 biotin (AL-1) (both produced in house) and rabbit anti-GFP (Thermofisher). After washing with PBS, the following secondary reagents were applied for 1 hour: Donkey anti-rat IgG Cy3 (Jackson Immunoresearch), streptavidin-APC (Biolegend) and donkey anti-rabbit IgG Alexa488 (Thermofisher). Finally, DAPI (4',6-

diamidino-2-phenylindole; Sigma) was used to stain the nuclei followed by mounting in DABCO (homemade). Images were acquired with a Zeiss AxioImager Z1 microscope and a AxioCam MRC5 camera.

Image analysis and cellular quantification

Image quantification was performed using the VIS Image Analysis software (Visiopharm). Splenic tissue was detected applying a 21 pixel mean $DAPI^+$ filter, followed by smoothening the edges and filling holes of the mask using the software's functions "close" and "fill holes", respectively. Next, the mask was converted to a region of interest (ROI), annotated in grey. Aberrant signals resulting from e.g., dust particles, tissue folds or air bubbles were manually excluded from these regions of interest (white). Within the detected total spleen ROI, a similar approach was used to detect regions positive for CD4 expression, in order to identify the T cell zone (T; salmon). The ROI for B cell zones (B) was automatically identified by excluding annotated T cell zones, and with relatively higher density of nuclei (blue). When needed, this ROI was manually adjusted to exclude areas with high accumulation of DAPI staining, such as at the edge of the tissue. An additional region of interest was defined around the T and B cell zones (50 pixels, PY). The remaining area of the spleen cells was referred to as red pulp (RP). Nuclear identification was based on the watershed signal of the $DAPI^+$ staining. The nuclear label was expanded with 5 pixels to allow detection of both nuclear and cytoplasmic fluorescent signal. Nuclear labels exceeding the manually set threshold for CD45.2 expression, were converted to $CD45.2^+$ labelled cells. Similarly, $CD45.2^+$ labelled cells surpassing the threshold for *Tcf7* expression were labelled as $Tcf7^{GFP+}$ cells. Threshold settings were identical between different samples. Finally, a counting frame was applied to ensure accurate counts for all $CD45.2^-$, $CD45.2^+$, $Tcf7^{GFP+}$ and EdU^+ cells within the four ROI (total spleen, T and B cell zone, and proximal zone). The obtained counts were then used to determine the frequency of single $CD45.2^+$ cells ($Tcf7^{GFP-}$ P14 cells), of double positive $CD45.2^+$ $Tcf7^{GFP+}$ ($Tcf7^{GFP+}$ P14 cells) and of EdU^+ cells among all subsets in each zone. The frequency of cells in the RP was obtained by subtracting T, B and PY counts from the cell counts in the total spleen ROI.

Data analyses

All bar and line graphs depict means ±SD. Statistical analyses were performed using Prism 7.0 or 8.0 (Graphpad Software). Paired and non- paired t tests (two-tailed) or one-way ANOVA were used according to the type of experiments. P-values ≤ 0.05 were considered significant (*: $p<0.05$; **: $p<0.001$; ***: $p<0.0001$); p-values >0.05; non-significant (ns)

Key Resources Table

Table 1 – Key resources

REAGENT OR RESOURCE	SOURCE	IDENTIFIER
Antibodies		
Rabbit anti-mouse/human Tcf1	Cell Signalling Technology	Clone C63D9; RRID: AB_2199302
F(ab')2-Donkey anti-Rabbit IgG (H+L) - PE	eBioscience	RRID:AB_1210761
Goat anti-Rabbit IgG (H+L) – AF647	Molecular Probes (Invitrogen)	RRID:AB_141663
24G2 supernatant (Fc block)		In house
H-2D^b / gp33-41 – APC (Tetramer)	TC Metrix	N/A
H-2D^b / np396 – APC (Tetramer)	TC Metrix	N/A
Anti-Mouse CD8a – APC, APC-eF780 or BV 650, AF700, BV785	eBioscience / BioLegend / In house	Clone: 53.6.7
Anti-Mouse CD45.1 – BV 785, Pacific Blue or AF647	BioLegend / In house	Clone A20.1
Anti-Mouse CD45.2 – PerCP-Cy5.5, APC-eFlour750, BV 650, PEF610 AF680	eBioscience / BioLegend	Clone: 104 Clone: Ali4A2
Anti-Mouse CD62L –BV 711, PE	eBioscience / BioLegend / In house	Clone: Mel14
Anti-Mouse CD69 – BV421, FITC	BD Biosciences	Clone: H1.2F3
Anti-Mouse CD127 – APC or PE	eBioscience / In house	Clone A7R34
Anti-Mouse CX3CR1 – BV711 or BV650	BioLegend	Clone: SA011F11
Anti-Mouse Ki67 – FITC	BD Biosciences	RRID:AB_396302
Anti-Mouse KLRG1 – PE Cy7 or BV 421	eBiosciences / BioLegend	Clone: 2F1
Anti-Mouse Lag3 (CD223) – PE or PerCPCy5.5	eBioscience	Clone: C9B7W
Anti-Mouse Ly108 – APC, PE Biotin	BioLegend/ eBioscience	Clone: 330-AJ Clone: 13G3-19D
Anti-Mouse PD-1 (CD279) - PECy7, BV711	BioLegend	Clone: RMP1-30
Anti-Mouse Tim3 (CD366) – APC, BV785, PE	BioLegend/BioLegend/ eBioscience	Clone: RMT3-23
Anti-Mouse Va2	BD Pharming	Clone: B20.1
Anti-CD44 APC eF780, Pacific Blue	eBioscience/In house	Clone IM7
Anti-mouse Sca1 – PE Cy7, AF700	eBioscience/Biolegend	Clone MP6-XT22
Anti-rabbit IgG (FITC)	eBioscience	Polyclonal; RRID:AB_253525

Donkey anti-rat IgG – Cy3	Jackson Immunoresearch	Cat #712-165-153; RRID:AB_2340667
Donkey anti-rabbit Alexa488	Life Technologies	Cat #R37118; RRID:AB_2556546
Donkey anti-rabbit IgG – Cy3	Jackson Immunoresearch	Cat# 711-165-152; RRID:AB_2307443
Rabbit anti-GFP	Thermofischer	
Rat anti-mouse CD4	eBioscience	Clone H129
Cytokines		
IL1α (Stock 10µg/ml)	Peprotech	211-11A
IL1β (Stock 10µg/ml)	Peprotech	211-11B
IL2 (Stock: 50 µg/ml)	Peprotech	212-12
IL3 (Stock 100µg/ml)	Peprotech	213-13
IL4 (Stock 20µg/ml)	Biolegend	574304
IL6 (Stock 20µg/ml)	Peprotech	216-16
IL7 (Stock 50µg/ml)	Peprotech	217-17 B
IL10 (Stock 10µg/ml)	Peprotech	210-10
IL12 (Stock 100µg/ml)	Peprotech	210-12 - 250UG
IL15 (Stock 10µg/ml)	Peprotech	210-15-10UG
IL18 (Stock 10µg/ml)	Biolegend	767002-10ug
IL21 (Stock 10µg/ml)	Peprotech	210-21-2ug
IL23 (Stock 10µg/ml)	Peprotech	200-23
IL27 (Stock 100µg/ml)	Thermo Fisher Scientific	14-8271-63
IL33 (Stock 100µg/ml)	Peprotech	210-33
GM-CSF (Stock 10µg/ml)	Peprotech	315-03
mSCF (Stock 100µg/ml)	Peprotech	250-03 B
TNFα (Stock 50µg/ml)	Peprotech	315-01A
TGFβ (Stock 20µg/ml)	Peprotech	100-21C
LIF (Stock 100µg/ml)	Peprotech	250-02
IGF-II (Stock 10µg/ml)	Peprotech	100-12
mFTL3L (Stock 100µg/ml)	Peprotech	250-31L B
IFNα (Stock 100ku)	Chemicon Int Brand	IF009
IFNβ (Stock 100ku)	Chemicon Int Brand	IF011
Bacterial and Virus Strains		
LCMV 53b Armstrong	D.Zehn, IVR-CHUV	In house
LCMV WE	C. Mueller, Uni Bern	In house
LCMV Clone 13	D.Zehn, IVR-CHUV	In house
Chemicals, Peptides and Recombinant Proteins		
Ammonium-Chloride-Potassium (ACK) buffer	In house	N/A
Peptide: LCMV glycoprotein amino acids 33-41 (gp33) (KAVYNFATM)	TC Metrix	N/A
Brefeldin A	Biolegend	Cat# 420601
Sunflower Seed Oil	Sigma-Aldrich	Cat# S5007
Tamoxifen	Sigma-Aldrich	Cat# T5648
Aphidicolin (Stock 2mg/ml)	Sigma-Aldrich	178273
Decitabine (Stock 10mM)	Sigma-Aldrich	A3656-5mg

DAPI (4',6-diamidino-2-phenylindol, Dihydrochloride)	MolecularProbes, ThermoFisher	Cat# D-1306
Mouse $CD8^+$ T cell enrichment kit	StemCell Technologies	Cat# 19853
Click-it Plus EdU Flow Cytometry Assay Kit	ThermoFisher	Cat #C10634
DynabeadsTM CD8 positive isolation kit	Life Technologies	Cat# 11333D
Intracellular Fix & Perm Buffer set	eBiosciences	Cat# 88-8824-00
FoxP3/Transcription factor staining buffer set	eBiosciences	Cat# 00-5523-00
MACS $CD8^+$ positive selection	Miltenyi Biotec	Cat# 130-116-478
CellTrace™ Violet Cell Proliferation kit	ThermoFisher Scientific	Cat# C34557
Zombie Acqua Fixable Viability Kit	Biolegend	Cat# 423101
DMEM (Dulbecco's Modified Eagle's Medium) 4500 mg/L glucose	10% FCS, 1% penicillin/streptomycin	GIBCO® Invitrogen GmbH, Germany
HBSS (Hanks' Balanced Salt solution) -$CaCl_2$ -$MgCl_2$		GIBCO® Invitrogen GmbH, Germany
Diphtheria Toxin (DT)	Sigma	D0564
EdU	ThermoFisher	Cat #C10634
Dithiothreitol (DTT)	Applichem	Cat # A3668
Experimental Models: Organisms/Strains		
Mouse: C57BL/6 (B6) (CD45.2)	Charles River Laboratories	Strain 027
Mouse: B6.SJL-Ptprc < a > (CD45.1)	Jackson Lab	Strain 002014; RRID: MGI_6200621
Mouse: B6; D2-Tg(TcrLCMV)327Sdz P14 T cell receptor (TCR) transgenic (CD45.2)	Pircher, Freiburg, Germany (Pircher et al., 1989)	RRID: MGI_3810256
Mouse: B6.129-Tm(*Tcf7*)Cle (*Tcf7*$^{-/-}$) (CD45.2)	H. Clevers, Utrecht, Netherlands (Verbeek et al., 1995)	RRID: MGI_4360712
Mouse: Vb5 TCRβ only transgenic (B6, CD45.1)	P. Fink (Seattle, USA) (Dillon et al., 1994)	N/A
Mouse: C.129S2-Stat4tm1Gru/J (CD45.2)	M Lohning (Berlin, Germany) (Kaplan et al., 1996)	N/A
Mouse: B6.Tg(*Tcf7*^{GFP})Whe (*Tcf7*^{GFP}) (CD45.2)	(Utzschneider et al., 2016b)	N/A
Mouse: B6.Gt(Rosa)26Sortm1(CA	J. Joyce, UNIL (Snippert et al., 2010)	N/A

G-Brainbow2.1)Cle (CD45.2)		
Mouse : B6.Tg(*Tcf7*$^{GFP\text{-}iCre}$) Whe (*Tcf7*$^{GFP\text{-}iCre}$) (CD45.2)	(Pais Ferreira et al., 2020)	N/A
Mouse: B6;129S6-Gt(ROSA)26SSortm9(CAG-tdTomato)Hze/J	Huelsken, EPFL (Madisen et al., 2010)	N/A
Mouse: B6.Tg(*Tcf7*$^{DTR\text{-}GFP}$)Whe (*Tcf7*$^{DTR\text{-}GFP}$) (CD45.2)	(Siddiqui et al., 2019)	
Software and Algorithms		
GraphPad Prism v7.0	https://graphpad-prism.software.informer.com/5.0/	RRID:SCR_002798
FlowJo v.10	Tree Star	RRID:SCR_008520
Adobe Illustrator CC2018	Adobe creative cloud	https://www.adobe.com/ch_fr/creativecloud
Visiopharm (v.2019.02)	https://www.visiopharm.com	

3.Results

3.1. Generation and validation of a *Tcf7* guided lineage tracing approach

The transcription factor Tcf1 (encoded by *Tcf7* gene) is expressed homogenously in all naive $CD8^+$ T cells and downregulated in most but not all $CD8^+$ T cells at the effector phase of an immune response to viral infection. Tcf1 is expressed in memory cells and it is essential for the formation of central memory $CD8^+$ T cells (T_{CM}) (Boudousquie et al., 2014; Jeannet et al., 2010; Zhao et al., 2010).

In order to follow the fate of Tcf1-expressing $CD8^+$ T cells during an immune response, the lab generated a genetically modified mouse strain, which allows to stably genetically mark Tcf1-expressing cells. More in detail, the lab designed a BAC (bacterial artificial chromosome) transgenic mouse strain expressing an eGFP-CreERT2 fusion protein (enhanced green fluorescent protein – T2A–Cre recombinase – modified estrogen ligand-binding domain (ERT2)) under the control of the *Tcf7* locus (termed *Tcf7*$^{GFP\text{-}iCre}$) (**Fig 12A**). This mouse line works as a *Tcf7* reporter mouse, as GFP expression reproduces the expression of *Tcf7*. Furthermore, the activity of Cre-ERT2 is controlled by the synthetic agonist tamoxifen (TAM). In the absence of TAM, Cre-ERT2 is sequestered in the cytoplasm. TAM induces the translocation of the Cre-ERT2 into the nucleus, where Cre can mediate the recombination of sequences flanked by loxP sites. Inducible Cre expression (iCre) is thus combined with the conditional expression of a fluorescent protein to track cells, in which recombination has occurred.

We obtained 8 *Tcf7*$^{GFP\text{-}iCre}$ founder mice that had been generated by Cyagen. Initial experiments addressed the expression of GFP (i.e. *Tcf7*$^{GFP\text{-}iCre}$) by naive $CD8^+$ T cells. In most founder mice, GFP expression in T cells was low (5% - 30%) and only 1 female showed a frequency of >90% GFP^+ cells among T cells, but not B cells (**Fig 12B, C**), in agreement with endogenous Tcf1 expression. This female was used to establish a transgenic line.

Tcf7$^{GFP\text{-}iCre}$ mice were crossed with Rosa26 loxP STOP loxP Confetti (*R26*^{Confetti}) knock-in mice (**Fig 12D**). In *R26*^{Confetti} mice, induction of Cre activity led to the stochastic and mutually exclusive, but stable expression of one of four fluorescent proteins (RFP, CFP, YFP and GFP) (**Fig 12D**). For the experiments described below, only RFP expression was followed. Cells expressing very high levels of GFP derived from the induction of recombined *R26*^{Confetti} construct, which appeared only following TAM injection, could be discriminated from the *Tcf7*$^{GFP\text{-}iCre+}$ cells and were removed from the analysis.

To verify the induction of Cre activity, we performed an *in vitro* experiment. Naive $CD8^+$ T cells from *Tcf7*$^{GFP\text{-}iCre}$ *R26*^{Confetti} mice were cultured *in vitro* in the presence of the metabolized 4-hydroxytamoxifen (4-OHT; 1nM to 2μM) for 24 hours (h)-72h. IL2 was added to ensure cell survival (**Fig 12E**). After 24h, RFP induction was low (less than 2% RFP^+ cells). Additionally, a concentration of 4-OHT below 100nM was inefficient to promote RFP induction, even after 72h of culture. On the other hand, cells cultured with 100nM-2μM of 4-OHT efficiently

generated RFP$^+$ cells both at 48h (6-9%) and at 72h (12-16.8%) (**Fig 12E, F**). We concluded that the *Tcf7*$^{GFP\text{-}iCre}$ construct allowed the inducible recombination of the *R26*^{Confetti} locus.

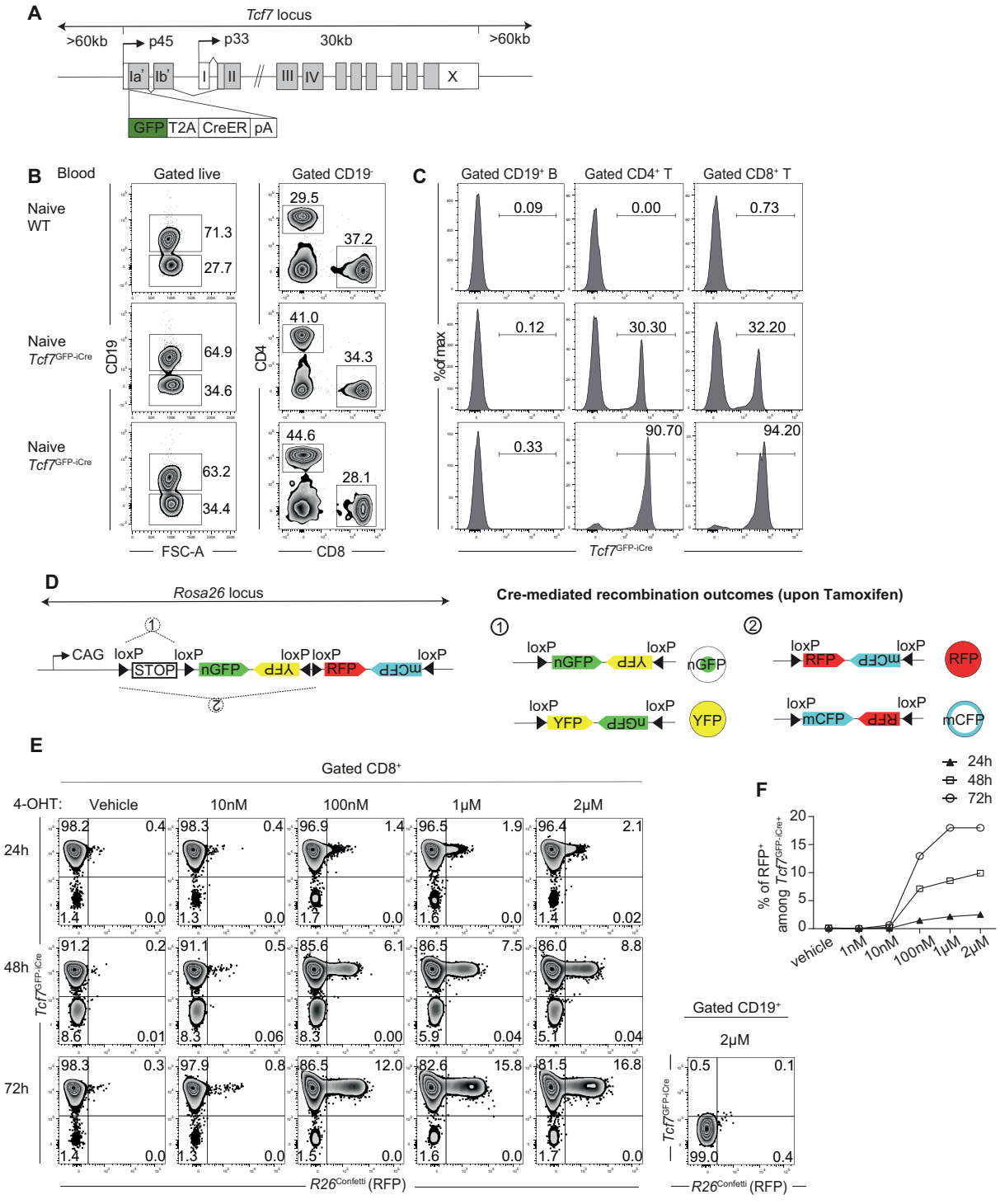

Figure 12 - Generation of a *Tcf7* guided lineage tracing model
(A) Schematic representation of the modified *Tcf7* locus. A green fluorescent protein-T2A-CreERT2 (termed GFP-iCre) fusion gene was inserted into the first exon the *Tcf7* locus on a >150kb BAC, which was then used to generate *Tcf7*$^{GFP\text{-}iCre}$ transgenic mice. **(B, C)** Blood cells from naive wild-type (WT) or *Tcf7*$^{GFP\text{-}iCre}$ transgenic founder mice were analysed for the GFP expression by B cells (CD19$^+$) and T cells (CD4$^+$ and CD8$^+$). Numbers depict the percentage of cells in the respective region. **(D)** Schematic representation of the modified *Rosa26*^{Confetti} locus. The Confetti cassette includes a STOP codon and two tandem invertible DNA segments, flanked by loxP sites in the

opposite orientation. Upon tamoxifen injection, stochastic Cre-mediated recombination leads to the excision and/or inversion of the cassette, switching on the gene expression of one of four possible fluorescent proteins: YFP, RFP, GFP or CFP. Adapted from (Livet et al., 2007). **(E)** Naive *Tcf7*$^{GFP\text{-}iCre}$ *R26*^{Confetti} CD8$^+$ T cells were treated *in vitro* with 4-OHT (4-hydroxytamoxifen) in the presence of IL2 (50 ng/ml) for 24hours (h) to 72h. Treatment of cells *in vitro* with 4-OHT allows the nuclear translocation of the Cre recombinase and thus the cleavage of loxP sites present on the Confetti cassette. **(F)** Frequency of RFP$^+$ cells expression among *Tcf7*$^{GFP\text{-}iCre+}$ cells. **(E, F)** The data shown derive from an experiment with n=1 per group.

We next verified RFP induction *in vivo*. Naive *Tcf7*$^{GFP\text{-}iCre}$ *R26*^{Confetti} mice were injected once with TAM. Five days later, RFP induction *in vivo* was observed in T cells but not in B cells, in agreement with the expression of *Tcf7*. RFP$^+$ cells were observed at comparable rates among CD4$^+$ and CD8$^+$ T cells (4.2% and 6.2%, respectively) (**Fig 13A**). As expected, no RFP$^+$ cells were observed in vehicle control injected mice (**Fig 13A**).

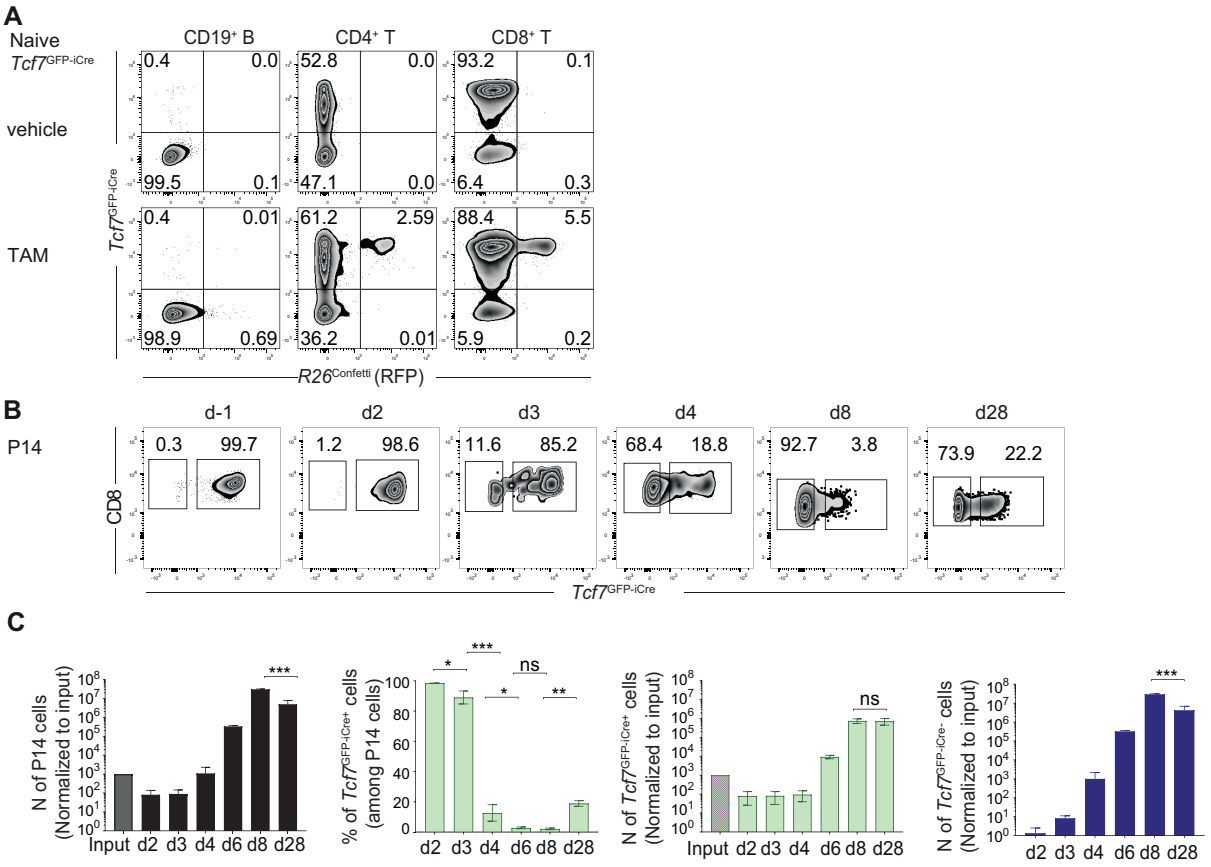

Figure 13 - Induction of RFP in naive *Tcf7*$^{GFP\text{-}iCre}$ *R26*^{Confetti} mice and *Tcf7*$^{GFP\text{-}iCre}$ expression during acute viral infection

(A) Naive *Tcf7*$^{GFP\text{-}iCre}$ *R26*^{Confetti} mice were injected once with Tamoxifen (2mg/ml) and analysed 5 days after. The expression of RFP (*R26*^{Confetti}) was analysed in B cells (CD19$^+$) and T cells (CD4$^+$ and CD8$^+$). **(B)** Expression of *Tcf7*$^{GFP\text{-}iCre}$ during LCMV infection. *Tcf7*$^{GFP\text{-}iCre}$ mice were crossed to P14 mice (specific for LCMV). *Tcf7*$^{GFP\text{-}iCre}$ P14 cells (CD45.2) were transferred into WT mice (CD45.1) followed by infection with LCMV WE. Expression of GFP (*Tcf7*$^{GFP\text{-}iCre}$) in P14 cells was followed over time. **(C)** Abundance of P14 cells over time (left); Frequency of *Tcf7*$^{GFP\text{-}iCre+}$ cells during an acute-resolved infection (centre left); Abundance of *Tcf7*$^{GFP\text{-}iCre+}$ (centre right) and *Tcf7*$^{GFP\text{-}iCre-}$ P14 cells (right) over time. The input number of P14 cells was 0.5-1×10^6 (d2-4 p.i.), 10^5 (d6 p.i.) or 10^4 cells (d8 and d28 p.i.). The output data are normalized to an input of 10^4 cells, whereby it is assumed that take is 10%, i.e. that 10^3 cells responded. **(A)** The data shown derive from 1 experiment with n=1 mouse per group. **(B-C)** The data shown are pooled from 2 independent experiments with total n=2-4 mice per group. Mean ±SD are shown. Statistics are based on One-Way ANOVA with Tukey's test **(C, E)** with *:p<0.05; **:p<0.01; ***:p<0.001; and (ns) p>0.05.

We also addressed the *Tcf7*$^{GFP\text{-}iCre}$ expression *in vivo*. *Tcf7*$^{GFP\text{-}iCre+}$ P14 cells were transferred into WT mice followed by LCMV WE infection, which causes an acute resolved infection, one day later. GFP (*Tcf7*$^{GFP\text{-}iCre}$) expression remained high until day 2 post infection (d2 p.i.), declined thereafter and was increased by d28 p.i. (**Fig 13B, C**). The number of total P14 cells was maximal at d8 p.i., while the frequency of cells expressing GFP (*Tcf7*$^{GFP\text{-}iCre}$) was minimal. At the memory phase (d28 p.i.), the number of P14 cells had decreased due to the contraction of *Tcf7*$^{GFP\text{-}iCre-}$ cells, while the absolute number of *Tcf7*$^{GFP\text{-}iCre+}$ cells remained unchanged (**Fig 13C**).

Thus, *Tcf7*$^{GFP\text{-}iCre}$ construct underwent the expected expression changes during the immune response to LCMV infection, in agreement with (Pais Ferreira et al., 2020), using a distinct *Tcf7*^{GFP} reporter.

3.2. Fate of *Tcf7*$^{+}$ CD8^{+} T cells during acute viral infection

3.2.1. Central memory CD8^{+} T cells derive from *Tcf7*$^{+}$ CD8^{+} T cells present at the peak of effector response

At the peak of the primary immune response to LCMV infection, we observed rare *Tcf7*$^{GFP\text{-}iCre+}$ CD8^{+} T cells (**Fig 13B, C**). We next addressed the fate of these cells (**Fig 14A**). *Tcf7*$^{GFP\text{-}iCre}$ *R26*^{Confetti} mice were infected with LCMV WE. As a control, we also infected mice lacking the *Tcf7*$^{GFP\text{-}iCre}$ allele (only *R26*^{Confetti}) (**Fig 14B**). At the peak of CD8^{+} T cell response, most virus-specific CD8^{+} T cells (H-2D^{b} gp33-tetramer^{+} CD8^{+} T cells, simplified here as gp33^{+} cells) had downregulated *Tcf7*$^{GFP\text{-}iCre}$ compared to naive CD8^{+} T cells and only a small subset of cells (1-2%) retained GFP expression (**Fig 14C**).

To ensure that the *Tcf7*$^{GFP\text{-}iCre}$ construct properly detected Tcf1^{+} cells, we sorted gp33^{+} cells expressing and lacking *Tcf7*$^{GFP\text{-}iCre}$ and stained for intranuclear Tcf1 protein. All gp33^{+} *Tcf7*$^{GFP\text{-}iCre+}$ cells expressed high levels of Tcf1 protein, while most gp33^{+} *Tcf7*$^{GFP\text{-}iCre-}$ cells lacked Tcf1 protein or expressed low levels (**Fig 14D**). Thus, the *Tcf7*$^{GFP\text{-}iCre}$ construct properly tracked Tcf1 expressing cells during viral infection.

Mice were then injected with TAM (1mg/ml for 5 consecutive days), starting at d8 p.i. (**Fig 14A**). Two days after the last injection (d14 p.i.), gp33^{+} cells contained a small population of RFP^{+} cells (0.38% of gp33^{+}). RFP^{+} cells were not detected in the absence of TAM injection or in TAM-administered mice that harboured only a *R26*^{Confetti} and lacked the *Tcf7*$^{GFP\text{-}iCre}$ allele (**Fig 14E, F, G**).

The vast majority of d14 gp33^{+} RFP^{+} cells were *Tcf7*$^{GFP\text{-}iCre+}$ (expressing intermediate levels of GFP from the *Tcf7*$^{GFP\text{-}iCre}$ allele) (**Fig 14E, H, I**). The GFP^{hi} population derived from the recombined *R26*^{Confetti} allele and was removed from the analysis, as discussed above. These data thus demonstrated the selective labelling of *Tcf7*$^{GFP\text{-}iCre+}$ cells and the absence of differentiation into *Tcf7*$^{GFP\text{-}iCre-}$ cells between d8 and d14 p.i.. Further, most d14 gp33^{+} RFP^{+}

Tcf7$^{GFP\text{-}iCre+}$ cells lacked the effector marker KLRG1 and expressed the central memory marker CD62L (**Fig 14J**). At the memory phase (d28 p.i.), gp33^{+} RFP^{+} cells were still uniformly *Tcf7*$^{GFP\text{-}iCre+}$ and most cells had a KLRG1^{-} CD62L^{+} T_{CM} phenotype (**Fig 14E, J**). Interestingly, the abundance of gp33^{+} RFP^{+} *Tcf7*$^{GFP\text{-}iCre+}$ cells did not significantly change between d14 and d28 p.i. (<2 fold decrease) (**Fig 14I**). Corresponding data were obtained for polyclonal CD8^{+} T cells specific for the np396^{+} epitope (**Fig 14K**). These data suggested that d8 *Tcf7*$^{+}$ cells gave quantitatively rise to T_{CM}.

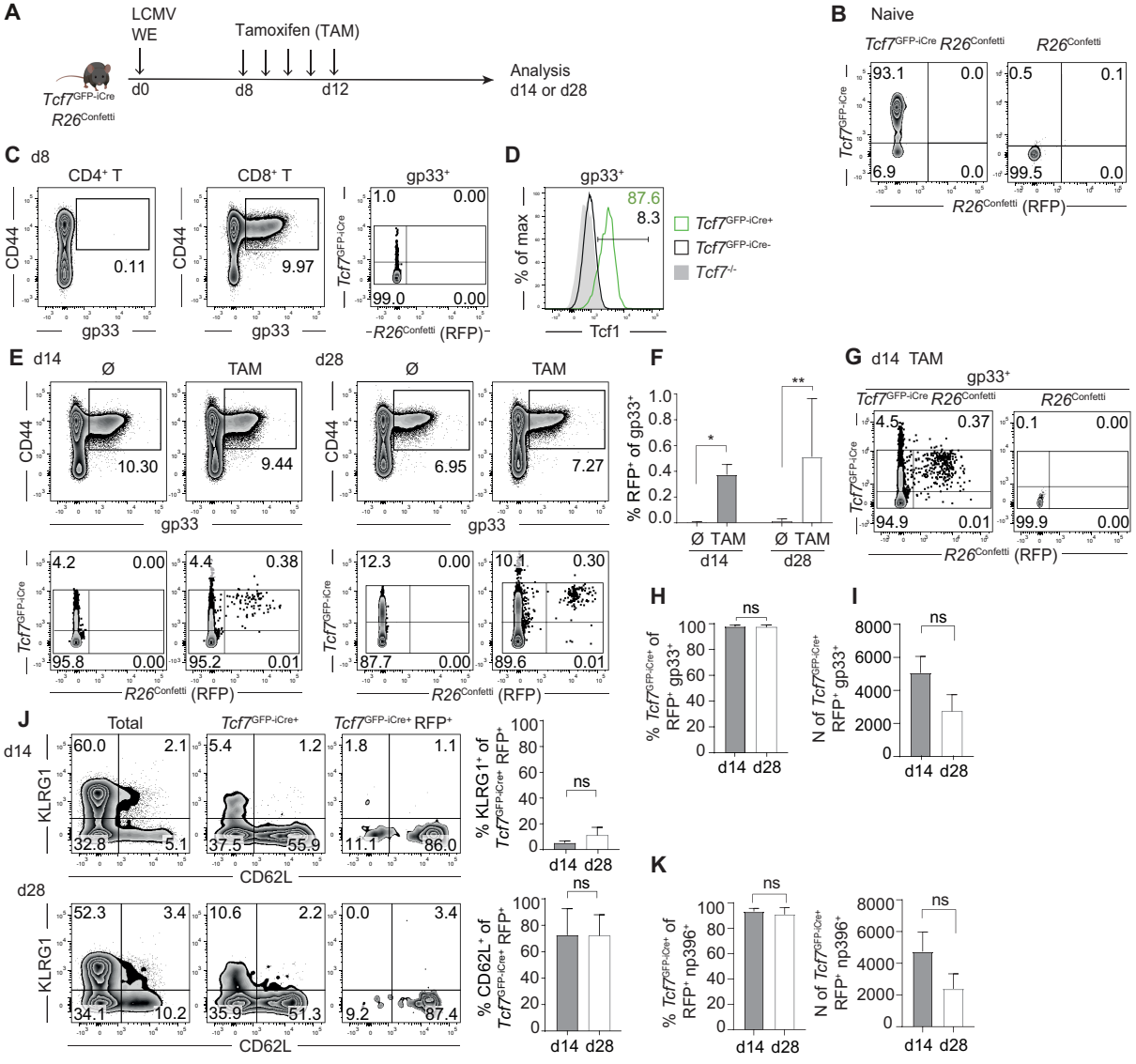

Figure 14 - Fate of *Tcf7*$^{GFP\text{-}iCre+}$ cells present at the peak of the primary response to LCMV infection
(A) Schematic representation of the experimental set-up. *Tcf7*$^{GFP\text{-}iCre}$ *R26*^{Confetti} mice (CD45.2) were infected with LCMV WE and either left untreated (Ø) or injected with 1 mg/ml Tamoxifen (TAM) starting on day 8 post-infection (d8 p.i.), daily for 5 consecutive days. **(B)** CD8^{+} T cells from naive *Tcf7*$^{GFP\text{-}iCre}$ *R26*^{Confetti} (left) or *R26*^{Confetti} mice (right) were analysed for the expression of GFP (*Tcf7*$^{GFP\text{-}iCre}$) and RFP (*R26*^{Confetti}). **(C)** At d8 p.i. (prior to TAM treatment) gated CD4^{+} and CD8^{+} T cells were stained with H-2D^{b} gp33 tetramer (gp33) and gp33^{+} CD44^{+} CD8^{+} T expressing or lacking *Tcf7*$^{GFP\text{-}iCre}$ were flow sorted. **(D)** The flow sorted *Tcf7*$^{GFP\text{-}iCre+}$ (green) and *Tcf7*$^{GFP\text{-}iCre-}$ (black) gp33^{+} CD44^{+} CD8^{+} T cells were analysed for Tcf1 protein expression compared to *Tcf7*$^{-/-}$ CD8^{+} T cells (grey fill). Numbers indicate the percentage of cells in the respective gate. **(E)** Following TAM infection, gated gp33^{+} CD44^{+} CD8^{+} T cells were analysed for the expression of GFP (*Tcf7*$^{GFP\text{-}iCre}$) and RFP (*R26*^{Confetti}) on d14 and d28 p.i. **(F)**

Fraction of RFP$^+$ cells among gp33$^+$ cells on d14 and d28 p.i. **(G)** Expression of GFP (*Tcf7*$^{GFP\text{-}iCre}$) and RFP (*R26*^{Confetti}) on gp33$^+$ CD44$^+$ CD8$^+$ T cells on d14 p.i. in TAM-treated *Tcf7*$^{GFP\text{-}iCre}$ *R26*^{Confetti} (left) or *R26*^{Confetti} mice (right) **(H)** Fraction of *Tcf7*$^{GFP\text{-}iCre+}$ RFP$^+$ cells among RFP$^+$ gp33$^+$ cells. **(I)** Abundance of gp33$^+$ *Tcf7*$^{GFP\text{-}iCre+}$ RFP$^+$ cells at d14 and d28 p.i. **(J)** Expression of KLRG1 and CD62L by gp33$^+$ cells (left), by *Tcf7*$^{GFP\text{-}iCre+}$ gp33$^+$ cells (centre) and by *Tcf7*$^{GFP\text{-}iCre+}$ RFP$^+$ gp33$^+$ cells (right) on d14 (top) and d28 pi. (bottom). Bar graphs on the right depict the frequency of KLRG1$^+$ (top) and CD62L$^+$ cells (bottom) among *Tcf7*$^{GFP\text{-}iCre+}$ RFP$^+$ cells. **(K)** Bar graphs show the fraction of *Tcf7*$^{GFP\text{-}iCre+}$ RFP$^+$ cells among np396$^+$ RFP$^+$ cells (left) and abundance of np396$^+$ *Tcf7*$^{GFP\text{-}iCre+}$ RFP$^+$ cells (right) at d14 and d28 p.i. **(A-K)** The data shown are pooled from 3 independent experiments with total n=5-6 mice per group. Mean ±SD are shown. Statistics are based on Non-paired two-tailed Student's test (A-K) with *:p<0.05; **:p<0.01; ***:p<0.001; and (ns) p>0.05.

To extend these data, we similarly addressed the fate of monoclonal d8 *Tcf7*$^+$ CD8$^+$ T cells. To this end, the *Tcf7*$^{GFP\text{-}iCre}$ *R26*^{Confetti} mouse line was crossed to a P14 T cell receptor (TCR) transgenic mouse line, in which all CD8$^+$ T cells express a TCR specific for the LCMV-derived gp33 epitope (**Fig 15A**). Naive *Tcf7*$^{GFP\text{-}iCre}$ *R26*^{Confetti} P14 cells were transferred into wild-type (WT) or *Tcf7*$^{GFP\text{-}iCre}$ recipients. The latter prevented the rejection of *Tcf7*$^{GFP\text{-}iCre}$ *R26*^{Confetti} P14 cells during the early memory phase (not shown). Mice were then infected with LCMV WE one day later (**Fig 15A**).

At d8 p.i., *Tcf7*$^{GFP\text{-}iCre}$ expression was downregulated in most P14 cells (**Fig 15B**). Flow sorted d8 *Tcf7*$^{GFP\text{-}iCre+}$ P14 cells expressed homogeneously high levels of Tcf1 protein, while d8 *Tcf7*$^{GFP\text{-}iCre-}$ P14 cells mostly lacked Tcf1 protein or expressed low levels (**Fig 15B**). Thus, the *Tcf7*$^{GFP\text{-}iCre}$ construct faithfully identified P14 cells expressing high levels of Tcf1 protein.

Two days after the last injection (d14 p.i.), P14 cells contained a small population of RFP$^+$ cells (0.4-0.6% of P14 cells) (**Fig 15C, D, E**). RFP$^+$ cells were not detected in naive mice or in infected mice in the absence of TAM, or in TAM-administered mice that harboured only the *R26*^{Confetti} allele (**Fig 15C**).

The vast majority of d14 RFP$^+$ P14 cells were *Tcf7*$^{GFP\text{-}iCre+}$, similar to the results obtained during the polyclonal response (**Fig 15E, F**). Along on the same line, at the memory phase, most *Tcf7*$^{GFP\text{-}iCre+}$ cells had a KLRG1$^-$ CD62L$^+$ central phenotype and differentiation into *Tcf7*$^{GFP\text{-}iCre-}$ cells was not observed (**Fig 15G**). The abundance of the RFP$^+$ *Tcf7*$^{GFP\text{-}iCre+}$ P14 cells was maintained from d14 to d28 p.i. (**Fig 15H**). These data thus identified a subset of effector cells that gave quantitatively rise to T_{CM}. This effector cell subset could thus be regarded as a T_{CM} precursor (T_{pCM}).

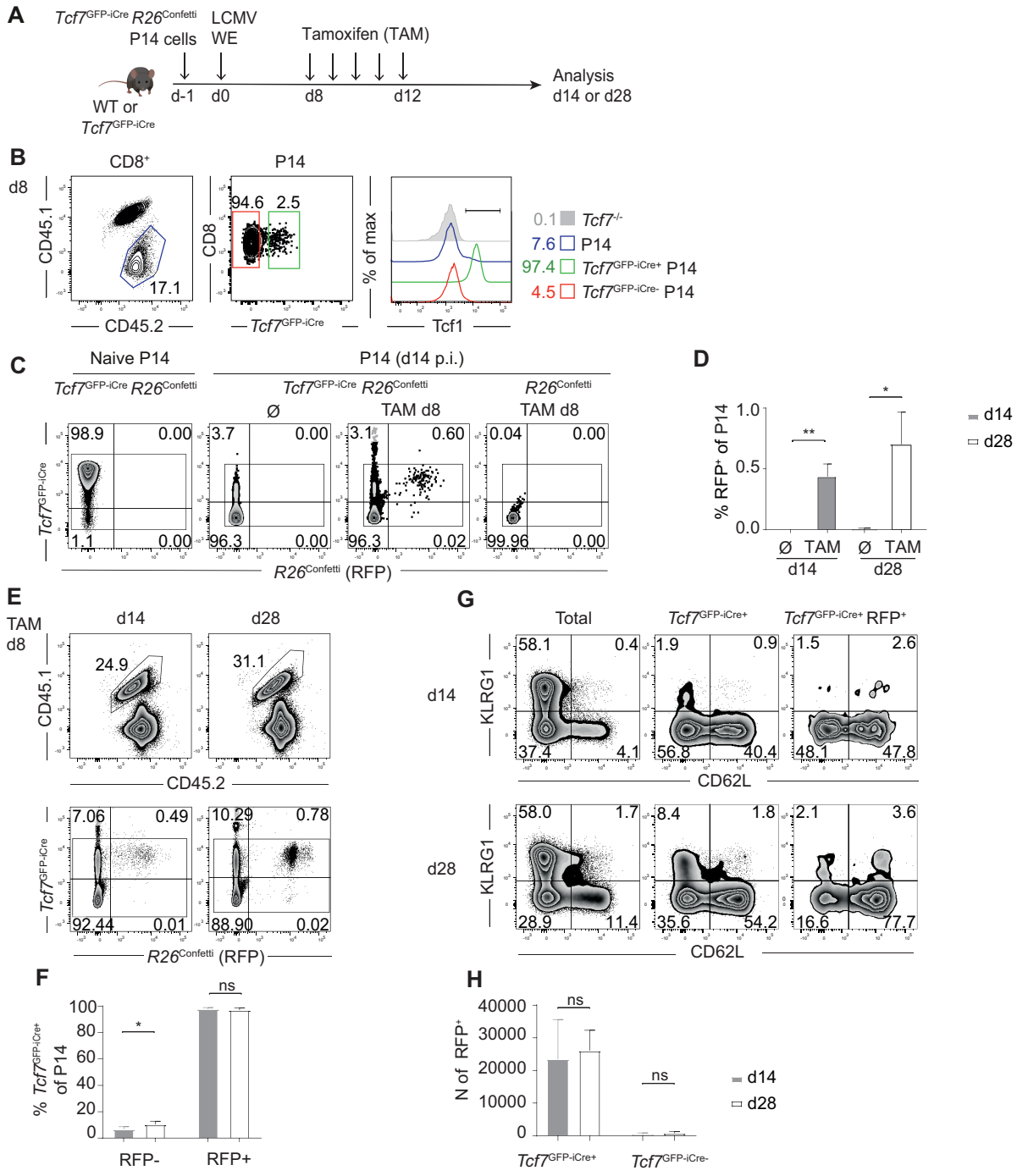

Figure 15 - Fate of monoclonal *Tcf7*$^{GFP\text{-}iCre+}$ P14 cells present at the peak of the primary response to LCMV infection

(A) Schematic representation of the experimental set-up. *Tcf7*$^{GFP\text{-}iCre}$ *R26*^{Confetti} P14 cells (CD45.2 or CD45.1/.2) were transferred into WT (CD45.1/.2 or CD45.2) or *Tcf7*$^{GFP\text{-}iCre+}$ (CD45.2) recipients and infected one day later with LCMV WE. Recipients were left untreated (Ø) or injected daily with 1mg/ml Tamoxifen (TAM) starting on d8 p.i., daily for 5 consecutive days. **(B)** At d8 p.i. (prior to TAM treatment), *Tcf7*$^{GFP\text{-}iCre+}$ and *Tcf7*$^{GFP\text{-}iCre-}$ P14 cells were sorted and stained for Tcf1 protein. The histogram overlay shows Tcf1 protein expression of total P14 cells (blue), and of flow sorted *Tcf7*$^{GFP\text{-}iCre+}$ (green) and *Tcf7*$^{GFP\text{-}iCre-}$ (red) P14 cells compared to *Tcf7*$^{-/-}$ CD8^{+} T cells (grey fill). Numbers indicate the percentage of cells in the respective gate. **(C)** GFP (*Tcf7*$^{GFP\text{-}iCre}$) and RFP (*R26*^{Confetti}) expression was analysed in naive *Tcf7*$^{GFP\text{-}iCre}$ *R26*^{Confetti} P14 cells (left) or at d14 p.i. by *Tcf7*$^{GFP\text{-}iCre}$ *R26*^{Confetti} (centre) or *R26*^{Confetti} P14 cells (right) without (Ø) or with TAM treatment (TAM). **(D)** Bar graphs show the percentage of RFP^{+} cells among P14 cells at d14 and d28 p.i. without (Ø) or with TAM treatment (TAM d8). **(E)** Gated P14 cells were analysed for the presence of GFP (*Tcf7*$^{GFP\text{-}iCre}$) and RFP (*R26*^{Confetti}) cells at d14 and d28 p.i. **(F)** Frequency of *Tcf7*$^{GFP\text{-}iCre+}$ cells among RFP^{-} and RFP^{+} P14 cells at d14 and d28 p.i. **(G)** Total P14 cells (left), *Tcf7*$^{GFP\text{-}iCre+}$ P14

cells (centre) or *Tcf7*$^{GFP\text{-}iCre+}$ RFP+ P14 cells (right) were analysed for the expression of KLRG1 versus CD62L at d14 (top) or d28p.i. (bottom). **(H)** Abundance of RFP^{+} *Tcf7*$^{GFP\text{-}iCre+}$ and RFP^{+} *Tcf7*$^{GFP\text{-}iCre-}$ P14 cells at d14 and d28 p.i. **(B-H)** The data shown are pooled from 2 independent experiments with total n=5 mice per group. Mean ±SD are shown. Statistics are based on Non-paired two-tailed Student's test **(D-H)** with *:p<0.05; **:p<0.01; ***:p<0.001; and (ns) p>0.05.

3.2.2. *Tcf7*$^{+}$ CD8^{+} T cells present at day 4 of the primary infection yield both central and effector memory CD8^{+} T cells but not terminal effector cells

The above data showed that d8 *Tcf7*$^{+}$ CD8^{+} T cells gave rise to T_{CM} cells but not effector memory cells (T_{EM}). The data thus implied that T_{EM} derived from a *Tcf7*$^{+}$ cell present at an earlier stage of the primary response. To investigate the timing of T_{CM} vs T_{EM} separation, we started the labelling of *Tcf7*$^{GFP\text{-}iCre+}$ cells at d4 p.i. (**Fig 16A**).

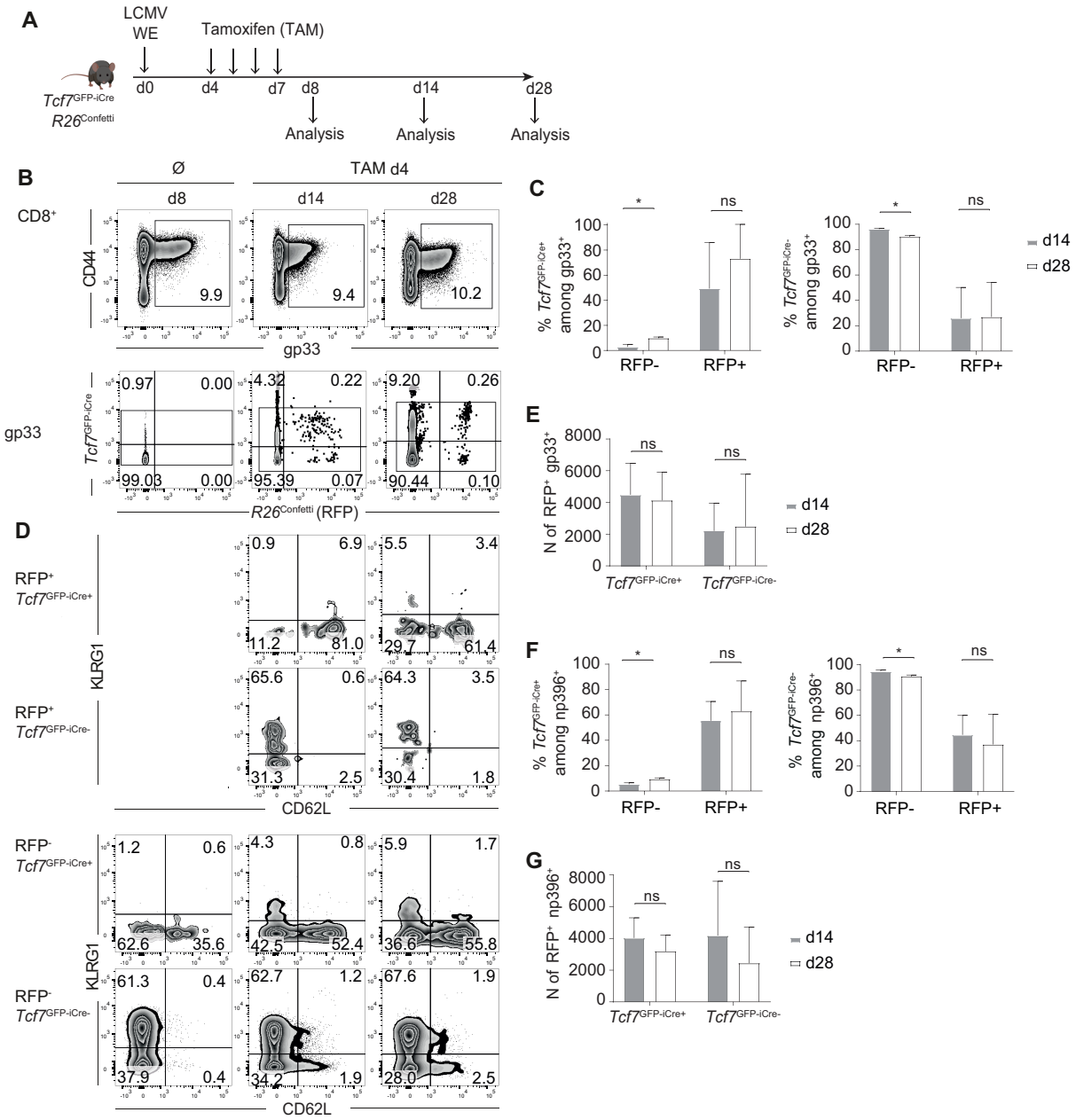

Figure 16 - Fate of *Tcf7*$^{GFP\text{-}iCre+}$ cells present at day 4 of the primary response to LCMV infection

(A) Schematic representation of the experimental set-up. *Tcf7*$^{GFP\text{-}iCre}$ *R26*^{Confetti} mice (CD45.2) were infected with LCMV WE and left untreated (Ø) or were injected with 1mg/ml Tamoxifen (TAM) starting on d4 p.i., daily for 4 consecutive days. **(B)** Gated gp33^{+} CD44^{+} CD8^{+} T cells were analysed for the expression of GFP (*Tcf7*$^{GFP\text{-}iCre}$) and RFP (*R26*^{Confetti}) in untreated mice at d8 p.i. (left), or in TAM treated mice at d14 (centre) or d28 (right) p.i.. **(C)** Fraction of *Tcf7*$^{GFP\text{-}iCre+}$ (left) and *Tcf7*$^{GFP\text{-}iCre-}$ cells (right) among RFP^{-} and RFP^{+} gp33^{+} subsets at d14 or d28 p.i.. **(D)** Expression of KLRG1 and CD62L by the indicated subsets of gp33^{+} cells on d8 (left), d14 (centre) and d28 pi. (right). **(E)** Abundance of gp33^{+} *Tcf7*$^{GFP\text{-}iCre+}$ RFP^{+} cells at d14 and d28 p.i. **(F)** Fraction of *Tcf7*$^{GFP\text{-}iCre+}$ (left) and *Tcf7*$^{GFP\text{-}iCre-}$ (right) among RFP^{-} and RFP^{+} np396^{+} cells at d14 and d28 p.i.. **(G)** Abundance of *Tcf7*$^{GFP\text{-}iCre+}$ RFP^{+} np396^{+} cells at d14 and d28 p.i. **(B-G)** The data shown are pooled from 2 independent experiments with total n=5 mice per group. Mean ±SD are shown. Statistics are based on Non-paired two-tailed Student's test (D-H) with *:p<0.05; **:p<0.01; ***:p<0.001; and (ns) p>0.05.

On d14 p.i., we again observed gp33^{+} RFP^{+} CD8^{+} T cells that maintained *Tcf7*$^{GFP\text{-}iCre+}$ expression (**Fig 16B, C**). These cells lacked KLRG1 and were enriched for CD62L expression. In addition, we also observed a gp33^{+} RFP^{+} population that lacked *Tcf7*$^{GFP\text{-}iCre}$ expression. Most of these cells expressed KLRG1 and lacked CD62L expression (**Fig 16D**). Corresponding populations of *Tcf7*$^{GFP\text{-}iCre+}$ and *Tcf7*$^{GFP\text{-}iCre-}$ gp33^{+} RFP^{+} were observed at d28 p.i. (**Fig 16B-D**). The abundance of RFP^{+} *Tcf7*$^{GFP\text{-}iCre+}$ cells did not change between d14 and d28 p.i. (**Fig 16E**), indicating that also d4 *Tcf7*$^{+}$ cells quantitatively yielded T_{CM}. Moreover, the presence of RFP^{+} *Tcf7*$^{GFP\text{-}iCre-}$ cells suggested that d4 *Tcf7*$^{+}$ cells also yielded T_{EM}. The fact that the abundance of gp33^{+} RFP^{+} *Tcf7*$^{GFP\text{-}iCre-}$ cells did not change between d14 and d28 p.i., suggested that d4 *Tcf7*$^{+}$ cells did not yield terminal effector cells (T_{EF}). Corresponding data were obtained for polyclonal np396^{+} CD8^{+} T cells (**Fig 16F, G**) and for monoclonal P14 cells (see next chapter). Collectively, these data showed that d4 *Tcf7*$^{+}$ cells gave quantitatively rise to T_{CM} and T_{EM} but not to T_{EF}.

3.2.3. Terminal effector cells derive from *Tcf7*$^{+}$ CD8^{+} T cells present at day 1 or 2 following infection

So far, the lineage tracing of *Tcf7*$^{GFP\text{-}iCre+}$ cells showed that d4 *Tcf7*$^{+}$ cells yielded T_{CM} and T_{EM} but not T_{EF}. To determine at what time point *Tcf7*$^{+}$ cells were programmed to yield T_{EF} cells, we transferred *Tcf7*$^{GFP\text{-}iCre}$ *R26*^{Confetti} P14 cells (CD45.1/.2) into WT (CD45.1 or CD45.2) or *Tcf7*$^{GFP\text{-}iCre}$ (CD45.2) recipient mice, which were infected with LCMV WE one day later. Starting at d1, d2, d3 or d4 p.i., mice received TAM injections on 3 consecutive days before their analysis at the peak of effector response (d8 p.i.) or at the memory phase (d28 p.i.) (**Fig 17A**).

At d8 p.i., the frequency and the abundance of RFP^{+} *Tcf7*$^{GFP\text{-}iCre+}$ P14 cells were relatively constant independent of when labelling was started (**Fig 17B, C**), although roughly 2-fold more RFP^{+} *Tcf7*$^{GFP\text{-}iCre+}$ cells were observed when labelling was started at d1 p.i.. This difference may result from an increased labelling efficiency at d1 p.i. due to higher *Tcf7*$^{GFP\text{-}iCre}$ levels. Irrespectively, the abundance of RFP^{+} *Tcf7*$^{GFP\text{-}iCre+}$ cells at d8 and d28 p.i. was the same for any given time-point (**Fig 17C**). Further, RFP^{+} *Tcf7*$^{GFP\text{-}iCre+}$ P14 cells lacked KLRG1 and many cells expressed CD62L, again independent of when labelling started (**Fig 17D**). Together,

these data suggested that *Tcf7*$^{+}$ cells present during all time-points of the primary response quantitatively yielded T_{CM}.

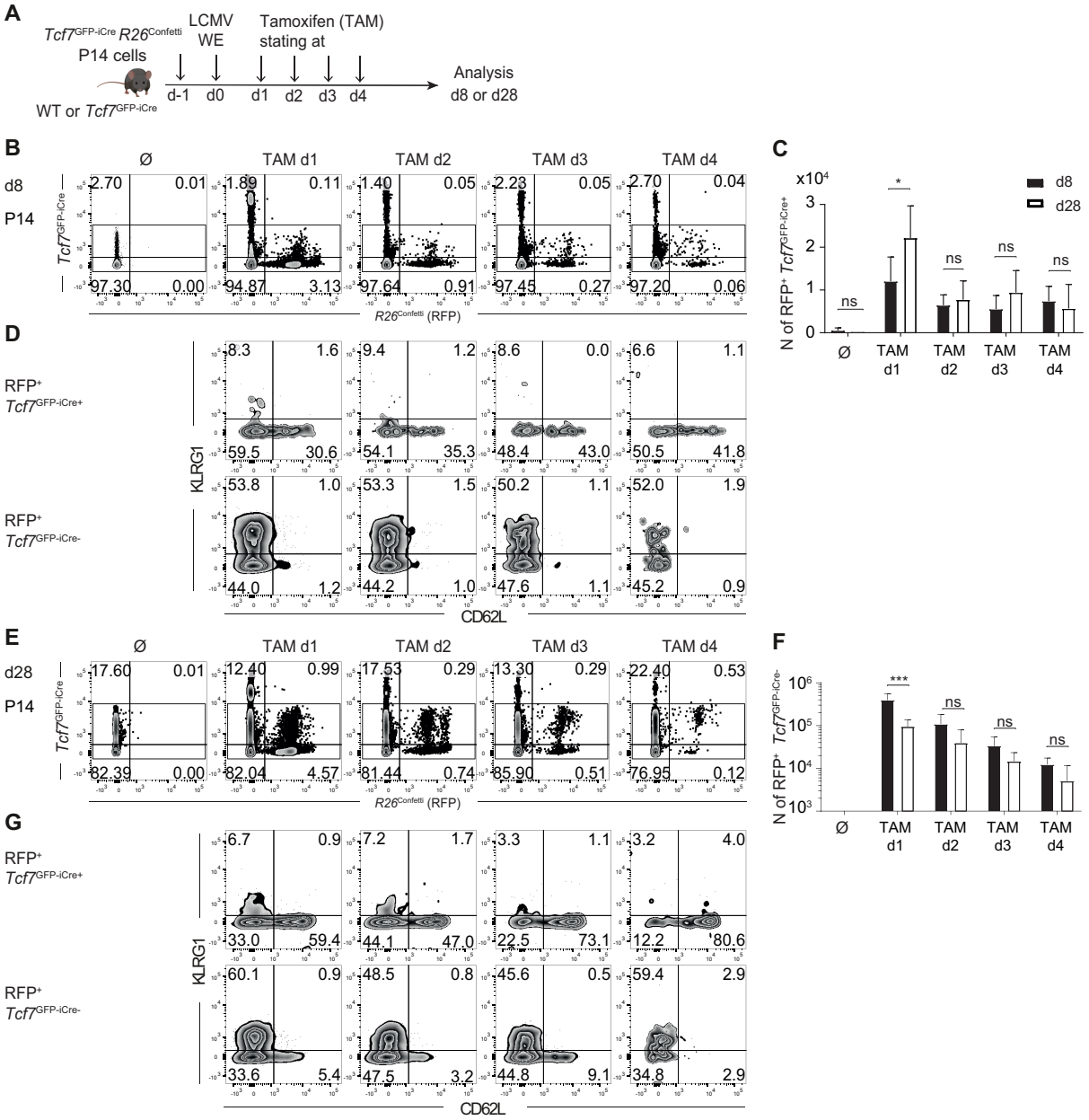

Figure 17 - Fate of *Tcf7*$^{GFP\text{-}iCre+}$ P14 cells present at day 1 through day 4 of the primary response to LCMV infection

(A) Schematic representation of the experimental set-up. *Tcf7*$^{GFP\text{-}iCre}$ *R26*^{Confetti} P14 cells (CD45.1/.2) were transferred into WT (CD45.1/.2 or CD45.2) or *Tcf7*$^{GFP\text{-}iCre+}$ (CD45.2) recipients and infected one day later with LCMV WE. Recipients were left untreated (Ø) or injected with 1mg/ml Tamoxifen (TAM) starting on d1, d2, d3 or d4 p.i., daily for 3 consecutive days. **(B)** GFP (*Tcf7*$^{GFP\text{-}iCre}$) and RFP (*R26*^{Confetti}) expression by P14 cells was analysed at d8 p.i.. The beginning of TAM-treatment is indicated as e.g. TAM d1. **(C)** Abundance of RFP^{+} *Tcf7*$^{GFP\text{-}iCre+}$ P14 cells at d8 and d28 p.i. **(D)** RFP^{+} *Tcf7*$^{GFP\text{-}iCre+}$ (top) or *Tcf7*$^{GFP\text{-}iCre-}$ P14 cells (bottom) were analysed for the expression of KLRG1 versus CD62L at d8 p.i.. **(E)** GFP (*Tcf7*$^{GFP\text{-}iCre}$) and RFP (*R26*^{Confetti}) expression by P14 cells was analysed at d28 p.i.. **(F)** Abundance of RFP^{+} *Tcf7*$^{GFP\text{-}iCre-}$ P14 cells at d8 and d28 p.i. **(G)** RFP^{+} *Tcf7*$^{GFP\text{-}iCre+}$ (top) or RFP^{+} *Tcf7*$^{GFP\text{-}iCre-}$ P14 cells (bottom) were analysed for the expression of KLRG1 versus CD62L at d28 p.i.. **(B-G)** The data shown are pooled from 2-3 independent experiments with n=9 (d8) or n=6 (d28) mice per group. Mean ±SD are shown. Statistics are based on Non-paired two-tailed Student's test **(C, F)** with *:p<0.05; **:p<0.01; ***:p<0.001; and (ns) p>0.05.

On the other hand, the frequency and the abundance of RFP$^+$ *Tcf7*$^{GFP\text{-}iCre\text{-}}$ P14 cells present at d8 p.i. was high when labelling was started at d1 but sharply decreased thereafter (**Fig 17E, F**). Furthermore, the abundance of RFP$^+$ *Tcf7*$^{GFP\text{-}iCre\text{-}}$ cells at d8 p.i. was significantly higher than d28 p.i., when labelling was started at d1, was still elevated when labelling was started at d2 (p=0.067), but was not different when labelling was started at d3 or d4 p.i. (**Fig 17F**). RFP$^+$ *Tcf7*$^{GFP\text{-}iCre\text{-}}$ P14 cells lacked CD62L and most expressed KLRG1 (**Fig 17G**), independent of when labelling was started. These data suggested that only *Tcf7*$^+$ cells present at d1 and d2 p.i. were able to yield T_{EF} cells. Furthermore, *Tcf7*$^+$ cells present during all time-points (d1 to d4) yielded T_{EM} and T_{CM}.

A short coming of the above experiments was that the labelling of *R26*^{Confetti} cells was inefficient and required TAM injection over several days i.e. when TAM injection was started at d1, labelling could actually occur anytime between d1 and d4 p.i.. To improve the labelling efficiency, we switched to a *R26*^{Tomato} reporter strain, which generates uniquely Tomato$^+$ (Tom) cells after TAM-induced recombination (**Fig 18A**). Indeed, *Tcf7*$^{GFP\text{-}iCre}$ *R26*^{Tomato} cells could be efficiently labelled *in vivo* using a single TAM injection at a 10-fold reduced dose (0.1mg) (not shown). Since the *in vivo* half-life of 1mg of TAM is about 16-24h (Wilson et al., 2014), labelling is likely restricted to around 24h post-injection.

As above, we transferred *Tcf7*$^{GFP\text{-}iCre}$ *R26*^{Tomato} P14 cells (CD45.1/.2) into WT or *Tcf7*$^{GFP\text{-}iCre}$ (CD45.2) recipient mice, followed by infection with LCMV WE one day later. Starting at d1, d2, d3 or d4 p.i., mice received a single TAM injection before analysis at d8 and d28 p.i. (**Fig 18B**). At d8 p.i., the frequency and the abundance of Tom$^+$ *Tcf7*$^{GFP\text{-}iCre+}$ P14 cells were relatively constant independent of when labelling started, although their abundance gradually decreased when labelling was started later (**Fig 18C, D**), similar to the effect seen above. Importantly, however, the abundance of Tom$^+$ *Tcf7*$^{GFP\text{-}iCre+}$ P14 cells at d8 and d28 p.i. was the same independent of when the labelling of *Tcf7*$^{GFP\text{-}iCre+}$ cells was started (**Fig 18D**). Further, the Tom$^+$ *Tcf7*$^{GFP\text{-}iCre+}$ P14 cells lacked KLRG1 and many expressed CD62L, independent of when labelling started (**Fig 18E**). These data confirmed that *Tcf7*$^+$ cells present at all time points of the primary response quantitatively yielded T_{CM}.

The frequency and the abundance of Tom$^+$ *Tcf7*$^{GFP\text{-}iCre\text{-}}$ P14 cells present at d8 p.i. was again high when labelling was started at d1 and d2 and sharply decreased when labelling started later (**Fig 18D**). Indeed, the abundance of Tom$^+$ *Tcf7*$^{GFP\text{-}iCre\text{-}}$ P14 cells at d8 was significantly higher than at d28 p.i. when labelling was started at d1 and d2 p.i., but was not different when starting at d3 or d4 p.i. (**Fig 18D, F**). Finally, the Tom$^+$ *Tcf7*$^{GFP\text{-}iCre\text{-}}$ P14 cells lacked CD62L and most expressed KLRG1, independent of when labelling started (**Fig 18G**). Thus, using a restricted labelling window confirmed that short-lived effector cells were generated transiently from *Tcf7*$^+$ cells that were present at d1 and d2 p.i.. Together, we found that CD8$^+$ T cells were programmed very early and transiently to differentiate into effector cells in their natural environment.

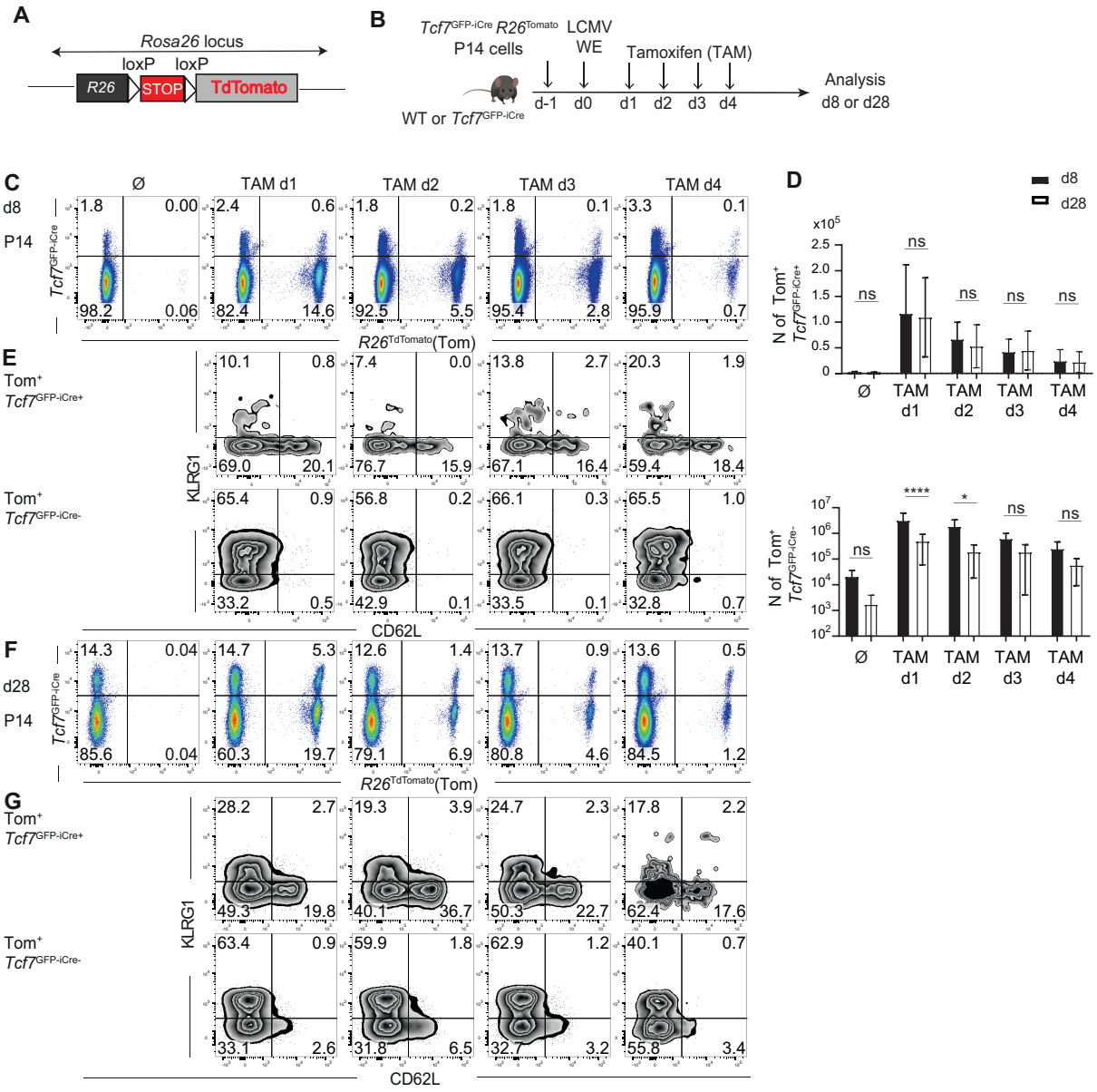

Figure 18 - Fate of *Tcf7*$^{GFP\text{-}iCre+}$ P14 cells present at day 1 through day 4 of the primary response to LCMV infection as determined using restricted labelling of *Tcf7*$^{GFP\text{-}iCre+}$ P14 cells

(A) Schematic representation of the modified *Rosa26*^{Tomato} locus. Cre-mediated excision of the STOP codon allows the expression of Tomato (Tom). **(B)** Schematic representation of the experimental set-up. *Tcf7*$^{GFP\text{-}iCre}$ *R26*^{Tomato} P14 cells (CD45.1/.2) were transferred into WT or *Tcf7*$^{GFP\text{-}iCre+}$ (CD45.2) recipients and infected one day later with LCMV WE. Recipients were left untreated (Ø) or injected with a single dose of 0.1mg/ml Tamoxifen (TAM) on d1, d2, d3 or d4 p.i.. **(C)** GFP (*Tcf7*$^{GFP\text{-}iCre}$) and Tom (*R26*^{Tomato}) expression by P14 cells was analysed at d8 p.i.. **(D)** Abundance of Tom^{+} *Tcf7*$^{GFP\text{-}iCre+}$ and Tom^{+} *Tcf7*$^{GFP\text{-}iCre-}$ P14 cells at d8 and d28 p.i. **(E)** Tom^{+} *Tcf7*$^{GFP\text{-}iCre+}$ (top) and Tom^{+} *Tcf7*$^{GFP\text{-}iCre-}$ P14 cells (bottom) were analysed for the expression of KLRG1 versus CD62L at d8 p.i.. **(F)** GFP (*Tcf7*$^{GFP\text{-}iCre}$) and Tom (*R26*^{Tomato}) expression by P14 cells was analysed at d28 p.i. **(G)** Tom^{+} *Tcf7*$^{GFP\text{-}iCre+}$ (top) and Tom^{+} *Tcf7*$^{GFP\text{-}iCre-}$ P14 cells (bottom) were analysed for the expression of KLRG1 versus CD62L at d28 p.i.. **(C-G)** The data shown are pooled from 3 independent experiments with total n=7 (d8) or n=9 (d28) mice per group and per time-point. Mean ±SD are shown. Statistics are based on Non-paired two-tailed Student's test **(C, F)** with *:p<0.05; **:p<0.01; ***:p<0.001; and (ns) p>0.05.

3.2.4. Tissue-resident memory cells mainly derive from peripheral *Tcf7*$^{+}$ CD8^{+} T cells present at day 2 post infection

The increased efficiency of Tomato induction further allowed us to trace tissue-resident cells (**Fig 19A**). Initially, we addressed the presence of tissue-resident RFP^{+} cells in non-hematopoietic tissues (lung and gut). For this purpose, we injected CD8α antibody conjugated with a fluorochrome i.v., 4 minutes before sacrificing the mouse. This excluded CD8^{+} T cells in the circulation from the analysis of cells isolated from tissues. Indeed, essentially all CD8^{+} T cells isolated from the gut (intestinal intraepithelial lymphocytes - IELs) lacked CD8α staining and were thus considered tissue-resident cells (not shown).

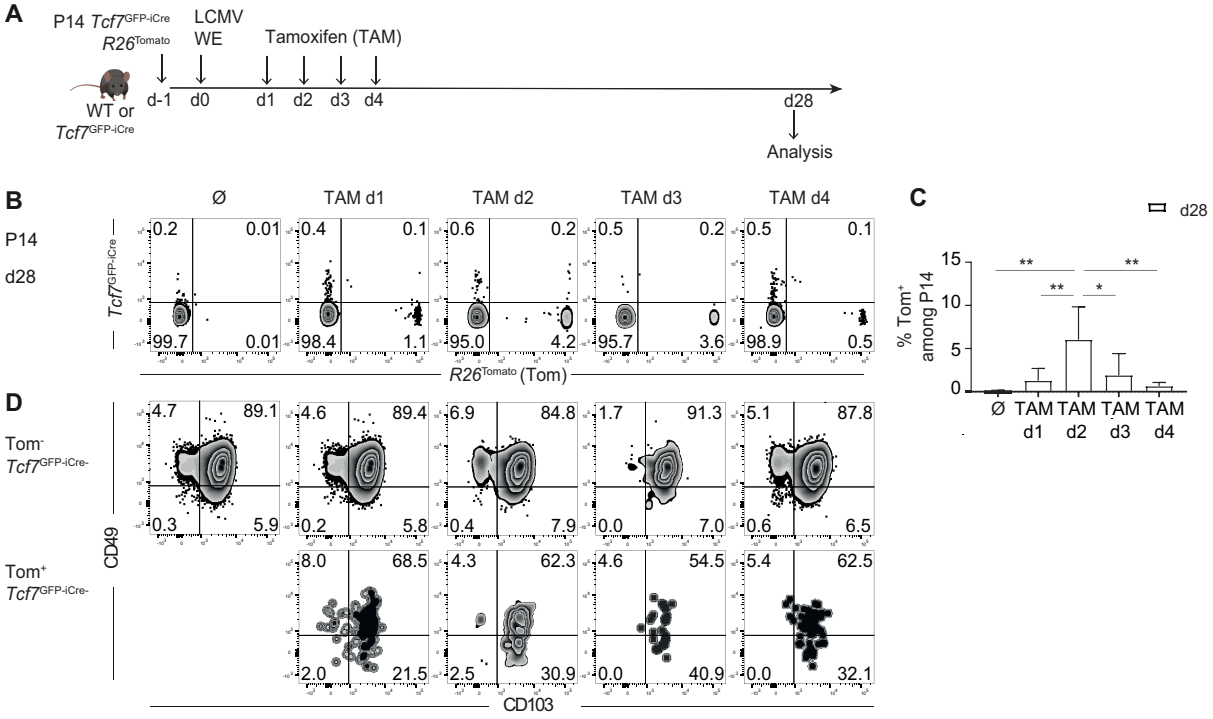

Figure 19 - Origin of tissue-resident memory cells
(A) Schematic representation of the experimental set-up. *Tcf7*$^{GFP\text{-}iCre}$ *R26*^{Tomato} P14 cells (CD45.1/.2) were transferred into *Tcf7*$^{GFP\text{-}iCre}$ (CD45.2) recipients and infected one day later with LCMV WE. Recipients were left untreated (Ø) or injected with a single dose of 0.1mg/ml Tamoxifen (TAM) on d1, d2, d3 or d4 p.i.. **(B)** Intraepithelial lymphocytes (IEL) present in the gut were isolated and at d28 p.i. GFP (*Tcf7*$^{GFP\text{-}iCre}$) and Tom (*R26*^{Tomato}) expression by P14 cells was analysed. **(C)** Frequency of Tom^{+} cells among P14 IEL cells at d28 p.i. **(D)** Expression of CD49 versus CD103 by Tom^{-} *Tcf7*$^{GFP\text{-}iCre\text{-}}$ P14 IEL (top) and Tom^{+} *Tcf7*$^{GFP\text{-}iCre\text{-}}$ P14 IEL (bottom) at d28 p.i..**(B-D)** The data shown are pooled from 3 independent experiments with total n=6-7 mice per group. Mean ±SD are shown. Statistics are based on One-Way ANOVA with Tukey's test **(C, E)** with *:p<0.05; **:p<0.01; ***:p<0.001; and (ns) p>0.05.

We analysed at which time-point of the primary infection *Tcf7*$^{GFP\text{-}iCre+}$ *R26*^{Tomato} P14 cells gave rise to tissue-resident memory cells present among gut IEL. We observed Tom^{+} IEL cells independent of whether labelling was started at d1 to d4 p.i. (**Fig 19B**), however labelled cells were most abundant when labelling of *Tcf7*$^{+}$ cells was started at d2 p.i. (**Fig 19C**). The vast majority of the Tom^{+} IEL were *Tcf7*$^{GFP\text{-}iCre\text{-}}$ and most of the cells expressed markers for tissue-resident memory cells, such as CD69 (not shown), CD49 and CD103 (**Fig 19D**). Thus, tissue-

resident memory cells chiefly derived from *Tcf7*$^{+}$ cells present at d2 p.i.. We also detected small populations of *Tcf7*$^{GFP\text{-}iCre+}$ IEL. However, such cells could only be identified with certainty among unlabelled (Tom^{-}) cells. Labelled Tom^{+} *Tcf7*$^{GFP\text{-}iCre+}$ IEL cells were likely too infrequent.

We also investigated the presence of Tom^{+} IEL at d8 p.i.. The presence of Tom^{+} IEL cells was maximal when labelling of *Tcf7*$^{GFP\text{-}iCre+}$ cells was started at d1 p.i. (**Fig 20A, B**) and gradually decreased thereafter. Phenotypically these cells were also *Tcf7*$^{GFP\text{-}iCre-}$ and expressed CD49 but few cells were CD103^{+} (**Fig 20C**). It is known for skin resident cells that CD103 upregulation occurs later (Mackay et al., 2013). When labelling was started at d1 p.i., the frequency of Tom^{+} IEL cells was higher at d8 p.i. compared to d28 p.i. (**Fig 20B**), suggesting that these cells contracted and thus represented in part short-lived tissue effector cells.

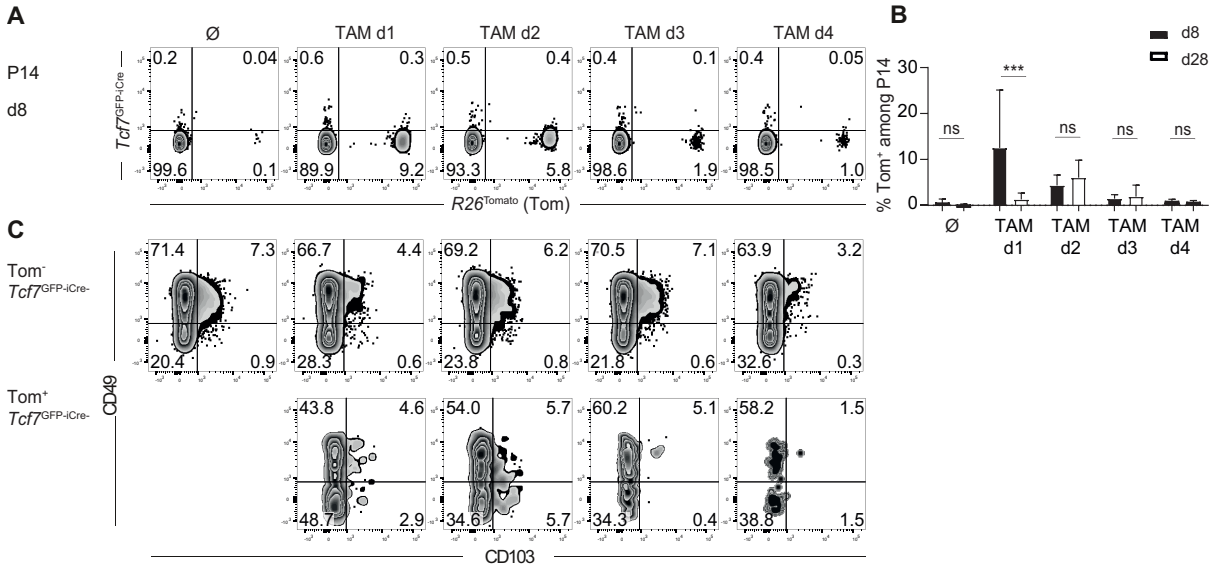

Figure 20 - Origin of P14 IEL cells present at the peak of the primary response
For the experimental set-up see legend to Figure 19. **(A)** GFP (*Tcf7*$^{GFP\text{-}iCre}$) and Tom (*R26*^{Tomato}) expression by P14 IEL cells was analysed at d8 p.i.. **(B)** Frequency of Tom^{+} cells among P14 IEL cells at d8 and d28 p.i. **(C)** Expression of CD49 versus CD103 by Tom^{-} *Tcf7*$^{GFP\text{-}iCre-}$ P14 IEL (top) and Tom^{+} *Tcf7*$^{GFP\text{-}iCre-}$ P14 IEL (bottom) at d8 p.i.. **(A-C)** The data shown are pooled from 3 independent experiments with n=7-8 mice per group. Mean ±SD are shown. Statistics are based on Non-paired two-tailed Student's test **(B, D)** with *:p<0.05; **:p<0.01; ***:p<0.001; and (ns) p>0.05.

As antigen-specific CD8^{+} T cells are not detected in the intestinal epithelium before d4.5 p.i. (Masopust et al., 2006), we concluded that tissue-resident memory cells are programmed in peripheral *Tcf7*$^{+}$ cells present at d2 p.i.. Tissue effector cells, like peripheral T_{EF} cells, mainly derived from peripheral *Tcf7*$^{+}$ present at d1 p.i..

3.2.5. *Tcf7*$^{+}$ CD8^{+} T cells are programmed to downregulate *Tcf7* and become terminal effector cells prior to the first cell division

Terminal effector cells derived from *Tcf7*$^{+}$ cells that are present before or at d2 post LCMV infection. Indeed, *Tcf7* was expressed at high levels in naive CD8^{+} T cells and remained expressed at high levels in all CD8^{+} T cells at d2 post LCMV infection (**Fig 13B**). To address whether these cells cycled, P14 cells were labelled with CTV (cell trace violet) prior to transfer into WT recipients (**Fig 21A**).

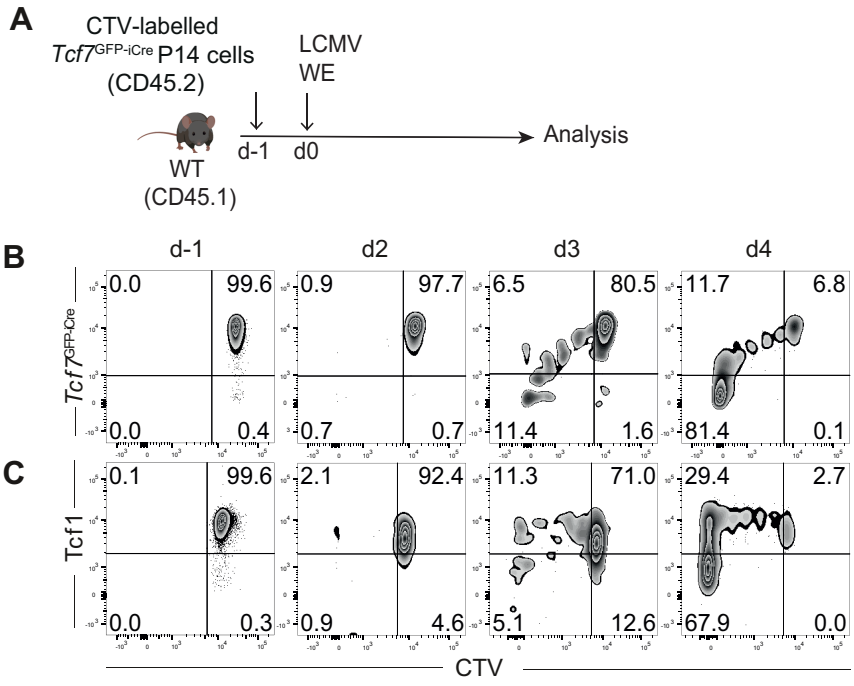

Figure 21 - Effector programming occurs prior to cell division
(A) Schematic representation of the experimental set-up. *Tcf7*$^{GFP\text{-}iCre}$ P14 cells (CD45.2) were labelled with CTV (cell trace violet) and transferred to WT (CD45.1) recipients, one day prior to infection with LCMV WE. **(B-C)** Expression of GFP (*Tcf7*$^{GFP\text{-}iCre}$) **(B)** or Tcf1 **(C)** versus CTV at the indicated time points prior to transfer to or after infection. **(A-C)** The data shown are representative of 3 independent experiments with total n=6 mice per group.

P14 cells in uninfected recipient mice maintained *Tcf7*^{GFP} or Tcf1 expression at high levels and they did not divide (not shown). In infected mice, cell division (CTV dilution) was not observed at d2 p.i. (**Fig 21B, C**). Cell division as well as *Tcf7* or Tcf1 downregulation were observed starting at d3 p.i. (**Fig 21B, C**) in agreement with (Lin et al., 2016). Similar results were obtained when mice were infected i.p. with acute LCMV Armstrong (Arm) strain (not shown), indicating that the virus strain or the route of infection did not influence the timing of cell division and Tcf1 downregulation. Thus, CD8^{+} T cells expressing high levels of *Tcf7* and Tcf1 were programmed to downregulate Tcf1 and differentiate into effector cells prior to the first cell division.

3.2.6. *Tcf7*$^{+}$ CD8^{+} T cells present at day 4 post-infection do not contribute to the terminal effector pool

Lineage tracing suggested that short-lived effector cells derived from *Tcf7*$^{+}$ cells prior to d4 p.i.. To independently confirm these findings, we determined whether d4 *Tcf7*$^{+}$ cells were indeed dispensable for the generation of T_{EF} cells. To do so, this lab has developed a lineage ablation system that allows the depletion of *Tcf7*$^{+}$ cells *in vivo* (Siddiqui et al., 2019). Briefly, a diphtheria toxin receptor (DTR) – T2A – GFP fusion gene was inserted into the *Tcf7* locus present on a BAC, which was then used to generate a transgenic mouse line. Injection of diphtheria toxin (DT) allows the ablation of *Tcf7*$^{DTR\text{-}GFP}$ expressing cells *in vivo* (Siddiqui et al., 2019).

We used this system to address whether ablation of d4 *Tcf7*$^{+}$ cells impacted the formation of T_{EF} cells. Naive *Tcf7*$^{DTR\text{-}GFP+}$ P14 cells were transferred into WT recipients, which were infected with LCMV Arm one day later (**Fig 22A**). As a control for possible DT toxicity, we also transferred naive *Tcf7*^{GFP} P14 cells into WT recipients. Mice were injected with DT at d4 and d5 p.i..

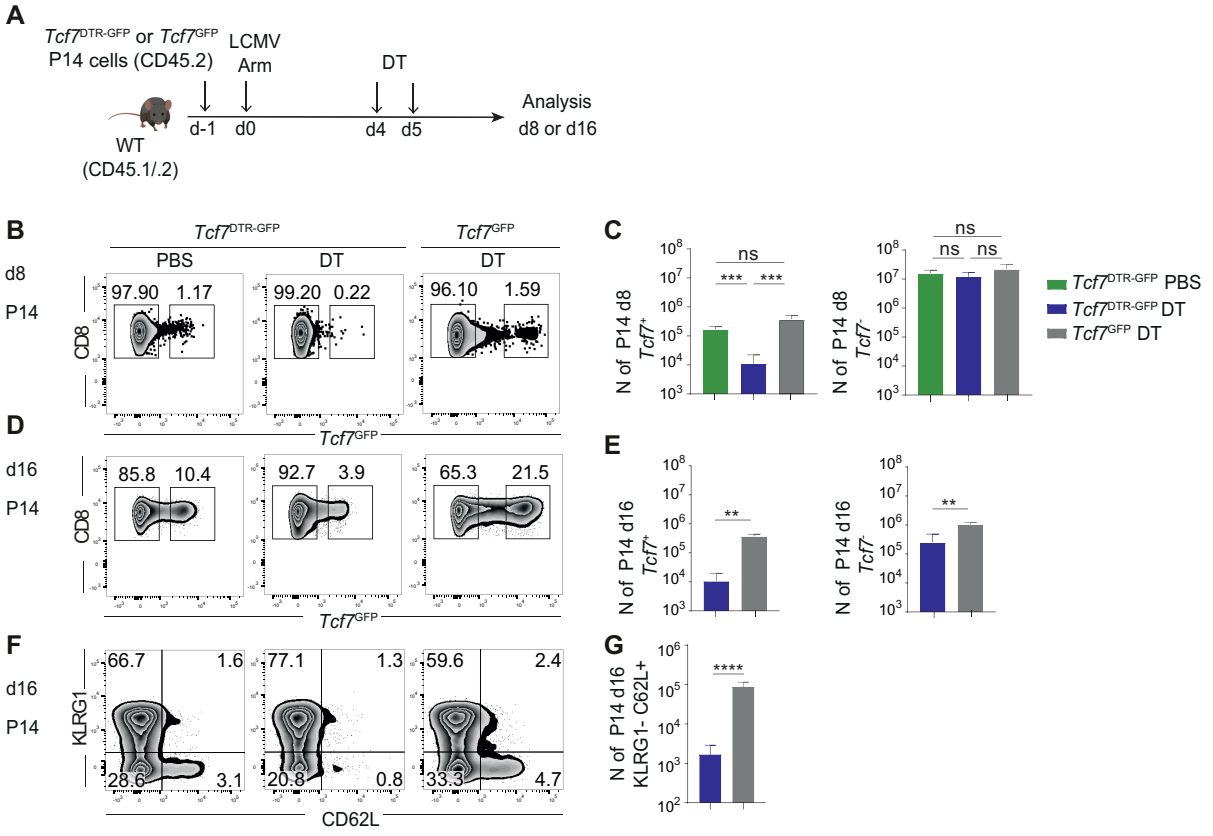

Figure 22 - Ablation of d4 *Tcf7*$^{+}$ cells deplete T_{CM} and reduced T_{EM} compartment
(A) Schematic representation of the experimental set-up. *Tcf7*$^{DTR\text{-}GFP}$ or *Tcf7*^{GFP} P14 cells (CD45.2) were transferred into WT (CD45.1/.2) recipients that were infected with LCMV Arm one day later. Recipients were injected twice with vehicle (PBS) or Diphtheria Toxin (DT) on d4 and d5 p.i.. **(B)** Expression of GFP was analysed by P14 cells on d8 p.i.. **(C)** Abundance of *Tcf7*$^{+}$ (*Tcf7*$^{DTR\text{-}GFP+}$ or *Tcf7*$^{GFP+}$) P14 (left) or *Tcf7*$^{-}$ (*Tcf7*$^{DTR\text{-}GFP\text{-}}$ or *Tcf7*$^{GFP\text{-}}$) P14 cells (right) on d8 p.i. **(D)** Expression of GFP by P14 cells was analysed on d16 p.i.. **(E)** Abundance of *Tcf7*$^{+}$ P14 (left) or *Tcf7*$^{-}$ P14 cells (right) on d16 p.i.. **(F)** Expression of KLRG1 versus CD62L by P14 cells was analysed on d16 p.i.. **(G)** Abundance of KLRG1^{-} CD62L^{+} P14 cells on d16 p.i.. **(B-G)** The data shown are pooled from 2 independent experiments with total n=10 mice per group. Mean ±SD are shown. Statistics are based on One-Way ANOVA with Tukey's test **(C, E, G)** with *:p<0.05; **:p<0.01; ***:p<0.001; and (ns) p>0.05.

At d8 p.i., DT treatment had profoundly depleted *Tcf7*$^{DTR\text{-}GFP+}$ cells (0.2-0.05% *Tcf7*$^{DTR\text{-}GFP+}$ of P14), compared to PBS-treated mice (1.2-1.6%) or DT-treated mice harbouring control *Tcf7*^{GFP} cells (1.5-2.0%) (**Fig 22B**). On the other hand, the abundance of *Tcf7*$^{DTR\text{-}GFP-}$ cells was comparable between the 3 groups of mice (**Fig 22C**). Thus, ablation of d4 *Tcf7*$^{+}$ cells did not alter the generation of d8 effector cells. These data confirmed that T_{EF} cells derived from *Tcf7*$^{+}$ cells that are present prior to d4 p.i. and suggested they derived from *Tcf7*$^{-}$ cells present at d4 p.i..

We further analysed the memory compartment of mice from which d4 *Tcf7*$^{+}$ cells had been depleted. However, as DT-treated mice became sick (independent of the depletion of *Tcf7*$^{DTR\text{-}GFP+}$ cells), we had to analyse these mice at d16 p.i., whereby we only compared mice that had been injected with DT. At d16 p.i. the abundance of *Tcf7*$^{DTR\text{-}GFP+}$ cells was very low and not different from that seen at d8 p.i. (**Fig 22D, E**). Thus, *Tcf7*$^{-}$ cells did not measurably re-express *Tcf7* between d8 and d16 p.i.. DT-treated mice harboured considerably fewer CD62L^{+} cells, consistent with the absence of a central memory compartment (**Fig 22F, G**). Further, the abundance of *Tcf7*$^{DTR\text{-}GFP-}$ cells at d16 was considerably lower than at d8 p.i., confirming that *Tcf7*$^{-}$ compartment had contracted and that T_{EF} cells had been present at d8 p.i.. Finally, the abundance of *Tcf7*$^{DTR\text{-}GFP-}$ cells at d16 p.i. was decreased (4-fold) compared to control mice (**Fig 22E**). Thus, both the d4 *Tcf7*$^{DTR\text{-}GFP+}$ and *Tcf7*$^{DTR\text{-}GFP-}$ compartments contributed to the T_{EM} compartment.

3.2.7. Developmental potential of *Tcf7*$^{+}$ and *Tcf7*$^{-}$ CD8^{+} T cells present at day 4 post-infection (in collaboration with Daniela Pais)

Lineage tracing and lineage ablation experiments showed that d4 *Tcf7*$^{+}$ CD8^{+} T cells yielded T_{CM} and T_{EM} cells but not short-lived effector cells (d8 *Tcf7*$^{-}$ cells). The latter derived from d4 *Tcf7*$^{-}$ cells, which also yielded T_{EM} cells. We first addressed whether there were phenotypic differences between d4 and d8 *Tcf7*$^{-}$ cells (**Fig 23A**).

Most d8 *Tcf7*$^{-}$ cells expressed KLRG1, while most d4 *Tcf7*$^{-}$ cells lacked KLRG1 (**Fig 23B**), a marker of terminally differentiated cells. Thus, the vast majority of d4 cells were *Tcf7*$^{-}$ KLRG1^{-} while the vast majority of d8 cells were *Tcf7*$^{-}$ KLRG1^{+} although *Tcf7*$^{-}$ KLRG1^{-} cells were also present (**Fig 23B**). *Tcf7*$^{-}$ KLRG1^{+} cells present at d8 p.i. also expressed high levels of CX3CR1 and lacked CD27 and CD62L, while d8 *Tcf7*$^{-}$ KLRG1^{-} had an intermediate expression of these markers, similar to d4 *Tcf7*$^{-}$ subsets (**Fig 23C, D**). Thus, d4 *Tcf7*$^{-}$ cells did not appear as differentiated as d8 *Tcf7*$^{-}$ cells.

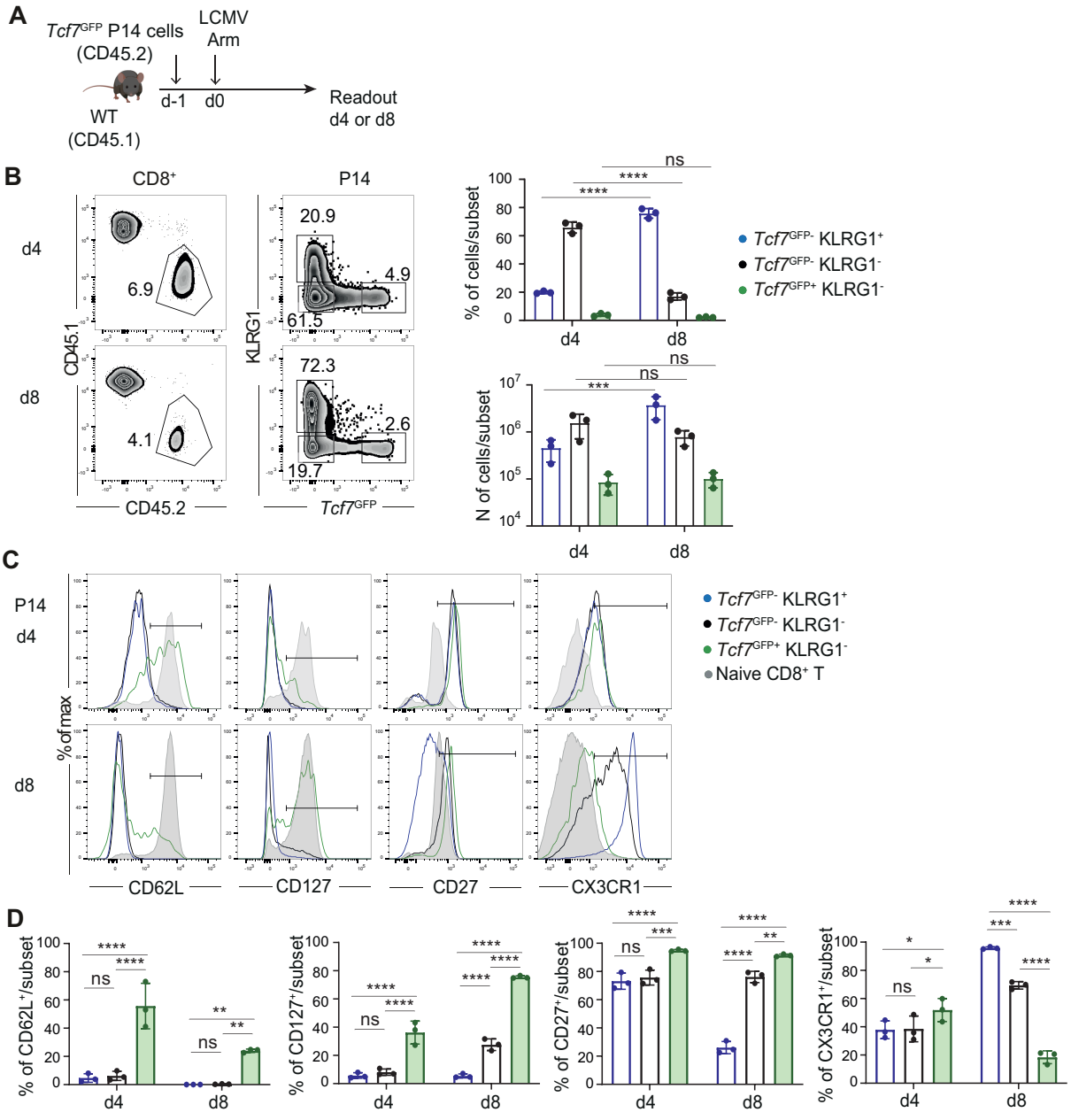

Figure 23 - Phenotype of *Tcf7*$^{GFP-}$ cells present at day 4 and 8 post LCMV-infection
(A) Schematic representation of the experimental set-up. 10^6 and 10^4 *Tcf7*^{GFP} P14 cells (CD45.2) were transferred into WT (CD45.1) recipients (for readout at d4 and d8 p.i., respectively). Mice were infected with LCMV Arm one day later. **(B)** Gated P14 cells were analysed for the expression of KLRG1 versus *Tcf7*^{GFP} on d4 and d8 p.i.. Bar graphs depict frequency and abundance of the indicated subsets of P14 cells at d4 and d8 p.i. **(C-D)** Expression of the indicated markers by *Tcf7*$^{+}$ KLRG1^{-} (green), *Tcf7*$^{-}$ KLRG1^{-} (black) and *Tcf7*$^{-}$ KLRG1^{+} (blue) at d4 and d8 p.i.. Bar graphs depict frequency of the cells expressing the indicated markers in the 3 subsets at d4 and d8 p.i..
(B-D) The data shown are representative of 2 independent experiments each with n=3 mice per group. Mean ±SD are shown. Statistics are based on One-Way ANOVA with Tukey's test **(B, D)** with *:p<0.05; **:p<0.01; ***:p<0.001; and (ns) p>0.05.

Since short-lived effector cells (d8 *Tcf7*$^{-}$) derived from d4 *Tcf7*$^{-}$ cells rather than d4 *Tcf7*$^{+}$ cells, we compared the developmental potential of d4 *Tcf7*$^{+}$, d4 *Tcf7*$^{-}$ KLRG1^{-} and d4 *Tcf7*$^{-}$ KLRG1^{+} cells to that of the corresponding d8 subsets. The 3 subsets were flow sorted and transferred into naive WT mice that were then infected with LCMV Arm (**Fig 24A**). Eight days

later (d4+8 or d8+8), we observed that d4 and d8 *Tcf7*$^+$ cells generated the highest number of progenies, whereby most cells were *Tcf7*$^-$ but *Tcf7*$^+$ cells were also present (**Fig 24B, C**). Twenty-eight days later (d4+28 or d8+28), the abundance of secondary *Tcf7*$^+$ was unchanged, while *Tcf7*$^-$ cells had contracted (**Fig 24D, E**). These data showed that d4 *Tcf7*$^+$ cells had stemness and were able to yield T_{EF} cells upon restimulation. Thus, in their natural environment, d4 *Tcf7*$^+$ cells do not seem to be exposed to the signals required for effector differentiation.

Restimulation of d4 *Tcf7*$^-$ KLRG1$^-$ and *Tcf7*$^-$ KLRG1$^+$ cells generated an intermediate number of progenies, similar to d8 *Tcf7*$^-$ KLRG1$^-$ cells. On the other hand, d8 *Tcf7*$^-$ KLRG1$^+$ cells yielded the lowest number of progenies. All progenies lacked *Tcf7* expression and most expressed KLRG1. The abundance of progenies was strongly reduced at d28 post-restimulation (**Fig 24D, E**), suggesting that all populations had the potential to generate terminal effector cells as well as effector memory cells. Unexpectedly, we observed *Tcf7*$^+$ memory cells that derived from restimulated d4 *Tcf7*$^-$ cells. This was also observed, although with low efficacy, when restimulating d8 *Tcf7*$^-$ cells. Thus, the *Tcf7* locus may not be stably shut down yet in some d4 *Tcf7*$^-$ cells and restimulation may allow some of these cells to re-express *Tcf7*. These *Tcf7* re-expressor cells may not be exactly the same as the ones that stably maintain *Tcf7* expression as many of the former cells express KLRG1. Finally, we noted that re-expression of *Tcf7* was not observed when d4 *Tcf7*$^+$ cells had been ablated (**Fig 22C, E**). Thus, *Tcf7* re-expression may be limited to situations of cell transfers. These experiments showed that d4 *Tcf7*$^+$ cells had stemness and that d4 *Tcf7*$^-$ cells had an intermediate developmental potential, which enabled these cells to yield terminally differentiated cells at d8 p.i..

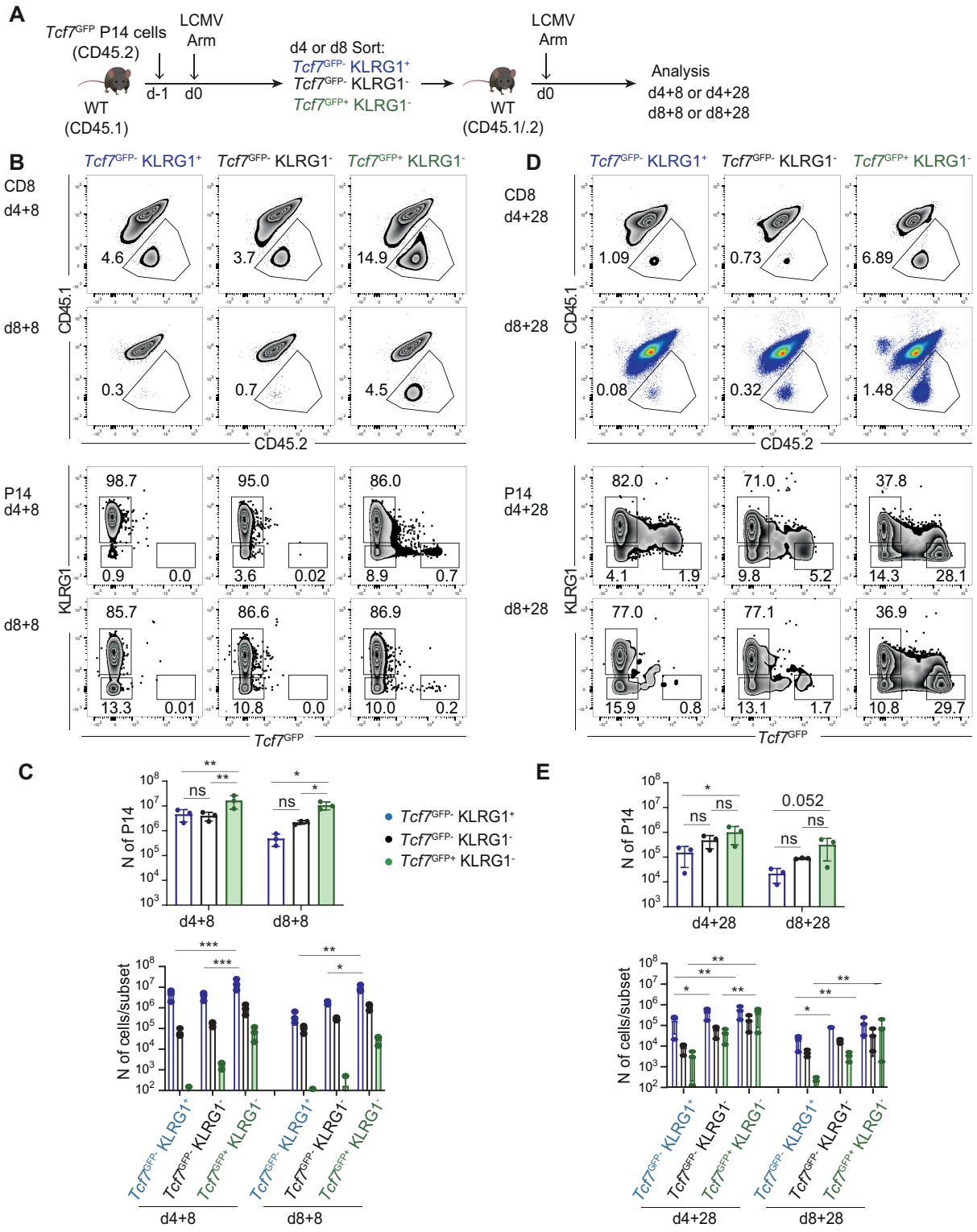

Figure 24 – Developmental potential of day 4 *Tcf7*$^+$ and *Tcf7*$^-$ cells
(A) Schematic representation of the experimental set-up. *Tcf7*^{GFP} P14 cells (CD45.2) were transferred into WT (CD45.1) recipients that were infected with LCMV Arm one day later. On d4 or d8 p.i. 10^4 *Tcf7*$^+$ KLRG1$^-$ (green), *Tcf7*$^-$ KLRG1$^-$ (black) and *Tcf7*$^-$ KLRG1$^+$ (blue) cells were sorted and transferred into secondary WT recipients, which were then infected with LCMV Arm. **(B)** Secondary P14 cells were analysed for the expression of *Tcf7*^{GFP} versus KLRG1 at d8 post-transfer (d4+8 or d8+8). **(C)** Abundance of secondary P14 cells and of secondary *Tcf7*$^+$ KLRG1$^-$ (green), *Tcf7*$^-$ KLRG1$^-$ (black) and *Tcf7*$^-$ KLRG1$^+$ (blue) cells. **(D)** Secondary P14 cells were analysed for the expression of *Tcf7*^{GFP} versus KLRG1 at d28 post-transfer (d4+28 or d8+28). **(E)** Abundance of secondary P14 cells and of secondary *Tcf7*$^+$ KLRG1$^-$ (green), *Tcf7*$^-$ KLRG1$^-$ (black) and *Tcf7*$^-$ KLRG1$^+$ (blue) cells.

(A-E) The data shown are representative of 2 independent experiments each with n=3 mice per group. Mean ±SD are shown. Statistics are based on One-Way ANOVA with Tukey's test **(C, E)** with *:p<0.05; **:p<0.01; ***:p<0.001; and (ns) p>0.05.

3.2.8. Localization of *Tcf7*$^{+}$ and *Tcf7*$^{-}$ CD8^{+} T cells in the spleen (in collaboration with Daniela Pais, the Luther Lab and the Joyce lab)

Given the distinct behaviour and fate of *Tcf7*$^{+}$ and *Tcf7*$^{-}$ cells, we addressed the localization and cycling of these cells using multicolour immunofluorescence. *Tcf7*^{GFP} P14 cells (CD45.2) were transferred into WT mice (CD45.1), which were then infected with LCMV Arm. Mice were injected with EdU (5-ethynyl-2'-deoxyuridine, a thymidine analog) 2h prior to sacrifice at d3, d4 or d6 p.i. (**Fig 25A**). Cross sections of the spleen were stained using DAPI (4',6-diamidino-2-phenylindole, nuclei, blue), anti-CD4 (T cell zone, pink), CD45.2 (P14 cells, red), anti-GFP (*Tcf7*^{GFP}, green) and EdU (cycling, orange). Stained spleen sections were scanned and subjected to image analysis using the Visiopharm software. First, the program identified the T cell zone (T) based on the CD4 staining (**Fig 25B**). Second, the B cell zone (B) was identified automatically based on an increased density of nuclei. An additional region of interest was defined around the T and B cell zones (50 pixels, termed PY). The remaining area of the spleen cells was referred to as red pulp (RP) (**Fig 25B**). P14 cells (DAPI^{+}, CD45.2^{+}) and *Tcf7*$^{+}$ P14 cells (DAPI^{+}, CD45.2^{+}, GFP^{+}) were identified automatically and assigned to the defined regions of the spleen.

At all time-points tested, P14 cells localized preferentially to the T cell zone, the PY or the RP, but rarely to the B cell zone (**Fig 25C, D**). At d3 p.i., *Tcf7*$^{GFP+}$ P14 cells were mainly located in the T cell zone and the PY. At d4, most *Tcf7*$^{GFP+}$ cells were in the T cell zone (41%), while they were comparably distributed to the T, the PY and the RP zones at d6 p.i.. *Tcf7*$^{GFP-}$ P14 cells were mainly located in the T cell zone and the PY at d3 p.i.. They were comparably distributed to the T zone, the PY and the RP at d4 p.i.. At d6 p.i., *Tcf7*$^{GFP-}$ P14 cells located predominantly in the RP. Thus, *Tcf7*$^{GFP+}$ P14 cells always localized to both T cell zone and PY and the localization changed only modestly over time. In contrast, *Tcf7*$^{GFP-}$ P14 cells increasingly localized to the RP along with a decrease of their presence in the T cell zone.

Cycling (EdU^{+}) P14 cells were very abundant at d3 and d4 p.i. and were reduced at d6 p.i. (**Fig 25C, D**). EdU^{+} *Tcf7*$^{GFP+}$ and *Tcf7*$^{GFP-}$ P14 cells did not show a preferential localization, indicating that there were no specialized niches in which *Tcf7*$^{+}$ and *Tcf7*$^{-}$ cells proliferated.

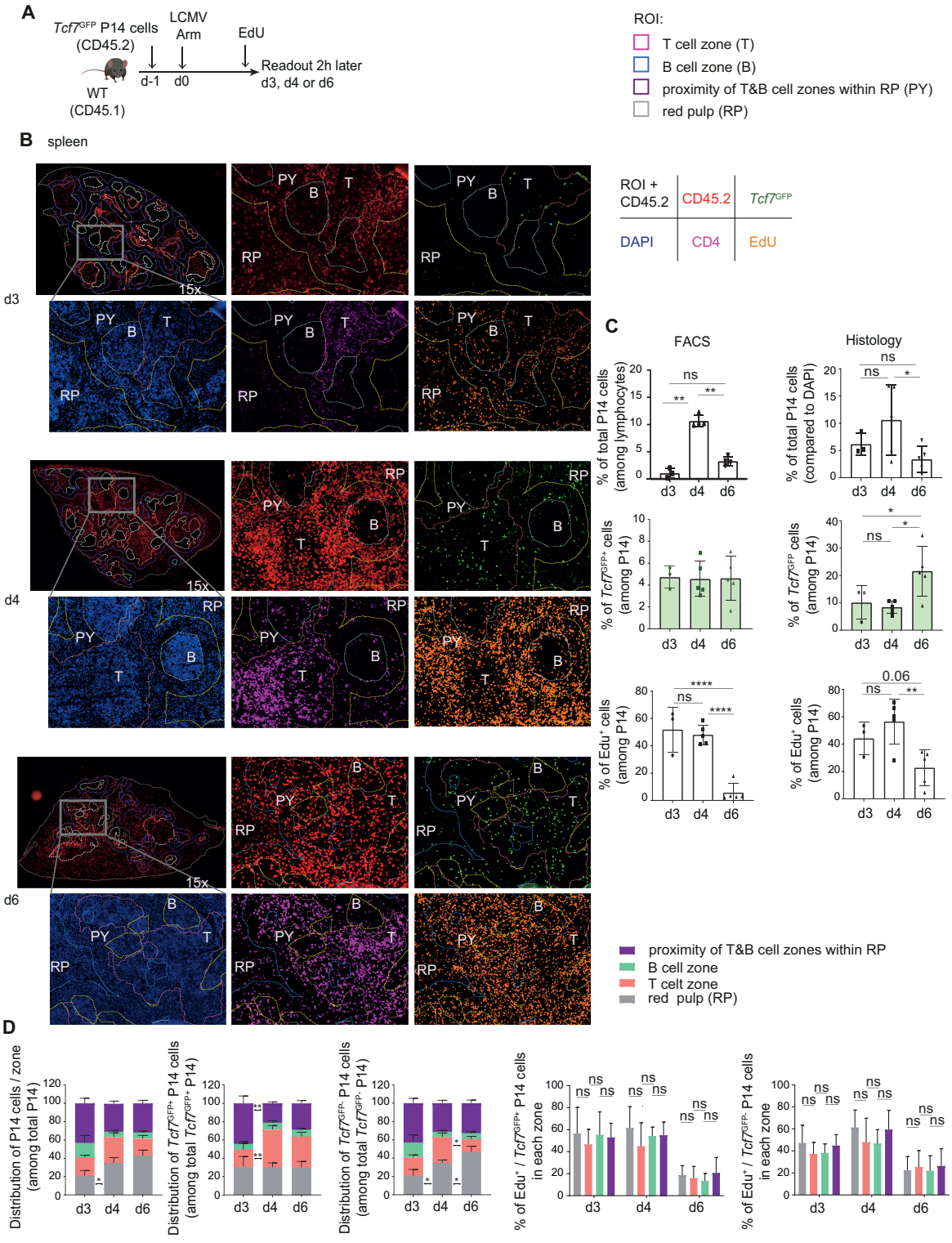

Figure 25 - Localization of *Tcf7*$^{GFP+}$ and *Tcf7*$^{GFP-}$ CD8^{+} T cells in the spleen
(A) Schematic representation of the experimental set-up. *Tcf7*^{GFP} P14 cells (CD45.2) were transferred into WT (CD45.1) recipients that were infected with LCMV Arm one day later. Recipients were injected with EdU 2h before sacrifice at d3, d4 or d6 p.i.. **(B)** Spleen cross sections were stained for CD45.2 (P14 cells, red), GFP (*Tcf7*^{GFP}, green), DAPI (nuclei, blue), CD4 (T cells, pink) and EdU (cycling, orange). Regions of interest (ROI) were defined using image analysis: T cell zone (CD4^{+}, T); B cell zone (nuclear dense, B); area in proximity of T and B cell zones (PY) and remaining area as red pulp (RP). **(C)** Frequency of cells determined by flow cytometry (left) or histology (right). From top to bottom: Frequency of total P14 cells (CD45.2^{+}) among total lymphocytes (flow cytometry) or DAPI^{+} cells (histology); Frequency of *Tcf7*$^{GFP+}$ cells (GFP^{+}) among P14 cells (CD45.2^{+}); Frequency of EdU^{+} cells among P14 cells. **(D)** Distribution of P14 cells, *Tcf7*$^{GFP+}$ or *Tcf7*$^{GFP-}$ P14 cells to each zone (left). Fraction of EdU^{+}

cells among *Tcf7*$^{GFP+}$ (left) and *Tcf7*$^{GFP-}$ P14 cells (right) in each zone. **(B-D)** The data shown are pooled from 2 independent experiments with a total of n=3-5 mice per group. Mean ±SD are shown. Statistics are based on One-Way ANOVA with Tukey's test **(C, D)** with *:p<0.05; **:p<0.01; ***:p<0.001; and (ns) p>0.05.

3.2.9. The distinct expansion of *Tcf7*$^{+}$ and *Tcf7*$^{-}$ CD8^{+} T cells is regulated in part by Tcf1

Naive *Tcf7*$^{+}$ cells give rise to d8 *Tcf7*$^{+}$ cells, which represent central memory precursors (T_{pCM}), and to d8 *Tcf7*$^{-}$ cells, most of which are terminal effector cells. While both cell types derive from naive CD8^{+} T cells, the abundance of *Tcf7*$^{+}$ and *Tcf7*$^{-}$ cells at d8 p.i. differs by a factor of around 50. We addressed whether this difference was due to differential cycling or survival of these populations.

WT P14 cells started to divide after d2 p.i. (**Fig 21B, C**), and the majority of cells had divided at d3.5 p.i. (**Fig 26A**). Cell division was associated with *Tcf7* and Tcf1 downregulation (**Fig 26A**). Cells retaining *Tcf7* expression had undergone fewer divisions than cells with low *Tcf7* expression. Indeed, *Tcf7*$^{+}$ cells had divided on average 3 times, while *Tcf7*$^{-}$ cells had efficiently diluted CTV (>6 divisions) (**Fig 26A**). We further addressed cycling of P14 cells based on EdU incorporation during a 2h pulse. This revealed that the fraction of cycling d4 *Tcf7*$^{-}$ cells was increased compared to d4 *Tcf7*$^{+}$ cells. At d6 p.i., the fraction of cycling *Tcf7*$^{-}$ cells was maintained, while that of *Tcf7*$^{+}$ cells was further reduced (**Fig 26B, C**). Thus, downregulation of *Tcf7* was associated with accelerated cell division.

We further tested the susceptibility of these populations to undergo apoptosis as judged by the activation of Caspase3. At d4 p.i., Caspase3 activation was somewhat higher in *Tcf7*$^{-}$ cells than in *Tcf7*$^{+}$ cells, while no difference was apparent in d6 subsets (**Fig 26D**). Together, these data suggested that the reduced abundance of *Tcf7*$^{+}$ cells at d8 p.i. was not due to increased apoptosis but rather based on a slower rate and a shortened period of cycling.

The slower cycling rate of *Tcf7*$^{+}$ cells prompted us to address whether this effect depended on Tcf1 protein expression. To address this issue, we used *Tcf7*^{GFP} P14 mice that lacked Tcf1 protein expression (Utzschneider et al., 2016b), hereafter called KO *Tcf7*^{GFP} P14 cells (**Fig 26E**). At d3.5 p.i., most KO *Tcf7*$^{GFP+}$ P14 cells had divided 5-6 times compared to 3 times for WT *Tcf7*$^{GFP+}$ P14 cells (**Fig 26E**). KO *Tcf7*$^{GFP-}$ cells had efficiently diluted CTV (>6 divisions), similar to WT *Tcf7*$^{GFP-}$ cells. Thus, the absence of Tcf1 protein expression in *Tcf7*$^{+}$ cells allowed *Tcf7*$^{+}$ cells to undergo more cell divisions. These data were corroborated using EdU incorporation (**Fig 26F, G**). At d4 p.i., KO *Tcf7*$^{GFP+}$ cells cycled as efficiently as KO *Tcf7*$^{GFP-}$ or WT *Tcf7*$^{GFP-}$ cells and more efficiently than d4 WT *Tcf7*$^{GFP+}$ cells. At d6 p.i., KO *Tcf7*$^{GFP+}$ cells cycled somewhat less than KO *Tcf7*$^{GFP-}$ cells but still more efficiently than d6 WT *Tcf7*$^{GFP+}$ cells (**Fig 26G**). Additionally, *Tcf7*$^{+}$ cell subset from KO mice had better survival capacity than WT cells slightly at d6 p.i. (**Fig 26H**). These data showed that the reduced cycling of *Tcf7*$^{+}$ cells compared to *Tcf7*$^{-}$ cells was mediated in part by the expression of Tcf1 protein.

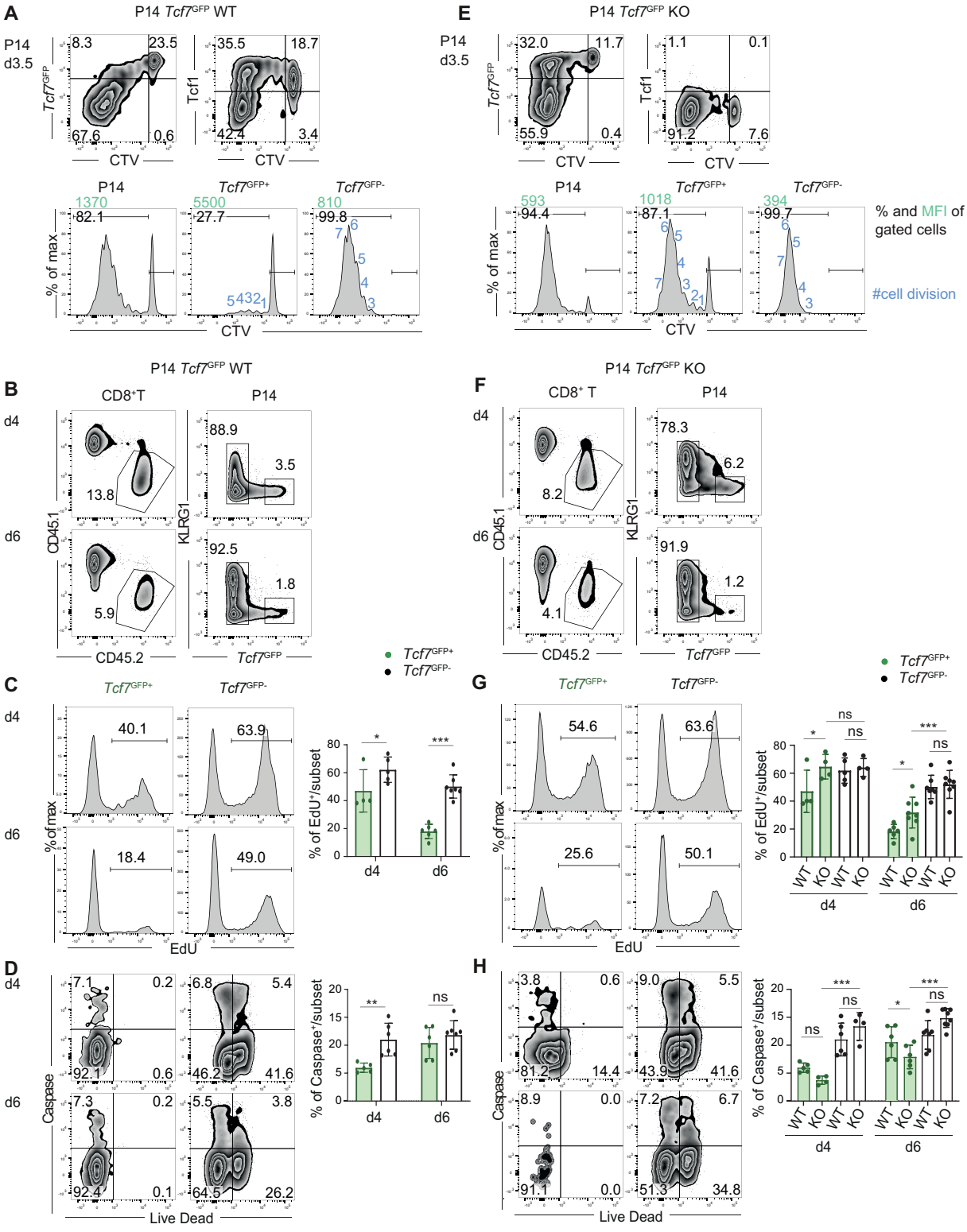

Figure 26 - Cell division, EdU incorporation and Caspase activation of *Tcf7*$^{+}$ and *Tcf7*$^{-}$ cells CD8^{+} T cells in the presence and absence of Tcf1

(A and E) For the experimental representation see legend to Figure 21. Briefly, WT or KO *Tcf7*^{GFP} P14 cells (CD45.2) were labelled with CTV and transferred to WT (CD45.1) recipients one day prior to infection with LCMV WE. **(B-D and F-H)** For the experimental representation see legend to Figure 25. Briefly, WT or KO *Tcf7*^{GFP} P14 cells (CD45.2) were transferred into WT (CD45.1) recipients. Recipients were infected with LCMV Arm one day later and injected with EdU 2h before sacrifice at d4 or d6 p.i.. **(A)** Gated WT *Tcf7*^{GFP} P14 cells analysed for the

expression of CTV versus GFP (*Tcf7*^{GFP}) or Tcf1 on d3.5 p.i. (top). Histograms (bottom) depict CTV expression in P14 (left), *Tcf7*$^{GFP+}$ P14 (centre) or *Tcf7*$^{GFP-}$ P14 (right). Numbers indicate the frequency (black) or Mean Fluorescence Intensity (MFI) of CTV (green) of the gated cells. Numbers in blue depict number of cell division. **(B)** Gated WT *Tcf7*^{GFP} P14 cells analysed for the expression of KLRG1 and GFP (*Tcf7*^{GFP}) on d4 and d6 p.i. **(C)** Gated WT *Tcf7*^{GFP} P14 cells analysed for EdU expression on *Tcf7*$^{+}$ and *Tcf7*$^{-}$ P14 cells**.** Bar graph depicts frequency of EdU-expressing cells of the indicated subset on d4 or d6 p.i.. **(D)** Gated WT *Tcf7*^{GFP} P14 cells analysed for the expression of Caspase3 versus Live Dead on *Tcf7*$^{+}$ and *Tcf7*$^{-}$ P14 cells. Bar graph depicts frequency of Caspase3-expressing cells of the indicated subset on d4 or d6 p.i.. **(E)** Gated KO *Tcf7*^{GFP} P14 cells analysed for the expression of CTV versus GFP or Tcf1 on d3.5 p.i. (top). Histograms (bottom) depict CTV expression in P14 (left), *Tcf7*$^{GFP+}$ P14 (centre) or *Tcf7*$^{GFP-}$ P14 (right). Numbers indicate the frequency (black) or MFI CTV (green) of gated cells. Numbers in blue depict number of cell division. **(F)** Gated KO *Tcf7*^{GFP} P14 cells analysed for the expression of KLRG1 and GFP on d4 and d6 p.i.. **(G)** Gated KO *Tcf7*^{GFP} P14 cells analysed for EdU expression on *Tcf7*$^{+}$ and *Tcf7*$^{-}$ P14 cells. Bar graph depicts frequency of EdU-expressing WT and KO *Tcf7*^{GFP} P14 cells of the indicated subset on d4 or d6 p.i.. **(H)** Gated KO *Tcf7*^{GFP} P14 cells analysed for the expression of Caspase3 versus Live Dead on *Tcf7*$^{+}$ and *Tcf7*$^{-}$ P14 cells. Bar graph depicts frequency of Caspase3-expressing WT and KO *Tcf7*^{GFP} P14 cells of the indicated subset on d4 or d6 p.i.. **(A and E)** The data shown are representative of 2 independent experiments with each n=3 mice per group. **(B-D and F-H)** The data shown are pooled from 2 independent experiments with total n=4-6 mice per group. Mean ±SD are shown. Statistics are based on Two-Way ANOVA with Tukey's test with *:p<0.05; **:p<0.01; ***:p<0.001; and (ns) p>0.05.

We also addressed the phenotype of WT and KO *Tcf7*^{GFP} P14 cells at d3.5 (**Fig 27A**). In line with the above data, KO *Tcf7*$^{GFP+}$ cells divided more, as judged by CTV dilution. However, the percentage of divided *Tcf7*$^{GFP+}$ cells that expressed CD25 or GzmB was not different between WT and KO cells (**Fig 27B-D**). Similarly, no difference was observed among *Tcf7*$^{GFP-}$ cells, which had completely diluted CTV.

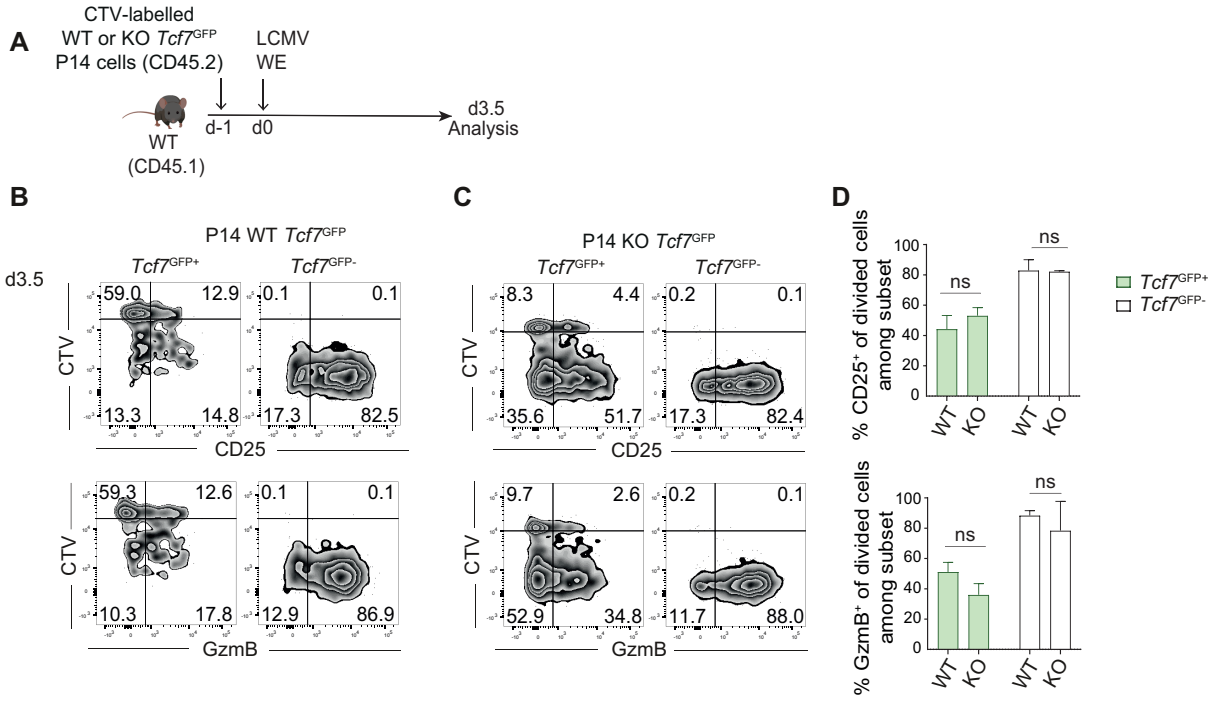

Figure 27 - Cell division and expression pattern of *Tcf7*$^{+}$ and *Tcf7*$^{-}$ cells in presence or absence of Tcf1 protein

(A) Schematic representation of the experimental set-up. WT or KO *Tcf7*^{GFP} P14 cells (CD45.2) were labelled with CTV and transferred into WT (CD45.1) recipients that were infected with LCMV WE one day later. **(B-C)** CTV versus CD25 (top) or GzmB (bottom) expression by WT **(B)** or KO **(C)** *Tcf7*$^{GFP+}$ P14 (left) or *Tcf7*$^{GFP-}$ P14 (right) was analysed at d3.5 p.i.. **(D)** Bar graph depicts frequency of CD25- (top) or GzmB-expressing cells (bottom) among divided cells of the indicated subset on d3.5 p.i.. **(A-D)** The data shown are representative from 2 independent experiments with total n=4 (KO) or n=6 (WT) mice per group. **(D)** Statistics are based on Two-Way ANOVA with Tukey's test with *:p<0.05; **:p<0.01; ***:p<0.001; and (ns) p>0.05.

Thus, Tcf1 protein expression was essential to limit the cycling and thus the expansion of *Tcf7*$^{+}$ cells during the primary response to infection. More efficient cycling of *Tcf7*$^{+}$ cells lacking Tcf1 may explain the impaired stemness of d8 *Tcf7*$^{GFP+}$ cells lacking Tcf1 observed before (Pais Ferreira et al., 2020).

3.3.1 Virus-specific CD8$^+$ T cell response to chronic viral infection in steady state

Our lab has identified memory-like CD8$^+$ T cells (T_{ML}) (defined as Tcf1$^+$ GzmB$^-$ PD1$^+$) that sustain the immune response to chronic viral infection. These cells have stem cell-like properties, they are able to expand, self-renew or differentiate into exhausted T cells (T_{EX}) (Tcf1$^-$ GzmB$^+$ PD1$^+$) (Utzschneider et al., 2016b). These insights are based on cell transfers into infection time- and infection type-matched secondary recipients or recall responses in naive secondary recipients. It is not known whether T_{ML} cells that reside in their natural environment self-renew and differentiate into T_{EX} during chronic viral infection. Further, it is not known at what rate exhausted cells are generated and turnover. These questions were addressed using the *Tcf7*-based lineage tracing model described in part 3.1.

First, we transferred *Tcf7*$^{GFP\text{-}iCre}$ *R26*^{Confetti} P14 cells (CD45.2$^+$) into Vβ5 mice (CD45.1$^+$), which express the β-chain of an Ovalbumin-specific TCR and thus show a reduced endogenous T cell response to LCMV. One day later these recipient mice were infected with LCMV cl13 (**Fig 28A**).

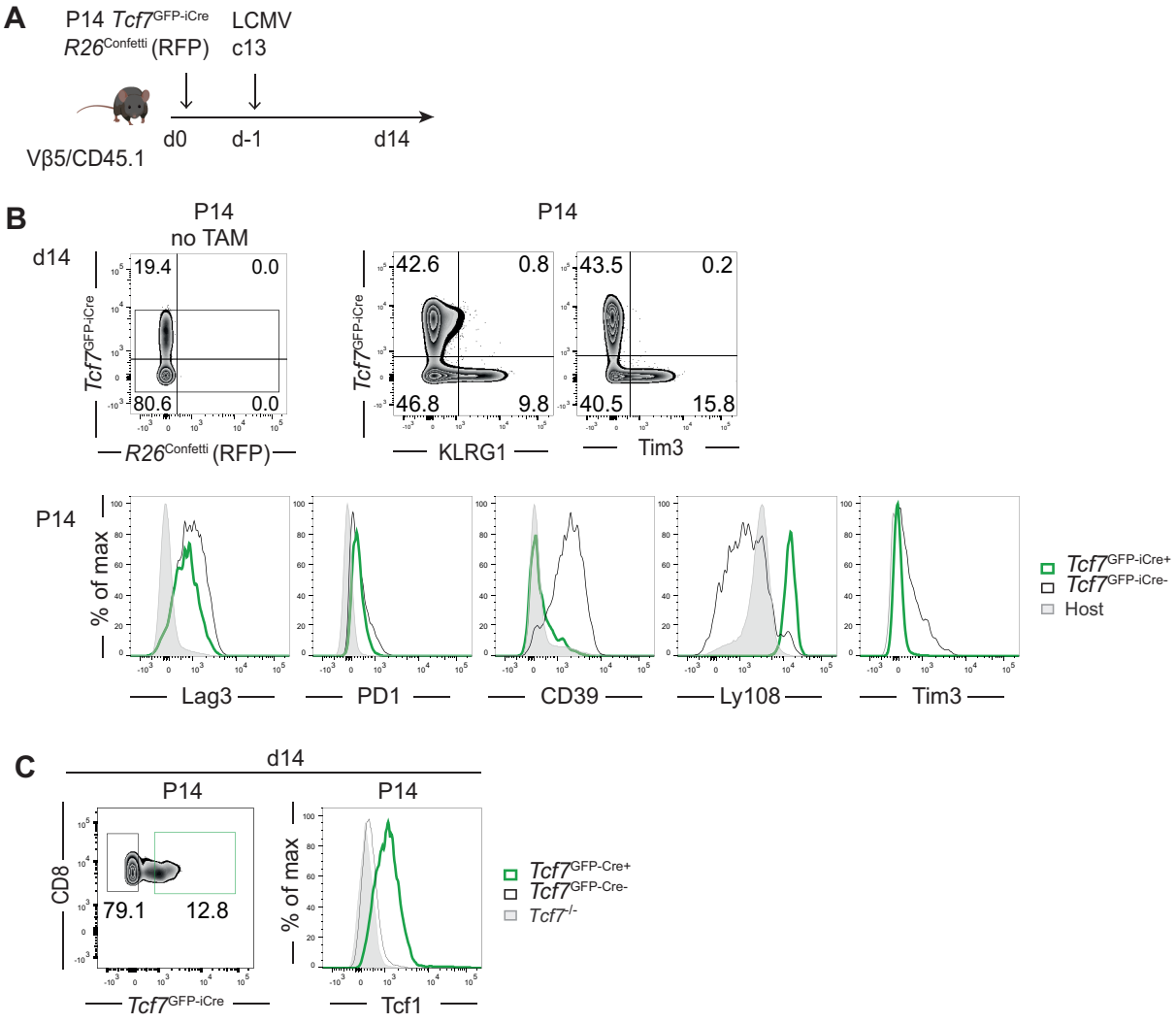

Figure 28 - *Tcf7*$^{GFP\text{-}iCre}$ expression by P14 cells responding to chronic infection

(A) *Tcf7*$^{GFP\text{-}iCre}$ *R26*^{Confetti} P14 cells (CD45.2) were transferred to Vβ5 mice and infected with LCMV cl13 one day later. **(B)** At d14 p.i., P14 cells were analysed for the expression of *Tcf7*$^{GFP\text{-}iCre}$ versus RFP (*R26*^{Confetti}) (left), KLRG1 (centre) or Tim3 (right). Histograms overlays depict the expression of Lag3, PD1, CD39, Ly108 and Tim3 by *Tcf7*$^{GFP\text{-}iCre+}$ (green) and *Tcf7*$^{GFP\text{-}iCre-}$ (black) P14 cells and compared to host CD8$^+$ T cells (grey fill). **(C)** Flow sorted *Tcf7*$^{GFP\text{-}iCre+}$ (green) and *Tcf7*$^{GFP\text{-}iCre-}$ (black) P14 cells were stained for Tcf1 protein and compared to *Tcf7*$^{-/-}$ cells (grey fill). **(A-B)** The data shown are representative of 2 independent experiments with total n=5 mice.

At d14 p.i., we observed a 10-20% of P14 cells expressing *Tcf7*$^{GFP\text{-}iCre+}$ (**Fig 28B**), similar to what was observed with another reporter mouse strain in the lab (Utzschneider et al., 2016b). As expected, cells expressing *Tcf7*$^{GFP\text{-}iCre+}$ co-expressed Slamf6 (Ly108), while *Tcf7*$^{GFP\text{-}iCre-}$ cells expressed CD39, and in part Tim3 and KLRG1 (**Fig 28B**). Both types of cells expressed PD1 and Lag3. Thus, *Tcf7*$^{GFP\text{-}iCre}$ expression properly discriminated T_{ML} from T_{EX}. To ensure the proper detection of Tcf1$^+$ cells by the *Tcf7*$^{GFP\text{-}iCre}$ construct, we flow sorted *Tcf7*$^{GFP\text{-}iCre+}$ and *Tcf7*$^{GFP\text{-}iCre-}$ P14 cells and stained them for Tcf1 protein. All *Tcf7*$^{GFP\text{-}iCre+}$ P14 cells expressed high levels of Tcf1 protein, while *Tcf7*$^{GFP\text{-}iCre-}$ P14 cells lacked Tcf1 protein (**Fig 28C**). Thus, the *Tcf7*$^{GFP\text{-}iCre}$ construct properly tracked Tcf1 expressing cells during chronic viral infection.

3.3.2 Self-renewal and differentiation of Memory-like *Tcf7*$^+$ T cells during chronic viral infection

Chronically-infected Vβ5 mice harbouring *Tcf7*$^{GFP\text{-}iCre}$ *R26*^{Confetti} P14 cells were injected with TAM at d14 p.i. (**Fig 29A**). Some mice were analysed 2 days after the last labelling (d18 p.i.), hereby named week 0. At this stage, we detected a small population of RFP$^+$ cells (1.5% of P14 cells) (**Fig 29B, C**). All these cells were *Tcf7*$^{GFP\text{-}iCre+}$ (**Fig 29B, D**). These data showed that only *Tcf7*$^{GFP\text{-}iCre+}$ cells had been labelled and that differentiation of *Tcf7*$^{GFP\text{-}iCre+}$ cells into *Tcf7*$^{GFP\text{-}iCre-}$ cells had not occurred between d14 and d18 p.i.. We then followed the size and the composition of the RFP$^+$ P14 population over time. One week later (d25 p.i.), the size of the RFP$^+$ population had not changed (1.6% of P14), but at 4 weeks post-labelling (d46 p.i.), the RFP$^+$ population showed a tendency to increase (3.6% of P14) (**Fig 29C**). Interestingly, the fraction of *Tcf7*$^{GFP\text{-}iCre+}$ RFP$^+$ cells did not change over time (1.3-1.5% of P14) (**Fig 29E**). Conversely, *Tcf7*$^{GFP\text{-}iCre-}$ RFP$^+$ cells were very rare at week 1 (0.1% of P14) but were considerably more abundant at week 4 (2.3% of P14) (**Fig 29E**).

Phenotypically, *Tcf7*$^{GFP\text{-}iCre+}$ RFP$^+$ cells expressed CD62L and Ly108 (not shown) and lacked the effector markers KLRG1 and Tim3, throughout the tracing period (**Fig 29F**), very similar to non-labelled *Tcf7*$^{GFP\text{-}iCre+}$ cells. On the other hand, at week 1, the rare *Tcf7*$^{GFP\text{-}iCre-}$ RFP$^+$ cells lacked KLRG1 and expressed low Tim3 levels. At week 4, *Tcf7*$^{GFP\text{-}iCre-}$ RFP$^+$ cells partially acquired both KLRG1 and Tim3, very similar to non-labelled *Tcf7*$^{GFP\text{-}iCre-}$ cells (**Fig 29F**).

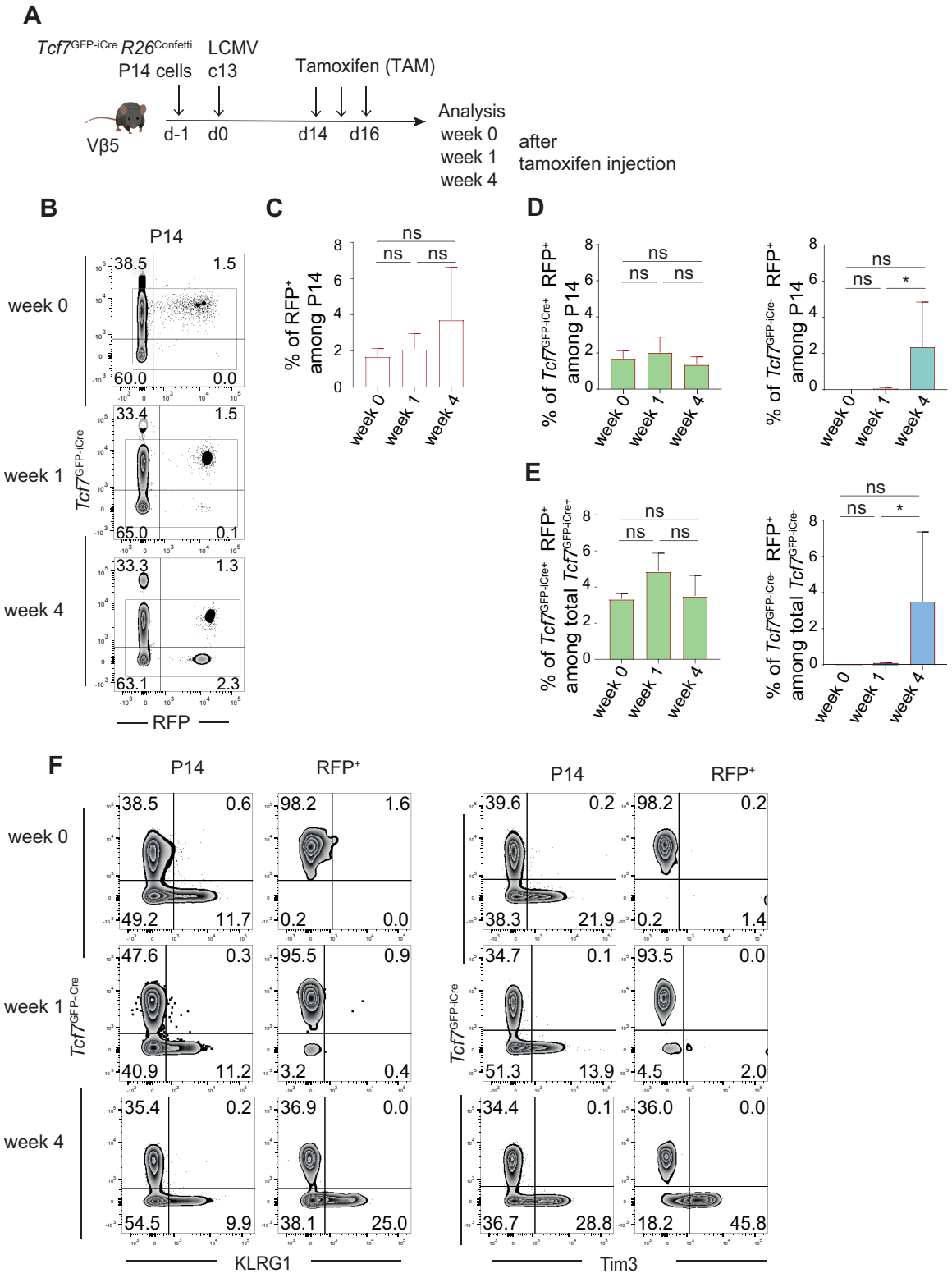

Figure 29 - Fate of *Tcf7*$^{GFP\text{-}iCre+}$ P14 cells during chronic infection
(A) *Tcf7*$^{GFP\text{-}iCre}$ *R26*^{Confetti} P14 cells (CD45.2) were transferred into Vβ5 mice and infected with LCMV cl13 one day later. Mice were injected with tamoxifen (TAM), starting at d14 p.i., daily for 3 consecutive days. **(B)** Gated P14 cells were analysed for GFP (*Tcf7*$^{GFP\text{-}iCre}$) versus RFP (*R26*^{Confetti}) expression 2 days after tamoxifen injection (named week 0), as well as 1 and 4 weeks later tamoxifen infection. **(C)** Frequency of RFP$^+$ among P14 cells. **(D)** Frequency of RFP$^+$ *Tcf7*$^{GFP\text{-}iCre+}$ (left) and RFP$^+$ *Tcf7*$^{GFP\text{-}iCre-}$ (right) among P14 cells over time. **(E)** Fraction of RFP$^+$ *Tcf7*$^{GFP\text{-}iCre+}$ among total *Tcf7*$^{GFP\text{-}iCre+}$ P14 cells over time (left). Fraction of RFP$^+$ *Tcf7*$^{GFP\text{-}iCre-}$ among total *Tcf7*$^{GFP\text{-}iCre-}$ P14 cells over time (right). **(F)** Expression of *Tcf7*$^{GFP\text{-}iCre}$ versus KLRG1 (left) or Tim3 (right) in total P14 or total

RFP$^+$ cells. **(A-F)** The data shown is from 1 experiment with n=3 mice per group. Mean ±SD are shown. Statistics are based on Non-paired two-tailed Student's test (A-K) with *:p<0.05; **:p<0.01; ***:p<0.001; and (ns) p>0.05.

Thus, *Tcf7*$^{GFP\text{-}iCre-}$ RFP$^+$ P14 cells gradually increased over time, and it took 4 weeks until the proportion of labelled *Tcf7*$^{GFP\text{-}iCre-}$ cells (RFP$^+$ *Tcf7*$^{GFP\text{-}iCre-}$ of total *Tcf7*$^{GFP\text{-}iCre-}$ cells) (3.51%) reached that of labelled *Tcf7*$^{GFP\text{-}iCre+}$ cells (RFP$^+$ *Tcf7*$^{GFP\text{-}iCre+}$ of total *Tcf7*$^{GFP\text{-}iCre+}$ cells) (3.75%) (**Fig 29E**). Thus, the turnover of the T_{EX} was surprisingly slow. As the *Tcf7*$^{GFP\text{-}iCre+}$ RFP$^+$ P14 cells generated *Tcf7*$^{GFP\text{-}iCre-}$ RFP$^+$ cells while maintaining the population of *Tcf7*$^{GFP\text{-}iCre+}$ RFP$^+$ P14 cells (**Fig 29D**), we concluded that *Tcf7*$^{GFP\text{-}iCre+}$ RFP$^+$ cells present in the spleen of chronically-infected mice self-renewed and yielded differentiated progeny.

Since the labelling efficiency using *Tcf7*$^{GFP\text{-}iCre}$ *R26*^{Confetti} cells was low, we used the *Tcf7*$^{GFP\text{-}iCre}$ *R26*^{Tomato} P14 mice to corroborate the above data (**Fig 18A**). We transferred *Tcf7*$^{GFP\text{-}iCre}$ *R26*^{Tomato} P14 cells (CD45.2$^+$) into Vβ5 mice (CD45.1$^+$) that were infected with LCMV cl13. At d14 p.i., mice were injected once with TAM. Some mice were analysed 2 days later (named week 0, hereafter). At this stage (d16 p.i.), we detected a considerable population of Tom$^+$ cells (8% of P14) (**Fig 30A, B**). All these cells were *Tcf7*$^{GFP\text{-}iCre+}$, confirming that only *Tcf7*$^{GFP\text{-}iCre+}$ cells had been labelled and that differentiation of *Tcf7*$^{GFP\text{-}iCre+}$ into *Tcf7*$^{GFP\text{-}iCre-}$ cells had not occurred between d14 and d16 p.i..

The size of the Tom$^+$ population was increased one week later (16-25% of P14) and was relatively stable at 2 and 3 weeks post-labelling (around 17% of P14) (**Fig 30A, B**). The fraction of *Tcf7*$^{GFP\text{-}iCre+}$ Tom$^+$ cells followed a similar trend and remained relatively stable at 2-3 weeks post-labelling (10-12% of P14). Conversely, *Tcf7*$^{GFP\text{-}iCre-}$ Tom$^+$ cells were absence at week 0, very rare at week 1 (2% of P14) and progressively increased at week 2 (7% of P14) and 3 (10% of P14) (**Fig 30C, D**). Phenotypically, *Tcf7*$^{GFP\text{-}iCre+}$ Tom$^+$ cells lacked the effector markers KLRG1 and Tim3, very similar to *Tcf7*$^{GFP\text{-}iCre-}$ cells (**Fig 30E**). On the other hand, at week 1, the rare *Tcf7*$^{GFP\text{-}iCre-}$ Tom$^+$ cells mostly lacked KLRG1 and expressed Tim3, while by week 2, *Tcf7*$^{GFP\text{-}iCre-}$ Tom$^+$ cells had acquired these markers, very similar to non-labelled *Tcf7*$^{GFP\text{-}iCre-}$ cells (**Fig 30E**).

At 3 weeks post-labelling, the proportion of labelled *Tcf7*$^{GFP\text{-}iCre-}$ cells (Tom$^+$ *Tcf7*$^{GFP\text{-}iCre-}$ of total *Tcf7*$^{GFP\text{-}iCre-}$ cells) (14%) had not yet reached that of labelled *Tcf7*$^{GFP\text{-}iCre+}$ cells (Tom$^+$ *Tcf7*$^{GFP\text{-}iCre+}$ of total *Tcf7*$^{GFP\text{-}iCre+}$ cells) (20%) (**Fig 30D**), similar to the slow turnover observed above. Further, even though Tom$^+$ *Tcf7*$^{GFP\text{-}iCre+}$ cells generated *Tcf7*$^{GFP\text{-}iCre-}$ cells, the population of Tom$^+$ *Tcf7*$^{GFP\text{-}iCre+}$ cells was relatively constant over time (week 0 versus week 3). These data confirmed that Tom$^+$ *Tcf7*$^{GFP\text{-}iCre+}$ cells present in the spleen of chronically-infected mice self-renewed and yielded differentiated progeny with a relatively slow turnover.

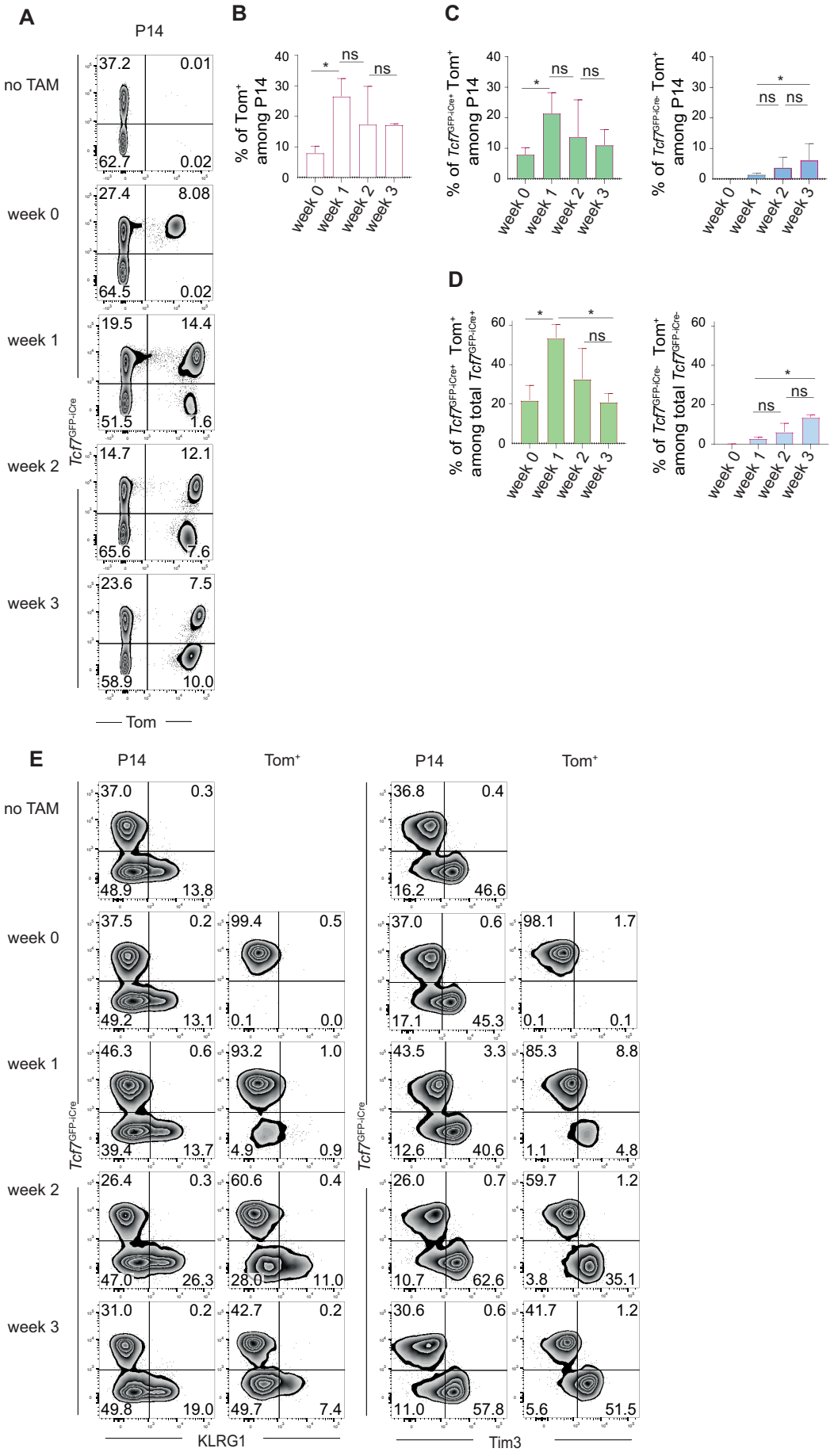
A
P14
no TAM
week 0
week 1
week 2
week 3
37.2
0.01
62.7
0.02
27.4
8.08
64.5
0.02
19.5
14.4
51.5
1.6
14.7
12.1
65.6
7.6
23.6
7.5
58.9
10.0
Tcf7GFP-iCre
Tom
B
% of Tom+ among P14
ns
*
ns
week 0
week 1
week 2
week 3
C
% of Tcf7GFP-iCre+ Tom+ among P14
% of Tcf7GFP-iCre- Tom+ among P14
D
% of Tcf7GFP-iCre+ Tom+ among total Tcf7GFP-iCre+
% of Tcf7GFP-iCre- Tom+ among total Tcf7GFP-iCre-
E
P14
Tom+
37.0
0.3
48.9
13.8
99.4
0.5
0.1
0.0
36.8
0.4
16.2
46.6
98.1
1.7
0.1
0.1
37.5
0.2
49.2
13.1
37.0
0.6
17.1
45.3
46.3
0.6
39.4
13.7
93.2
1.0
4.9
0.9
43.5
3.3
12.6
40.6
85.3
8.8
1.1
4.8
26.4
0.3
47.0
26.3
60.6
0.4
28.0
11.0
26.0
0.7
10.7
62.6
59.7
1.2
3.8
35.1
31.0
0.2
49.8
19.0
42.7
0.2
49.7
7.4
30.6
0.6
11.0
57.8
41.7
1.2
5.6
51.5
KLRG1
Tim3

Figure 30 - Fate of *Tcf7*$^{GFP\text{-}iCre+}$ P14 cells during chronic infection as determined using restricted labelling
(A) *Tcf7*$^{GFP\text{-}iCre}$ *R26*^{Tomato} P14 cells (CD45.2^{+}) were transferred into Vβ5 mice (CD45.1^{+}) and infected with LCMV cl13 one day later. Mice were injected with tamoxifen (TAM) once at d14 p.i.. Gated P14 cells were analysed for the expression of GFP (*Tcf7*$^{GFP\text{-}iCre}$) versus Tomato (*R26*^{Tomato}) shortly after tamoxifen injection (week 0), and weekly until three weeks later. **(B)** Frequency of Tom^{+} cells among P14 cells. **(C)** Frequency of Tom^{+} *Tcf7*$^{GFP\text{-}iCre+}$ (left) or Tom^{+} *Tcf7*$^{GFP\text{-}iCre-}$ (right) among P14 cells over time. **(D)** Fraction of Tom^{+} *Tcf7*$^{GFP\text{-}iCre+}$ among total *Tcf7*$^{GFP\text{-}iCre+}$ cells over time (left). Fraction of Tom^{+} *Tcf7*$^{GFP\text{-}iCre-}$ among total *Tcf7*$^{GFP\text{-}iCre-}$ cells over time (right). **(E)** Expression of *Tcf7*$^{GFP\text{-}iCre}$ versus KLRG1 (left) or Tim3 (right) in total P14 or total Tom^{+} cells. **(A-E)** The data shown is from 1 experiment with n=3 mice per group. Mean ±SD are shown. Statistics are based on Non-paired two-tailed Student's test (A-K) with *:p<0.05; **:p<0.01; ***:p<0.001; and (ns) p>0.05.

3.3.3 Heterogeneity of CD8^{+} T cells responding to chronic infection and differentiation trajectory downstream of Memory-like T cells

Initial studies showed that T_{ML} CD8^{+} T cells continuously yielded T_{EX} CD8^{+} T cells during chronic infection (Im et al., 2016; Utzschneider et al., 2016b; Wang et al., 2019; Wu et al., 2016). We addressed whether there was further heterogeneity among CD8^{+} T cells responding to chronic infection. Based on bulk RNAseq, we identified Ly108 as a marker for memory-like cells (Utzschneider et al., 2016b). Here, we tested CX3CR1 as a marker of exhausted cells. Indeed, staining of Ly108 versus CX3CR1 identified 3 main subpopulations of CD8^{+} T cells responding to chronic infection (**Fig 31A**).

To further address heterogeneity of CD8^{+} T cells responding to chronic infection, we performed multicolour flow cytometry using the following markers (Tcf7, Ly108, CX3CR1, PD1 and CD39) and presented the data in a t-SNE format (**Fig 31B**). This identified 3 main clusters of cells. Two of these subsets lacked CX3CR1. *Tcf7* expression was present on one subset, co-expressed with Ly108 and intermediate levels of PD1, but lacking all the other markers. This cluster represented T_{ML} cells (encircled with an orange frame). The other CX3CR1^{-} population, lacked *Tcf7* and Ly108 but expressed high levels of PD1 and CD39. These cells may correspond to a terminally exhausted (called T_{TEX}) subset (blue frame). The remaining cluster of cells expressed CX3CR1 (black frame). A minority of CX3CR1^{+} cells expressed elevated levels of Ly108 and low levels of CD39, while most cells expressed low levels of Ly108 and intermediate levels of CD39 (**Fig 31B**). Based on their intermediate phenotype this subset was termed transitory subset (T_{trans}, black frame).

A second staining panel further assessed cell cycling. This distinguished 4 main clusters of cells (**Fig 31C**). The T_{ML} subset (Tcf1^{+} CX3CR1^{-}) (orange frame) and the terminally exhausted (T_{TEX}) (Tcf1^{-} CX3CR1^{-}) (dark blue frame) subsets were predominantly quiescent (mKi67^{-}). The transitory CX3CR1^{+} population contained a cycling (T_{trans1}, pink frame) and a non-cycling subset (T_{trans2}, cyan frame). The latter included occasional Tcf1^{+} cells.

We directly assessed cycling in CD8^{+} T cells separated based on Ly108 versus CX3CR1 expression. Subsets lacking CX3CR1 (Ly108^{+} T_{ML} cells and Ly108^{-} T_{TEX} cells) were mostly quiescent (**Fig 31D**). However, some CX3CR1^{+} (T_{trans}) cells cycled relatively efficiently (**Fig 31D**). This suggested sequential stages in which some Ly108^{+} cells acquired CX3CR1 and actively started to cycle, followed by downregulation of Ly108 and continued cycling,

eventually returning to a post-cycling CX3CR1^{+} state, before downregulating CX3CR1 to become terminally differentiated.

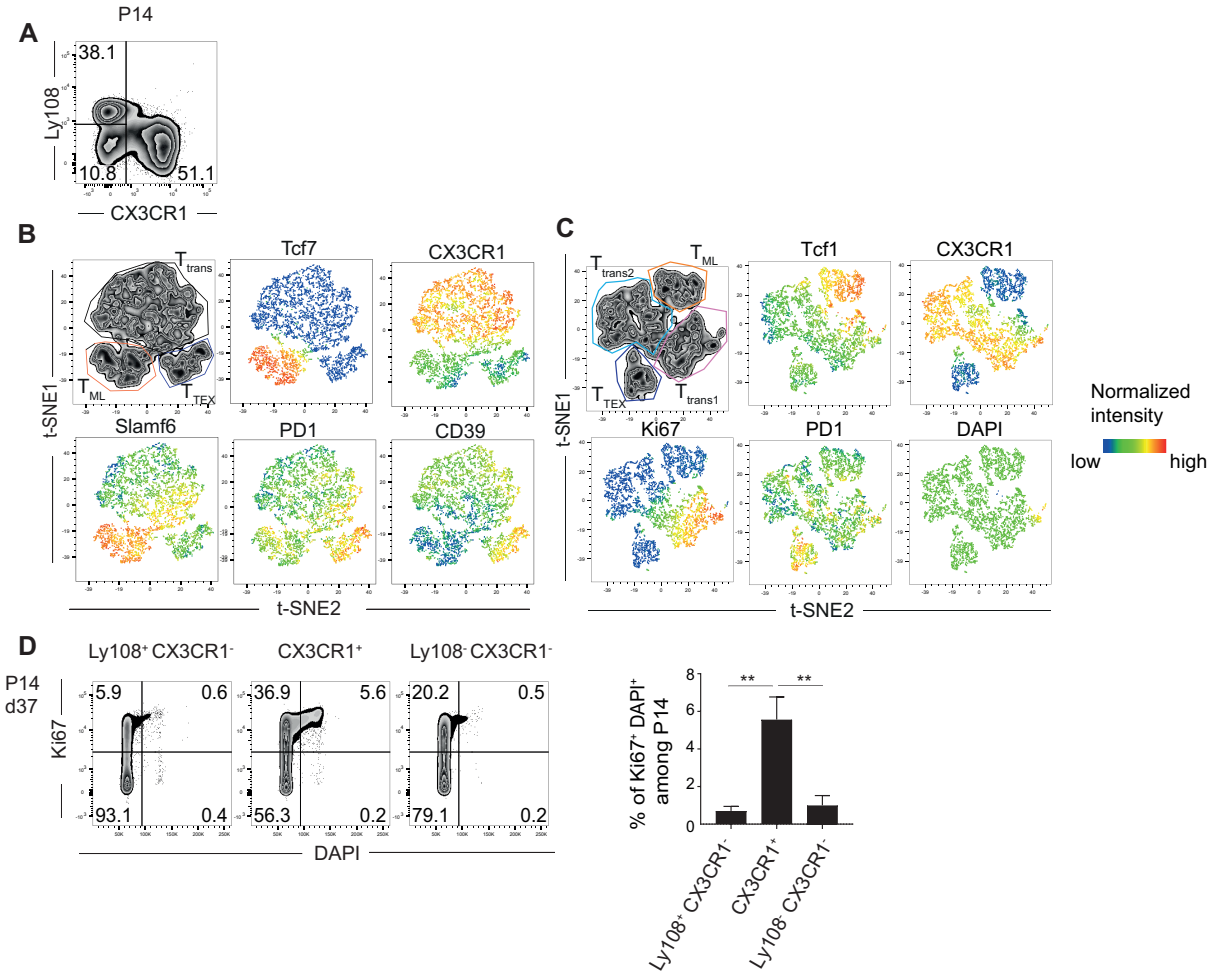

Figure 31 - Heterogeneity of CD8^{+} T cells responding to chronic infection
Tcf7$^{GFP\text{-}iCre}$ *R26*^{Tomato} P14 cells (CD45.2^{+}) were transferred into Vβ5 mice (CD45.1^{+}) and infected with LCMV cl13 one day later. Mice were injected with TAM once at d14 p.i.. **(A)** Expression of Ly108 versus CX3CR1 on total P14 cells. **(B)** t-distributed stochastic neighbour embedding (t-SNE) projection of P14 cells, coloured according to their cluster annotation, based on Tcf7, Ly108, CX3CR1, PD1 and CD39 expression. **(C)** t-SNE projection of P14 cells, coloured according to their cluster annotation, based on Tcf1, CX3CR1, Ki67 and DAPI expression. **(D)** Cycling profile (expression of Ki67 versus DAPI) by CD8^{+} T cell subsets defined by differential Ly108 versus CX3CR1 expression at d37 p.i. Bar graph depicts frequency of Ki67^{+} DAPI^{+} cells among P14 cells. **(D)** The data shown is from 1 experiment with n=3 mice per group. Mean ±SD are shown. Statistics are based on One-way ANOVA with *:p<0.05; **:p<0.01; ***:p<0.001; and (ns) p>0.05.

While this study was underway, other groups reported heterogeneity of exhausted CD8^{+} T cells (Beltra et al., 2020; Hudson et al., 2019; Zander et al., 2019). However, these studies differed regarding the differentiation trajectories downstream of T_{ML}. Consistent with the above suggestion, a linear differentiation model suggested that T_{ML} cells give rise to CX3CR1^{+} transitory exhausted cells (T_{trans}) and these then differentiate into terminally exhausted CX3CR1^{-} cells (T_{TEX}) (Beltra et al., 2020; Hudson et al., 2019). Other papers suggested that

T_{ML} give rise to CX3CR1$^+$ T_{trans} or CX3CR1$^-$ T_{TEX} (Chen et al., 2019; Zander et al., 2019). Unfortunately, these subsets have been described using different sets of markers (CD69, CD101, Tox, CX3CR1, Tim3), which may contribute in part to the distinct outcome/interpretation of the differentiation trajectories (Beltra et al., 2020; Hudson et al., 2019; Zander et al., 2019). Hereby, we addressed the trajectories of *Tcf7*$^+$ T_{ML} cells using lineage tracing.

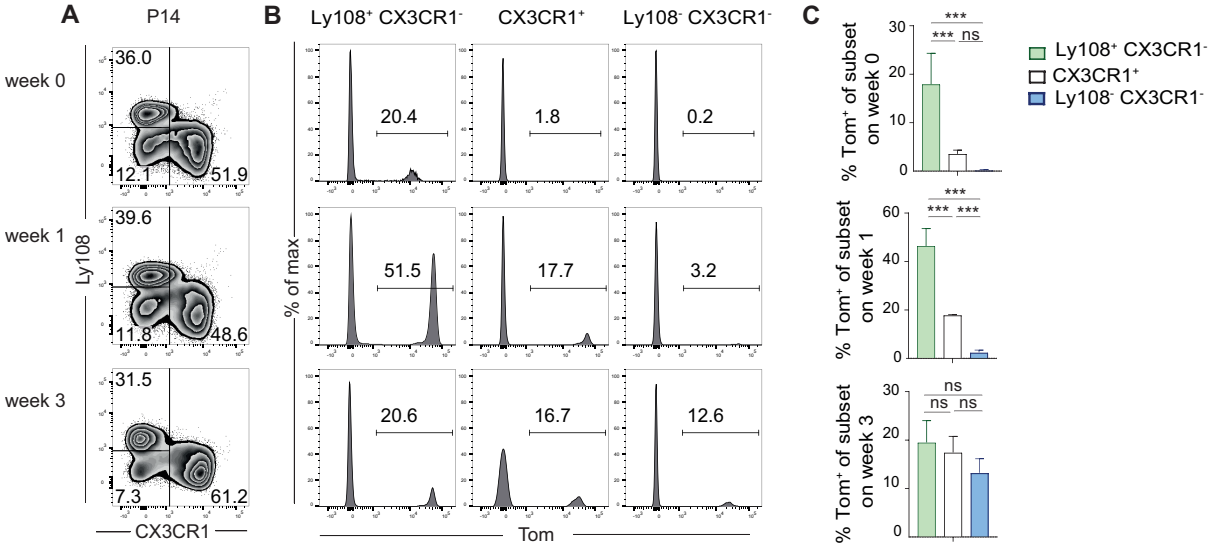

Figure 32 - Differentiation trajectory of *Tcf7*$^{GFP\text{-}iCre+}$ CD8$^+$ T cells during chronic infection
Tcf7$^{GFP\text{-}iCre}$ *R26*^{Tomato} P14 cells (CD45.2$^+$) were transferred into Vβ5 mice (CD45.1$^+$) and infected with LCMV cl13 one day later. Mice were injected with TAM once at d14 p.i.. **(A)** Expression of Ly108 versus CX3CR1 on gated P14 cells over time. **(B)** Histograms depict the expression of Tom by P14 Ly108$^+$ CX3CR1$^-$ (left), P14 CX3CR1$^+$ (centre) and P14 Ly108$^-$ CX3CR1$^-$ (right) cells. Numbers depict frequency of positive within the gated cells. **(C)** Bar graphs show frequency of total Tom$^+$ cells among subsets identified by Ly108 and CX3CR1 differential expression on week 0 (top), 1 (middle) or 3 (bottom) post-labelling. **(A-C)** The data shown derive from 1 experiment with n=3 mice per group. Mean ±SD are shown. Statistics are based on Non-paired two-tailed Student's test with *:p<0.05; **:p<0.01; ***:p<0.001; and (ns) p>0.05.

We transferred *Tcf7*$^{GFP\text{-}iCre}$ *R26*^{Tomato} P14 cells (CD45.2$^+$) into Vβ5 mice (CD45.1$^+$) that were infected with LCMV cl13 one day later. At d14 p.i., mice were injected once with TAM. Some mice were analysed 2 days later (named week 0) and then weekly for 3 weeks. Total P14 cells contained 3 main subpopulations of Ly108 versus CX3CR1 defined cells, which remained relatively constant over time (**Fig 32A**). When looking at labelled cells on week 0, we observed that almost all Tom$^+$ cells were Ly108$^+$ and very few labelled CX3CR1$^+$ were present (**Fig 32B, C**). At week 1, Tom$^+$ cells were predominantly Ly108$^+$. Interestingly, a fraction of CX3CR1$^+$ were also Tom$^+$ cells, while labelled Ly108$^-$ CX3CR1$^-$ were almost inexistant. This suggested that some Tom$^+$ Ly108$^+$ cells upregulated CX3CR1$^+$, before cells lacking both Ly108 and CX3CR1 become detectable. At week 3, the fraction of Tom$^+$ Ly108$^-$ CX3CR1$^-$ cells had become similar to that of Tom$^+$ CX3CR1$^+$ and Ly108$^+$ CX3CR1$^-$ cells. Thus, the data

suggested that T_{ML} cells differentiated into CX3CR1^{+} transitory exhausted cells (T_{trans}) that accumulated, prior to further differentiation to Ly108^{-} CX3CR1^{-} terminally exhausted cells (T_{TEX}), in a linear differentiation trajectory.

3.4. Extrinsic signals that regulate the expression of Tcf1 in CD8$^+$ T cells *in vitro*

Tcf1 is expressed by all naive CD8$^+$ T cells. During acute infection, Tcf1 is downregulated in most but not all CD8$^+$ T cells during the effector phase and is expressed in memory cells (Boudousquie et al., 2014; Jeannet et al., 2010; Zhao et al., 2010). Downregulation of Tcf1 thus correlated with effector differentiation, while maintenance of Tcf1 expression was required for memory formation. These observations indicated an important role of the signals that controlled Tcf1 expression in effector versus memory differentiation. A productive T cell response depends on the activation of naive CD8$^+$ T cell via T cell receptor (TCR; signal 1), co-stimulatory molecules (such as CD28, CD27; signal 2) and inflammatory cytokines (IL12, type I IFN; signal 3) (Masopust and Schenkel, 2013). Using a DC vaccination system, the lab had found that systemic inflammatory signals were responsible for the downregulation of Tcf1 and effector differentiation (Danilo et al., 2018). Here we were interested to establish an *in vitro* system to identify cytokines that suppress or induce Tcf1 expression in order to modulate effector versus memory differentiation.

3.4.1. Suppression of Tcf1 expression in activated T cells by IL12 *in vitro*

To address whether cytokines modulated Tcf1 expression *in vitro*, naive CFSE-labelled P14 cells were cultured with gp33 peptide-pulsed splenocytes (**Fig 33A**).

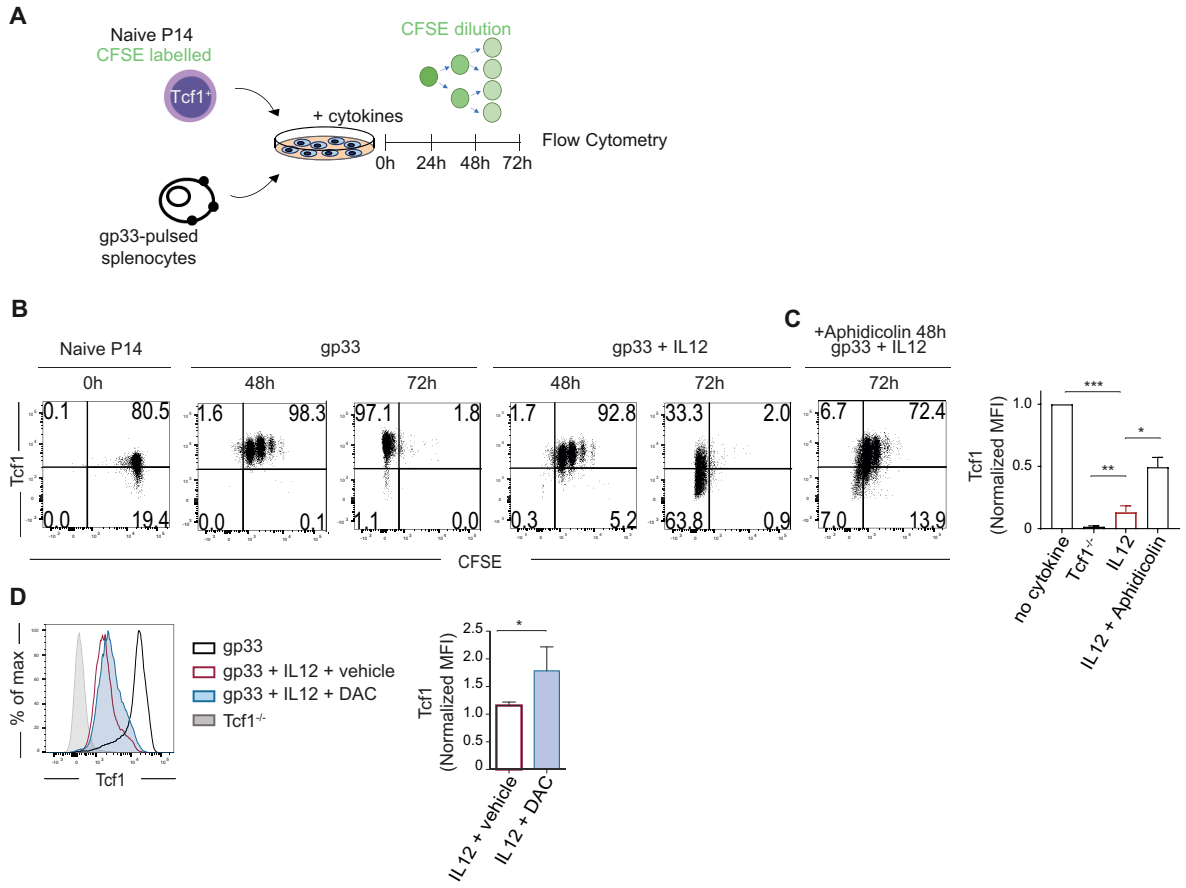

Figure 33 - Tcf1 is downregulated upon culture with proinflammatory cytokines *in vitro*
(A) Schematic representation of the experimental set-up. CFSE-labelled P14 cells were activated *in vitro* with gp-33 peptide-pulsed splenocytes. **(B)** Expression of Tcf1 versus CFSE of P14 cells prior to cell culture (left) or upon 48h

or 72h without (centre) or upon addition of IL12 (right). **(C)** Gated stimulated P14 cells cultured with IL12 were analysed for expression of Tcf1 versus CFSE upon addition of aphidicolin (1µg) at 48h post-stimulation. Bar graph depicts normalized MFI of Tcf1 of P14 cells cultured under the indicated conditions for 72h. **(D)** Expression of Tcf1 of stimulated P14 cells (black), cultured with IL12 and vehicle (red) or Decitabine (DAC) (blue filled) added at 48h, and analysed after 72h post gp33-stimulation, compared to $Tcf1^{-/-}$ (grey fill). Bar graphs depict the MFI of Tcf1 in P14 cells cultured under the indicated conditions, normalized to with IL12 and vehicle (red). **(A-D)** The data shown are representative of at least 2 independent experiments with total n>4 per group. Mean ±SD are shown. Statistics are based on Non-paired two-tailed Student's test with *:p<0.05; **:p<0.01; ***:p<0.001; and (ns) p>0.05.

At 48h post-stimulation, P14 cells had undergone few cell divisions and by 72h they had completely diluted CFSE (**Fig 33B**). In the process, P14 cells maintained high levels of Tcf1 expression (**Fig 33B**). Addition of IL12 did not change Tcf1 during the first 3 divisions at 48h, but induced abrupt Tcf1 downregulation at 72h of stimulation (**Fig 33B**). Thus, the inflammatory cytokine IL12 suppressed Tcf1 expression in activated $CD8^+$ T cells.

As Tcf1 suppression occurred after the first 3 cell divisions, we tested whether it depended on cell division. We thus activated $CD8^+$ T cells in the presence of Aphidicolin, which is a DNA polymerase inhibitor that blocks cell cycle progression at the G1/S phase. Adding Aphidicolin to IL12-stimulated $CD8^+$ T cells at 48h after activation, efficiently arrested cell cycle progression (no further CFSE dilution) at 72h. Interestingly, this prevented Tcf1 downregulation (**Fig 33C**). Thus, IL12-mediated Tcf1 downregulation depended on cell cycling.

To test whether IL12 suppressed Tcf1 based on epigenetic mechanisms, we treated activated cells with the DNA methyltransferase inhibitor Decitabine (DAC), which prevents *de novo* DNA methylation. Adding DAC to $CD8^+$ T cells at 48h after activation, improved Tcf1 expression in IL12-stimulated cells (**Fig 33D**). This indicated that IL12 induced epigenetic silencing of Tcf1 in cycling cells.

3.4.2. Regulation of Tcf1 expression in activated T cells by cytokines *in vitro*

We tested in a similar fashion a whole panel of cytokines for their ability to suppress Tcf1 expression. In addition to IL12, IL4 and to a lesser extent IL27 and IFNβ were also able to suppress Tcf1 expression (**Fig 34A**). Thus, only certain pro-inflammatory cytokines as well as IL4 (in agreement with (Maier et al., 2011)) were able to downregulate Tcf1 in activated $CD8^+$ T cells *in vitro*.

As we found no cytokines that increased Tcf1 expression in activated $CD8^+$ T cells *in vitro*, we next tested whether certain cytokines were able to counteract IL12-mediated Tcf1 downregulation. We found that TGFβ efficiently opposed IL12-mediated Tcf1 downregulation *in vitro* (**Fig 34B, C**). This was not a general property of immunoregulatory cytokines, as IL10 did not oppose IL12-mediated Tcf1 downregulation. Since Tcf1 suppression required cell division (**Fig 33C**) and TGFβ is known to reduce $CD8^+$ T cell proliferation (Kehrl et al., 1986), we addressed the proliferation of the P14 cells. Addition of TGFβ alone reduced CFSE dilution, but this was restored to normal upon addition of IL12 (**Fig 34C, D**). Thus, IL12-mediated Tcf1 downregulation was reverted by TGFβ and this was not due to reduced cycling of the cells.

Interestingly, TGFβ also prevented Tcf1 downregulation induced by IL27 and IFNβ, but failed to reverse IL4-mediated Tcf1 downregulation (**Fig 34E**). These data suggested that not all cytokines regulate Tcf1 through the same mechanism.

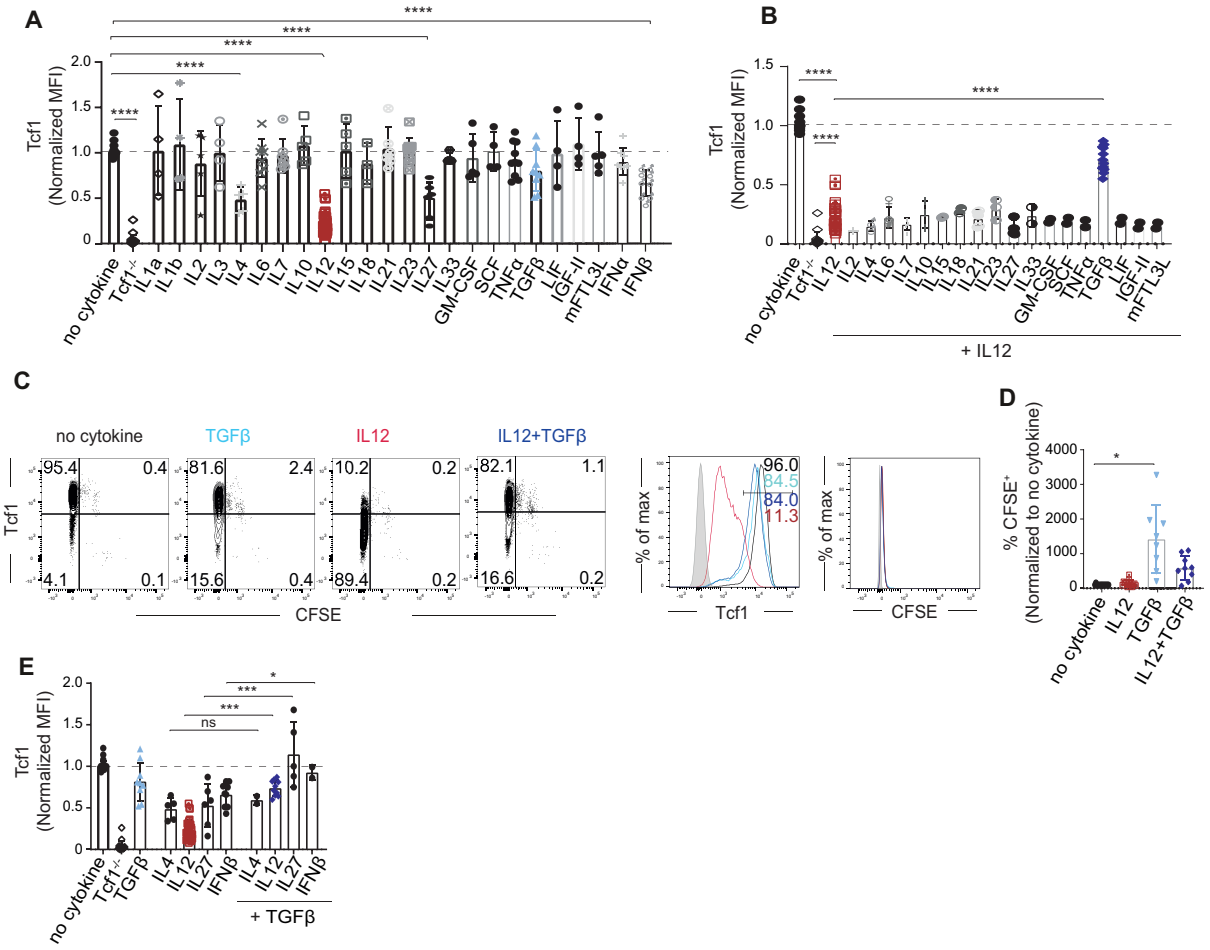

Figure 34 - Addition of TGFβ reverts IL12-mediated Tcf1 *in vitro*
(A-B) Bar graphs depict Normalized MFI of Tcf1 of P14 cells cultured on the indicated conditions after 72h post gp33-stimulation, compared to culture without any cytokine. **(C)** Expression of Tcf1 versus CFSE of P14 cells stimulated (left), upon addition of TGFβ (centre left), IL12 (centre right) or IL12 and TGFβ (right), after 72h of culture. Histograms depicts Tcf1 (left) or CFSE (right) expression of stimulated P14 cells (black), cultured with TGFβ (cyan), IL12 (red) or IL12+TGFβ (dark blue), compared to Tcf1$^{-/-}$ (grey fill). Numbers depict frequency of positive within the gated cells. **(D)** Frequency of normalized CFSE^{+} P14 cells, upon the indicated conditions. **(E)** Normalized MFI of Tcf1 of stimulated P14 cells, upon the indicated conditions. **(A-E)** The data shown are representative of at least 2 independent experiments with total n>4 per group. Mean ±SD are shown. Statistics are based on Non-paired two-tailed Student's test with *:p<0.05; **:p<0.01; ***:p<0.001; and (ns) p>0.05.

IL12 binding to IL12Rβ leads to the activation of JAK2 and then to STAT4 and, to a lesser extent STAT5. IL12R signalling can also active STAT1 through TYK2 (Gollob et al., 1998). We tested whether STAT4 was required for Tcf1 downregulation by IL12. Indeed, IL12 failed to downregulate Tcf1 when added to activated STAT4-deficient P14 cells (**Fig 35A, B**).

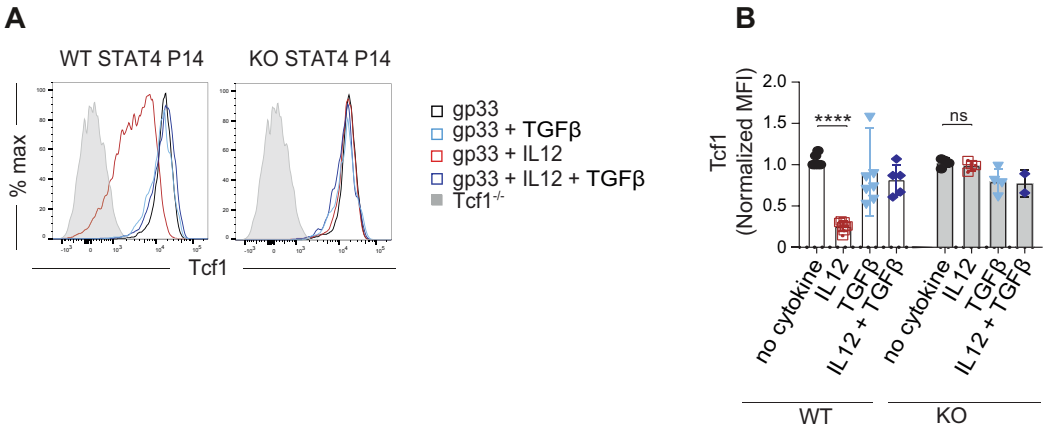

Figure 35 - IL12-mediated Tcf1 downregulation is dependent on STAT4 signalling *in vitro*
(A) Histograms depicts Tcf1 expression of WT (left) or KO STAT4 P14 cells (right) at the indicated conditions. **(B)** Bar graph depicts Tcf1 normalized MFI of WT or KO STAT4 P14 cells at the indicated conditions. **(A-B)** The data shown are representative of at least 2 independent experiments with total n=2-7 per group. Mean ±SD are shown. Statistics are based on Non-paired two-tailed Student's test with *:p<0.05; **:p<0.01; ***:p<0.001; and (ns) p>0.05.

Altogether, we found that Tcf1 expression was regulated by cytokines, whereby IL4, IL12, IL27 and IFNβ downregulated Tcf1. IL12-mediated Tcf1 downregulation depends on STAT4 signalling. TGFβ prevented Tcf1 downregulation by IL12, IL27 and IFNβ but not by IL4. Future experiments are needed to address how IL12/STAT4 signalling suppresses (rather than activates) Tcf1 expression and how TGFβ prevents this.

Personal contributions to published or planned publications

Danilo, M., Chennupati, V., **Silva, J.G.**, Siegert, S. & Held, W. (2018). Suppression of Tcf1 by Inflammatory Cytokines Facilitates Effector CD8 T Cell Differentiation. *Cell Reports*, 22, 2107-2117.

- Performed *in vitro* assays with naive $CD8^+$ T cells stimulated with gp33 peptide-pulsed splenocytes (Fig. 4A-C, E, Fig. S3C of the manuscript).

Pais Ferreira, D., **Silva, J.G.**, Wyss, T., Fuertes Marraco, S.A, Scarpellino, L., Charmoy, M., Maas, R., Siddiqui, I., Tang, L., Joyce, J.A., Delorenzi, M., Luther, S.A., Speiser, D.E., Held, W. (2020). Central Memory $CD8^+$ T Cells Derive From Stem-like *Tcf7*^{hi} Effector Cells In the Absence of Cytotoxic Differentiation. *Immunity*, 53, 1-16.

- Performed *in vivo* lineage cell tracing experiments of $Tcf1^+$ effector-phase $CD8^+$ T cells during acute infection (Fig. 3A-E; Fig. S5A-I of the manuscript).

Silva, J.G., Pais Ferreira, D., Wyss, T., Charmoy, M., Held, W. *Tcf7* guided fate mapping delineates the origin of effector and memory $CD8^+$ T cell lineages during acute viral infection. *In preparation*

4.Discussion

The central aim of this thesis was to address the developmental origin of memory and effector cells in their natural environment. To do so, we followed $CD8^+$ T cells expressing Tcf1, knowing that Tcf1 was expressed in all naive $CD8^+$ T cells, was not needed for the formation of effector cells but was required for the formation of central memory cells in response to acute resolved infection (Jeannet et al., 2010; Zhou et al., 2010).

4.1. *Tcf7* guided lineage tracing

To track *Tcf7*$^+$ cells, we expressed a GFP-Cre-ERT2 fusion protein under the control of the *Tcf7* locus. This was combined with the conditional expression of a fluorescent reporter (*R26*^{Confetti} or *R26*^{Tomato}). Together, this system allowed us to inducibly and stably label *Tcf7*-expressing cells in their natural environment during a primary response to infection.

A recent paper suggested that Cre-mediated recombination had a negative effect when induced in proliferating T cells (Kurachi et al., 2019). Indeed, $CD8^+$ T cells rapidly proliferate at the early phase of an infection. By using the *R26*^{Tomato} reporter, which could be efficiently induced, we were able to limit Cre activity to a relatively brief period of around 24h. Moreover, we saw only minor differences in the abundance of labelled cells when labelling was started at d1 p.i. (when $CD8^+$ T cells did not yet proliferate) compared to when cell labelling was started at d4 p.i. (when most $CD8^+$ T cells proliferate). Rather than toxicity, we believe that the reduced expression levels of the *Tcf7*$^{GFP\text{-}iCre}$ construct observed after d1 p.i. led to a reduced labelling efficiency.

4.2. Identification of Central Memory T cells

Two main models have been proposed to explain effector vs memory cell formation. The linear differentiation model suggested that all cells pass through a lytic effector phase before dedifferentiation into non-lytic central memory cells (T_N>T_{EF}> T_{CM}) (Bannard et al., 2009; Kalia et al., 2010; Youngblood et al., 2017). Alternatively, another model proposed that, upon stimulation, naive cells yield cells with central memory traits (stem cell-like properties and lack of lytic activity) and that further stimulation of these cells generate effector cells with lytic activity (T_N> T_{CM} >T_{EF}) (Henning et al., 2018; Kakaradov et al., 2017; Pace et al., 2018). Recent work by this lab has identified a population of virus-specific *Tcf7*$^+$ $CD8^+$ T cells that is present at the peak of the primary response of infection. These cells lack lytic activity and have all the functional properties of central memory cells (Pais Ferreira et al., 2020). These findings are not compatible with the linear differentiation model.

Using lineage tracing, this thesis first showed that the virus-specific *Tcf7*$^+$ $CD8^+$ T cells present at the peak of the primary response gave quantitatively rise to T_{CM} cells. Importantly, this was shown in the absence of cell transfer, in intact mice *in vivo*. Thus, these data identified effector-phase *Tcf7*$^+$ $CD8^+$ T cells as central memory precursors (T_{pCM}). On the other hand, T_{pCM} cells present at d8 p.i. did not yield T_{EM} or T_{EF}. However, T_{pCM} cells had the potential to yield T_{EF}, T_{EM} or T_{CM} in response to restimulation (Pais Ferreira et al., 2020). Together, the

data thus suggested that, at the peak of the primary response, the *Tcf7*$^{+}$ CD8^{+} T cells were no longer exposed to the signals required for T_{EM} or T_{EF} differentiation.

4.3. Effector programming

The above data suggested that T_{EM} and T_{EF} derived from *Tcf7*$^{+}$ CD8^{+} T cells that are present at earlier timepoints of the primary response. Indeed, we found that T_{EF} derived transiently from *Tcf7*$^{+}$ CD8^{+} T cells that were present at d1 and d2 p.i., but not later time points of the infection. These data are compatible with and considerably extend a previously suggested autopilot model (**Fig 36**).

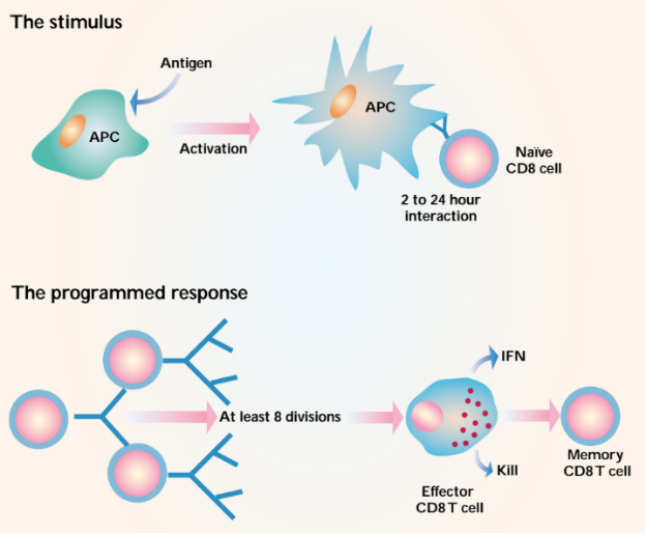

Figure 36 - Autopilot model suggested as a mechanism of fate-decision upon activation of a CD8^{+} T cells
Naive CD8^{+} T cells are committed to expand and differentiate upon only 2h-24h of exposure to an antigen presenting cell (APC). Subsequent division and differentiation occurred without requirement of further antigenic stimulation. (Bevan and Fink, 2001)

Using an engineered APC system, it was shown that the commitment of a naive CD8^{+} T cell to expand and differentiate required only 2h of exposure to APC. Thus, subsequent division and differentiation occurred without further antigenic stimulation (van Stipdonk et al., 2001). Effector programming at very early time-points of an infection has also been suggested *in vivo* (Borsa et al., 2019; Buchholz et al., 2013; Gerlach et al., 2013; Joshi et al., 2007; Mercado et al., 2000; Obar et al., 2011). Cell transfer experiments confirmed that naive CD8^{+} T cells primed during the first 24 hours were prone to expand and differentiate independent of further antigen recognition (Kaech and Ahmed, 2001). Thus, if naive CD8^{+} T cells receive an optimal early exposure to APC, they don't require any other signal to complete their proliferation and differentiation. This was similarly seen when shortening bacterial infection using antibiotics (Joshi et al., 2007; Mercado et al., 2000). However, these studies have some caveats. Following adoptive transfer, although expansion and differentiation occurred, the

efficacy was low compared to the natural response. Antibiotic treatment curtailed infection but did not completely eliminate the antigen. We found that early effector programming indeed occurred in intact mice, when cells remained in their natural environment during an ongoing immune response. In addition, our data revealed that effector programming was transient, as minimal differentiation of *Tcf7*$^+$ cells into effector cells occurred after d2 p.i..

Several studies suggest that the majority of antigen-specific cells have been activated by antigen encounter at 2 days post-infection (our data and (Chang et al., 2007; Lin et al., 2016; Mercado et al., 2000). At this time-point, *Tcf7* and Tcf1 remained uniformly expressed at high levels in all CD8$^+$ T cells and no cell division had occurred yet (our data and (Lin et al., 2016). Thus, the data suggested that effector programming occurred prior to the first cell division in cells that expressed high levels of Tcf1. It is clear that the production of inflammatory cytokines, which can be detected within hours after infection, precedes CD8$^+$ T cell division (Baazim et al., 2019; Pham et al., 2009). This raises the possibility that inflammatory cytokines, such as type I IFN signals during LCMV infection, may play a role in effector programming. Further experiments will be needed to identify the signals required for effector programming.

Effector programming means that the signals to differentiate *Tcf7*$^+$ cells into effector cells are only present during the first 2 days of the infection. It likely does not mean that a programmed *Tcf7*$^+$ CD8$^+$ T cell will exclusively give rise to effector cells. Indeed, a clonal analysis of the primary response has shown that single naive CD8$^+$ T cells will in most cases give rise to both effector and memory precursor cells (Gerlach et al., 2010; Stemberger et al., 2007). However, clone sizes as well as the relative presence of effector versus memory precursor cells are highly variable. Together with our findings, this suggested that the signals that naive cells are exposed to during the first 2 days are very heterogeneous. Variable signalling inputs based on antigen and co-stimulation from DC (Shin et al., 2019) and perhaps from the inflammatory cytokines may thus explain the clonal variability.

4.4. Effector differentiation

This thesis provided additional insights into effector differentiation following effector programming. After d2 p.i., *Tcf7*$^+$ cells started to divide, while still maintaining high levels of *Tcf7* and Tcf1 during the initial 3-4 cell divisions. Thus, Tcf1 protein was not segregating asymmetrically during the first cell division. Rather, after the initial 3-4 cell divisions, Tcf1 levels decreased precipitously in most of the cells, in agreement with (Lin et al., 2016). These data do not rule out a role for asymmetric division in effector versus memory differentiation. Rather they indicated that Tcf1 plays no role in asymmetric division. Interestingly, during the initial divisions, *Tcf7* levels were reduced gradually yet more rapidly than those of Tcf1 protein. Similar to Tcf1, *Tcf7* levels also dropped off sharply in most cells after 3-4 cell divisions. In the remaining cells, the gradual reduction of *Tcf7* expression, seemed to generate a gradient of *Tcf7* expression levels depending on how many times a cell had divided.

We also addressed the signals involved in the downregulation of Tcf1. By establishing an *in vitro* stimulation system, we found that Tcf1 downregulation required cell division and depended on the presence of inflammatory cytokines. Initial data found that the inflammatory cytokine IL12 potently suppressed Tcf1, in a STAT4-dependent fashion. The mechanism responsible for the suppressive effect of STAT4, an activator of transcription, requires further investigation. We also obtained evidence that IL12-mediated Tcf1 suppression involved epigenetic silencing via *de novo* DNA methylation. However, it is known that IL12 does not play a role in effector differentiation during LCMV infection (Keppler et al., 2009).

It is known that infection with LCMV generates a strong type I IFN response (Muller et al., 1994; van den Broek et al., 1995) and that terminal differentiation in response to LCMV depends on type I IFN acting on $CD8^+$ T cells (Wiesel et al., 2012). IL27 is also greatly upregulated in viral infections (Harker et al., 2018). We thus tested a whole panel of cytokines for their potential to suppress Tcf1. We found that IFNβ had some, but relatively weak capacity to suppress Tcf1, while IFNα had no effect. Similarly, IL27 was able to suppress Tcf1 weakly *in vitro*. Preliminary experiments showed that combining IFNβ and IL27 had an additive effect on Tcf1 suppression (not shown). We thus believe that the combined action of IFNβ and IL27 suppresses Tcf1 in early proliferating $CD8^+$ T cells during LCMV infection and that this is essential for effector differentiation. Further experiments will be needed to verify this possibility *in vivo*.

While T_{EF} derived from *Tcf7*$^+$ cells present at d2 p.i., lineage tracing showed that the *Tcf7*$^+$ cells present at d4 p.i. did no longer yield T_{EF}. This was independently confirmed based on the ablation of d4 *Tcf7*$^+$ cells. Ablation of d4 *Tcf7*$^+$ cells precluded central memory formation, as expected, but did not alter the generation of T_{EF}. Thus, d4 *Tcf7*$^+$ cells did not contribute to the terminal effector pool, in line with the lineage tracing data. Notwithstanding, d4 *Tcf7*$^+$ cells readily yielded T_{EF} cells (as well as central memory cells) in recall stimulation experiments. This means that d4 *Tcf7*$^+$ cells have the potential to yield T_{EF} but that, in their natural environment, at d4 p.i., *Tcf7*$^+$ cells were no longer exposed to the signals required for effector differentiation. Based on the above *in vitro* data, it is tempting to speculate that antigen, costimulation and/or IFNβ and IL27 levels have dropped below a threshold needed to drive effector differentiation of *Tcf7*$^+$ cells. This prediction remains to be verified.

Finally, we addressed the question why effector cells (that are *Tcf7*$^-$) outnumber central memory precursors (that are *Tcf7*$^+$) by a factor of >50, at the peak of the primary response. Indeed, both types of cells initially derive from *Tcf7*$^+$ naive cells. We found that cell survival was not very different between *Tcf7*$^+$ and *Tcf7*$^-$ cells. Rather, the abundance of *Tcf7*$^+$ cells was lower due to their reduced rate and more limited duration of cell division, compared to *Tcf7*$^-$ cells. The slower rate of cycling of *Tcf7*$^+$ cells prompted us to address whether this effect depended on Tcf1 protein expression. Indeed, we found that the limited cycling of *Tcf7*$^+$ compared to *Tcf7*$^-$ cells was mediated in part by Tcf1 protein expression. Thus, Tcf1 protein expression was essential to limit the cycling and thus the expansion of *Tcf7*$^+$ cells during the

primary response to infection. The more efficient cycling of *Tcf7*$^+$ cells lacking Tcf1 may contribute to the impaired stemness of such cells observed at the peak of the primary response (Pais Ferreira et al., 2020). Irrespectively, the data provide an explanation for why effector cells greatly outnumber central memory precursor cells at the peak of the primary response.

4.5. Developmental origin of the various memory populations

The developmental origin of memory cells has been a major open question in immunology (Henning et al., 2018). According to a **linear differentiation model**, naive cells give rise to effector cells and memory precursor cells, which both have lytic function. The latter need to dedifferentiate (loose lytic activity) following viral clearance to become memory T cells (T_N >T_{EF} >T_{CM}) (Kalia et al., 2010; Youngblood et al., 2017). A caveat of this model has been that memory precursors do not quantitatively give rise to memory and most cells die during the contraction phase. Thus, it remained possible that MPEC include a rare non-lytic subset that gives quantitatively rise to memory.

An alternative explanation, termed **decreasing potential model**, is that T_N give rise to cells that have central memory properties and that such cells eventually yield T_{CM} and, upon further stimulation, T_{EF} cells (T_N> T_{CM} >T_{EF}) (Pace et al., 2018; Restifo and Gattinoni, 2013). However, effector-phase CD8$^+$ T cells that respond to infection and that have central memory function, had not been identified.

Our lab has identified a CD8$^+$ T cell subset expressing *Tcf7* that is present at the peak of the primary response, that lacks a cytotoxic gene expression program and lytic activity, but possesses all the functional properties associated with T_{CM} (Pais Ferreira et al., 2020). This thesis showed that these cells give quantitatively rise to T_{CM}. These findings are not compatible with the linear differentiation model but consistent with decreasing potential model.

A further prediction of the decreasing potential model is that cells with functional properties of T_{CM} should be present throughout the primary response. Consistent with this notion, we found *Tcf7*$^+$ cells at all stages of the primary response (**Fig 37**). Further experiments will be needed to address whether these cells lack a cytotoxic gene expression program and lytic activity at all stages of the primary response. We did show, however, that *Tcf7*$^+$ cells present at d4 p.i. had the potential to yield T_{EF} and T_{CM} following restimulation. Furthermore, fate mapping showed that d4 *Tcf7*$^+$ cells also gave quantitatively rise to T_{CM}. Moreover, *Tcf7*$^+$ cells present at d1, d2 and d3 p.i. also gave quantitatively rise to T_{CM}. In addition, fate mapping showed that d1 and d2 *Tcf7*$^+$ cells also yielded T_{EF}. We concluded that cells with functional properties of T_{CM} were present throughout the primary response. Indeed, priming of naive cells initially yielded divided cells that retained *Tcf7* expression and further stimulation (with inflammatory cytokines) was needed to obtain differentiated cells. Based on the lineage tracing data, priming of naive cells is thought to directly yield cells with T_{CM} properties and effector cells derive from these cells upon further stimulation.

Fate mapping also addressed the developmental origin of T_{EM}. We initially found that d8 *Tcf7*$^+$ cells did not yield T_{EM}, indicating that the relevant signals were no longer present at d8 p.i.. Ablation of *Tcf7*$^+$ cells at d10 p.i. confirmed that T_{EM} quantitatively derived from *Tcf7*$^-$ cells present at d10 (Pais Ferreira et al., 2020). Fate mapping showed that T_{EM} arose from *Tcf7*$^+$ cells present at d4 p.i.. Lineage ablation further showed that T_{EM} can also derive from *Tcf7*$^-$ cells present at d4 p.i.. Finally, T_{EM} derived from *Tcf7*$^+$ cells present at all time points prior to d4. Thus, T_{EM} derived from *Tcf7*$^+$ cells present from d1 to d4 p.i. but not d8 p.i.. Thus, T_{EM} generation seems to progressively occur from *Tcf7*$^-$ cells after d4 p.i.. We also attempted to identify a putative T_{EM} precursor. Most *Tcf7*$^-$ cells present at d4 lacked KLRG1, while most d6 and d8 *Tcf7*$^-$ cells expressed KLRG1, in agreement with (Joshi et al., 2007; Sarkar et al., 2008). These data raised the possibility that T_{EM} derived from *Tcf7*$^-$ KLRG1$^-$ cells. Indeed, the developmental potential of d8 *Tcf7*$^-$ KLRG1$^-$ cells appeared intermediate between *Tcf7*$^+$ and *Tcf7*$^-$ KLRG1$^+$ cells. However, fate mapping of *Tcf7*$^-$ KLRG1$^-$ cells (using a specific marker that would still have to be identified) would be needed to verify the developmental potential of these cells.

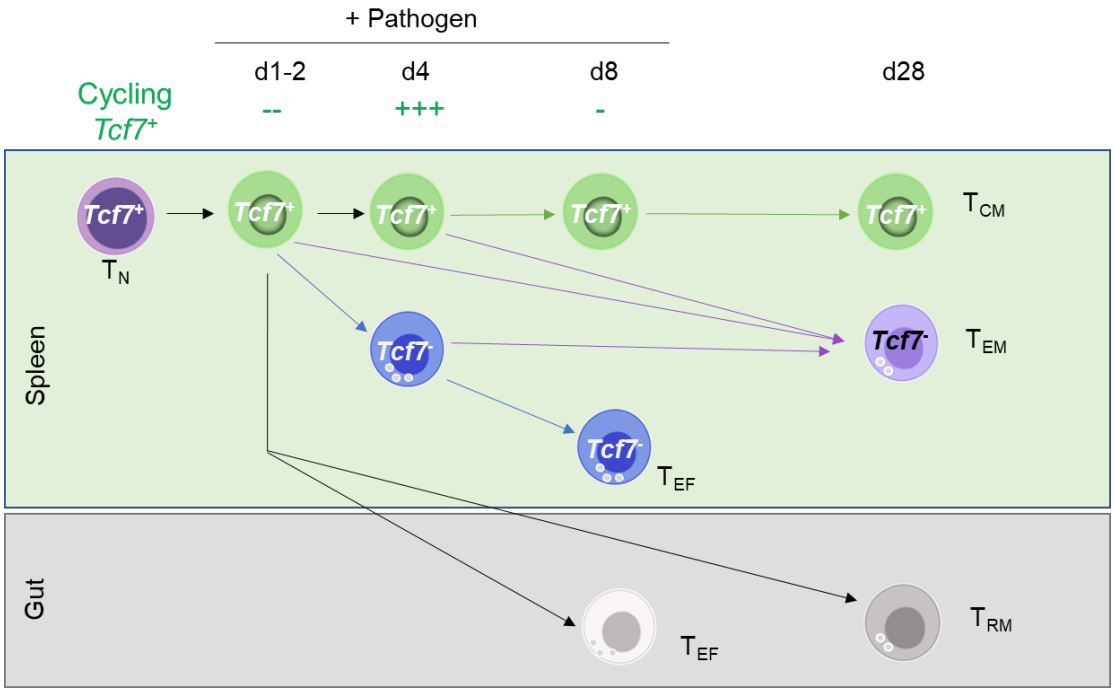

Figure 37 – Fate of *Tcf7*$^+$ CD8$^+$ T cells during an acute infection
Tcf7$^+$ cells present throughout the primary response have functional characteristics of T_{CM}. These early *Tcf7*$^+$ cells will give quantitatively yield T_{CM}. D1-2 *Tcf7*$^+$ cells, which do not yet divide, can give rise to all other CD8$^+$ T cell types, including T_{EM}, T_{RM} and terminal effector cells. At d4 p.i., *Tcf7*$^+$ cells do no longer yield terminal effector cells. T_{EM} derive from both d4 *Tcf7*$^+$ and *Tcf7*$^-$ cells. At d8 p.i., *Tcf7*$^+$ cells uniquely yield T_{CM}. Even though the fate of *Tcf7*$^+$ cells is progressively restricted, d4 and d8 *Tcf7*$^+$ cells have comparable developmental potential upon recall stimulation. T_N: Naive T cells; T_{CM}: Central Memory T cells; T_{EM}: Effector Memory T cells; T_{RM}: Tissue-resident Memory cells; T_{EF}: effector T cells.

We further used fate mapping to address the developmental origin of tissue-resident memory cells. We found that *Tcf7*$^+$ cells were programmed to yield tissue-resident memory cells from d1 to d4 p.i., although a clear peak was observed at d2 p.i.. As antigen-specific

$CD8^+$ T cells are not detected in the intestinal epithelium before d4.5 p.i. (Masopust et al., 2006), we propose that tissue-resident memory cells were programmed in *Tcf7*$^+$ cells present in secondary lymphoid organs around d2 p.i.. T_{RM} derived from d2 *Tcf7*$^+$ cells were mostly *Tcf7*$^-$. This suggested that d2 *Tcf7*$^+$ cells underwent differentiation in the periphery before their emigration into tissue. It has been previously suggested that T_{RM} cells derive from cells that had previously expressed KLRG1 (Herndler-Brandstetter et al., 2018). If so, d2 *Tcf7*$^+$ cells may undergo effector differentiation and acquire KLRG1 before or after their emigration into tissues. We also observed very rare *Tcf7*$^+$ cells among T_{RM}. However, their frequency was too low to see whether some of these had been labelled. Thus, the T_{RM} compartment seem to include a *Tcf7*$^+$ subset. It will be of interest to determine whether this *Tcf7*$^+$ compartment plays a role in the long-term maintenance of T_{RM}.

Altogether, we showed that the central memory compartment derived from *Tcf7*$^+$ cells present at all time points of the $CD8^+$ T cell response to an acute infection. In contrast, T_{EM} derived from *Tcf7*$^+$ cells present until d4 p.i., while T_{EF} were generated until d2 p.i.. Most T_{RM} are programmed in peripheral *Tcf7*$^+$ cells at d2 p.i. (**Fig 37**). Even though the fate of *Tcf7*$^+$ cells is progressively restricted, d4 and d8 *Tcf7*$^+$ cells have comparable developmental potential upon recall stimulation. The relevant signals acting on *Tcf7*$^+$ cells thus seem to change during the course of infection. It will be of interest to determine the precise contribution of the TCR, costimulation and inflammation to the distinct phases of the primary response identified herein.

4.6. Renewal and differentiation of T_{ML} during chronic viral infection

This lab and others have identified T_{ML} (defined as Tcf1$^+$ GzmB$^-$ PD1$^+$ $CD8^+$ T cells) that sustain the immune response to chronic viral infection. These T_{ML} cells have stem cell-like properties, as they are able to expand, self-renew and differentiation into T_{EX} cells (Tcf1$^-$ GzmB$^+$ PD1$^+$ $CD8^+$ T cells) (Im et al., 2016; Utzschneider et al., 2016b). However, these findings are based on cell transfers into infection time- and type-matched secondary recipients or recall responses in naive secondary recipients, which may differ from steady-state conditions *in vivo*. In the context of haematopoiesis, hematopoietic stem cells are required for long-term self-renewal and differentiation following transplantation, but have a limited contribution during native haematopoiesis in an unperturbed system (Sun et al., 2014). Here, we addressed whether T_{ML} cells residing in their natural environment self-renew and continuously differentiate into T_{EX} during chronic viral infection and if so, at what rate these exhausted cells are generated and turnover.

We found that *Tcf7*$^+$ T_{ML} cells, labelled during chronic infection, progressively yielded differentiated *Tcf7*$^-$ T_{EX} progeny. At the same time, the pool of labelled *Tcf7*$^+$ T_{ML} cells remained present in relatively stable proportions (except for a transient increase in 1 experiment). These data suggested that T_{ML} indeed maintained a stable progenitor pool (i.e. self-renewed) while at the same time yielded T_{EX}. Thus, our data confirmed the stem cell-like properties of T_{ML}

cells residing in their natural environment in secondary lymphoid organs. We further noted that the generation of T_{EX} was surprisingly slow. When some T_{ML} were labelled at d14 p.i., it took at least 4 weeks until the fraction of labelled T_{EX} corresponded to that of labelled T_{ML}. Thus, the time span needed to renew the $CD8^+$ T cell compartment in chronic infection was around 4 weeks.

Our own data and recently published studies suggest that T_{EX} are heterogeneous (Beltra et al., 2020; Chen et al., 2019; Hudson et al., 2019; Zander et al., 2019). However, these studies suggested two distinct models for the differentiation trajectories downstream of T_{ML} (**Fig 38**). A linear differentiation model suggested that T_{ML} cells give rise to $CX3CR1^+$ transitory exhausted cells and that these then differentiated into terminally exhausted $CX3CR1^-$ cells (Beltra et al., 2020; Hudson et al., 2019). Other papers suggested that T_{ML} cells give rise separately to $CX3CR1^+$ transitory exhausted or $CX3CR1^-$ terminally exhausted cells (Chen et al., 2019; Zander et al., 2019).

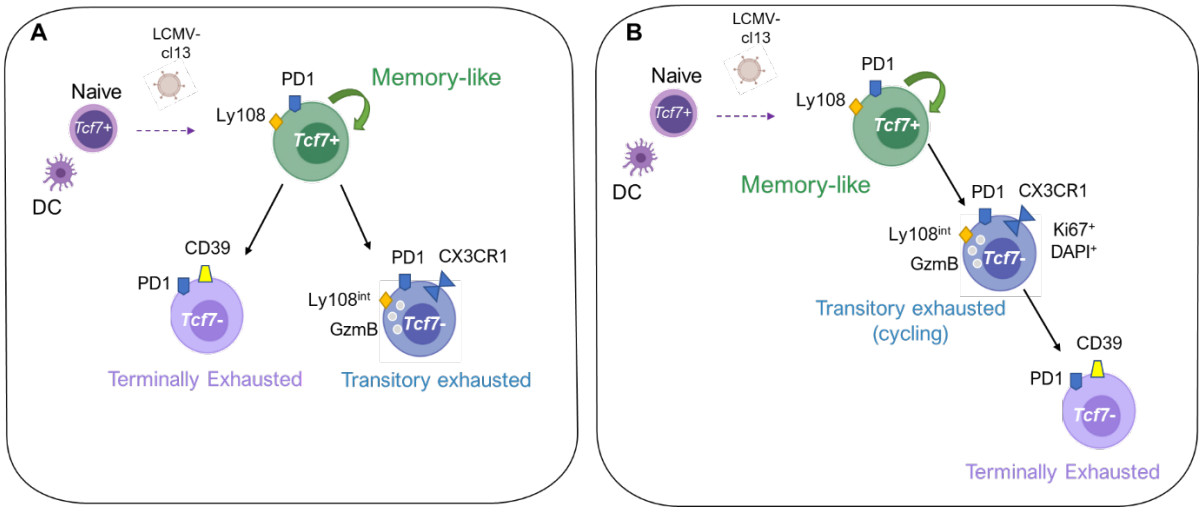

Figure 38 – Fate trajectory of *Tcf7*$^+$ $CD8^+$ T cell during a chronic infection
(**A**) Bifurcative model: *Tcf7*$^+$ population can give rise to a $CX3CR1^-$ exhausted subset or to a $CX3CR1^+$ cytolytic subset; (**B**) Linear Trajectory: *Tcf7*$^+$ stem-like population differentiate into a $CX3CR1^+$ transitory population, which then can differentiate into a $CX3CR1^-$ exhausted subset. Our model supported the latter linear trajectory model and included the cycling potential of cells: Quiescent *Tcf7*$^+$ Memory-like cells can differentiate into a transitory $CX3CR1^+$ population, which presents heterogeneity regarding Ly108 expression and which comprises some cells with cycling potential. These cells can further differentiate and may finally lead to a terminally exhausted stage.

We thus used lineage tracing to address the trajectories of labelled *Tcf7*$^+$ cells using differential Ly108 versus CX3CR1 expression. As labelled transitory exhausted cells appeared before and accumulated more rapidly than terminally exhausted, our lineage tracing data supported a linear differentiation from T_{ML} to transitory exhausted cells ($CX3CR1^+$), which then gave rise to terminally exhausted ($CX3CR1^-$ $Ly108^-$) cells.

4.7. Significance

Vaccines are one of the most important advances in modern medicine. Vaccination requires the potent induction of memory responses in order to provide long-lasting protection. Most current vaccines protect based on the induction of antibodies. The lack of protective vaccines against certain pathogens such as HIV, HCV and others generates strong interest in developing T cell-based vaccines (Shin, 2018). Among T cells, T_{CM} cells are thought to confer most potent protection, due to their longevity and stem cell-like properties, i.e. to rapidly re-generate a complete response resembling a primary response. To improve the generation of T_{CM} based vaccines, it is initially crucial to better understand the developmental origin of T_{CM} and the signals that impact the generation of T_{CM}. This thesis shows that T_{CM} derive from a rare subset of cells that is present throughout the primary immune response to infection. These rare cells seem to derive directly from naive cells. Thus, the primary expansion of naive cells in a way that prevents effector differentiation may improve T_{CM} formation. An early detection and quality control of the relevant precursor cells during vaccination may thus help to improve T_{CM} formation.

In addition to prophylactic vaccines, therapeutic vaccines would be helpful to treat chronic infections and cancer. Here, it will be important to ensure that vaccines do not further amplify the exhausted $CD8^+$ T cell phenotype acquired during chronic antigen exposure (Klebanoff et al., 2006). Appropriately targeting memory-like $CD8^+$ T cells to expand them without differentiating them may be essential to improve such immune response. Along this line, we began to address the influence of cytokines on the regulation of Tcf1, the master regulator of T_{CM} and T_{ML} and consequently T cell stemness. Understanding the molecular basis and regulation of T cell stemness will likely help to improve T cell mediated protection in response to vaccination and improve T cell function in circumstances of antigen persistence such as chronic infection and cancer.

References

Ahmed, R., and D. Gray. 1996. Immunological memory and protective immunity: understanding their relation. *Science* 272:54-60.

Ahmed, R., A. Salmi, L.D. Butler, J.M. Chiller, and M.B. Oldstone. 1984. Selection of genetic variants of lymphocytic choriomeningitis virus in spleens of persistently infected mice. Role in suppression of cytotoxic T lymphocyte response and viral persistence. *J Exp Med* 160:521-540.

Alfei, F., K. Kanev, M. Hofmann, M. Wu, H.E. Ghoneim, P. Roelli, D.T. Utzschneider, M. von Hoesslin, J.G. Cullen, Y. Fan, V. Eisenberg, D. Wohlleber, K. Steiger, D. Merkler, M. Delorenzi, P.A. Knolle, C.J. Cohen, R. Thimme, B. Youngblood, and D. Zehn. 2019. TOX reinforces the phenotype and longevity of exhausted T cells in chronic viral infection. *Nature* 571:265-269.

Alon, R., H. Rossiter, X. Wang, T.A. Springer, and T.S. Kupper. 1994. Distinct cell surface ligands mediate T lymphocyte attachment and rolling on P and E selectin under physiological flow. *J Cell Biol* 127:1485-1495.

Amsen, D., K. van Gisbergen, P. Hombrink, and R.A.W. van Lier. 2018. Tissue-resident memory T cells at the center of immunity to solid tumors. *Nat Immunol* 19:538-546.

Asano, M.S., and R. Ahmed. 1996. CD8 T cell memory in B cell-deficient mice. *J Exp Med* 183:2165-2174.

Baazim, H., M. Schweiger, M. Moschinger, H. Xu, T. Scherer, A. Popa, S. Gallage, A. Ali, K. Khamina, L. Kosack, B. Vilagos, M. Smyth, A. Lercher, J. Friske, D. Merkler, A. Aderem, T.H. Helbich, M. Heikenwalder, P.A. Lang, R. Zechner, and A. Bergthaler. 2019. CD8(+) T cells induce cachexia during chronic viral infection. *Nat Immunol* 20:701-710.

Badovinac, V.P., K.A. Messingham, A. Jabbari, J.S. Haring, and J.T. Harty. 2005. Accelerated CD8+ T-cell memory and prime-boost response after dendritic-cell vaccination. *Nat Med* 11:748-756.

Banerjee, A., S.M. Gordon, A.M. Intlekofer, M.A. Paley, E.C. Mooney, T. Lindsten, E.J. Wherry, and S.L. Reiner. 2010. Cutting edge: The transcription factor eomesodermin enables CD8+ T cells to compete for the memory cell niche. *J Immunol* 185:4988-4992.

Bannard, O., M. Kraman, and D.T. Fearon. 2009. Secondary replicative function of CD8+ T cells that had developed an effector phenotype. *Science* 323:505-509.

Barber, D.L., E.J. Wherry, D. Masopust, B. Zhu, J.P. Allison, A.H. Sharpe, G.J. Freeman, and R. Ahmed. 2006. Restoring function in exhausted CD8 T cells during chronic viral infection. *Nature* 439:682-687.

Battegay, M., S. Cooper, A. Althage, J. Banziger, H. Hengartner, and R.M. Zinkernagel. 1991. Quantification of lymphocytic choriomeningitis virus with an immunological focus assay in 24- or 96-well plates. *J Virol Methods* 33:191-198.

Battegay, M., D. Moskophidis, A. Rahemtulla, H. Hengartner, T.W. Mak, and R.M. Zinkernagel. 1994. Enhanced establishment of a virus carrier state in adult CD4+ T-cell-deficient mice. *J Virol* 68:4700-4704.

Becker, T.C., E.J. Wherry, D. Boone, K. Murali-Krishna, R. Antia, A. Ma, and R. Ahmed. 2002. Interleukin 15 is required for proliferative renewal of virus-specific memory CD8 T cells. *J Exp Med* 195:1541-1548.

Beltra, J.C., S. Manne, M.S. Abdel-Hakeem, M. Kurachi, J.R. Giles, Z. Chen, V. Casella, S.F. Ngiow, O. Khan, Y.J. Huang, P. Yan, K. Nzingha, W. Xu, R.K. Amaravadi, X. Xu, G.C. Karakousis, T.C. Mitchell, L.M. Schuchter, A.C. Huang, and E.J. Wherry. 2020. Developmental Relationships of Four Exhausted CD8(+) T Cell Subsets Reveals Underlying Transcriptional and Epigenetic Landscape Control Mechanisms. *Immunity* 52:825-841 e828.

Bergthaler, A., L. Flatz, A. Verschoor, A.N. Hegazy, M. Holdener, K. Fink, B. Eschli, D. Merkler, R. Sommerstein, E. Horvath, M. Fernandez, A. Fitsche, B.M. Senn, J.S. Verbeek, B. Odermatt, C.A. Siegrist, and D.D. Pinschewer. 2009. Impaired antibody response causes persistence of prototypic T cell-contained virus. *PLoS Biol* 7:e1000080.

Bevan, M.J., and P.J. Fink. 2001. The CD8 response on autopilot. *Nat Immunol* 2:381-382.

Blackburn, S.D., H. Shin, W.N. Haining, T. Zou, C.J. Workman, A. Polley, M.R. Betts, G.J. Freeman, D.A. Vignali, and E.J. Wherry. 2009. Coregulation of CD8+ T cell exhaustion by multiple inhibitory receptors during chronic viral infection. *Nat Immunol* 10:29-37.

Blattman, J.N., R. Antia, D.J. Sourdive, X. Wang, S.M. Kaech, K. Murali-Krishna, J.D. Altman, and R. Ahmed. 2002. Estimating the precursor frequency of naive antigen-specific CD8 T cells. *J Exp Med* 195:657-664.

Borsa, M., I. Barnstorf, N.S. Baumann, K. Pallmer, A. Yermanos, F. Grabnitz, N. Barandun, A. Hausmann, I. Sandu, Y. Barral, and A. Oxenius. 2019. Modulation of asymmetric cell division as a mechanism to boost CD8(+) T cell memory. *Sci Immunol* 4:

Bottcher, J.P., M. Beyer, F. Meissner, Z. Abdullah, J. Sander, B. Hochst, S. Eickhoff, J.C. Rieckmann, C. Russo, T. Bauer, T. Flecken, D. Giesen, D. Engel, S. Jung, D.H. Busch, U. Protzer, R. Thimme, M. Mann, C. Kurts, J.L. Schultze, W. Kastenmuller, and P.A. Knolle. 2015. Functional classification of memory CD8(+) T cells by CX3CR1 expression. *Nat Commun* 6:8306.

Boudousquie, C., M. Danilo, L. Pousse, B. Jeevan-Raj, G.S. Angelov, V. Chennupati, D. Zehn, and W. Held. 2014. Differences in the transduction of canonical Wnt signals demarcate effector and memory CD8 T cells with distinct recall proliferation capacity. *J. Immunol.* 196:2784-2791.

Brooks, D.G., M.J. Trifilo, K.H. Edelmann, L. Teyton, D.B. McGavern, and M.B. Oldstone. 2006. Interleukin-10 determines viral clearance or persistence in vivo. *Nat Med* 12:1301-1309.

Buchholz, V.R., M. Flossdorf, I. Hensel, L. Kretschmer, B. Weissbrich, P. Graf, A. Verschoor, M. Schiemann, T. Hofer, and D.H. Busch. 2013. Disparate individual fates compose robust CD8+ T cell immunity. *Science* 340:630-635.

Cannarile, M.A., N.A. Lind, R. Rivera, A.D. Sheridan, K.A. Camfield, B.B. Wu, K.P. Cheung, Z. Ding, and A.W. Goldrath. 2006. Transcriptional regulator Id2 mediates CD8+ T cell immunity. *Nat Immunol* 7:1317-1325.

Carlson, C.M., B.T. Endrizzi, J. Wu, X. Ding, M.A. Weinreich, E.R. Walsh, M.A. Wani, J.B. Lingrel, K.A. Hogquist, and S.C. Jameson. 2006. Kruppel-like factor 2 regulates thymocyte and T-cell migration. *Nature* 442:299-302.

Chang, J.T., V.R. Palanivel, I. Kinjyo, F. Schambach, A.M. Intlekofer, A. Banerjee, S.A. Longworth, K.E. Vinup, P. Mrass, J. Oliaro, N. Killeen, J.S. Orange, S.M. Russell, W. Weninger, and S.L. Reiner. 2007. Asymmetric T lymphocyte division in the initiation of adaptive immune responses. *Science* 315:1687-1691.

Chen, Y., R. Zander, A. Khatun, D.M. Schauder, and W. Cui. 2018. Transcriptional and Epigenetic Regulation of Effector and Memory CD8 T Cell Differentiation. *Front Immunol* 9:2826.

Chen, Z., Z. Ji, S.F. Ngiow, S. Manne, Z. Cai, A.C. Huang, J. Johnson, R.P. Staupe, B. Bengsch, C. Xu, S. Yu, M. Kurachi, R.S. Herati, L.A. Vella, A.E. Baxter, J.E. Wu, O. Khan, J.C. Beltra, J.R. Giles, E. Stelekati, L.M. McLane, C.W. Lau, X. Yang, S.L. Berger, G. Vahedi, H. Ji, and E.J. Wherry. 2019. TCF-1-Centered Transcriptional Network Drives an Effector versus Exhausted CD8 T Cell-Fate Decision. *Immunity* 51:840-855 e845.

Cornberg, M., L.L. Kenney, A.T. Chen, S.N. Waggoner, S.K. Kim, H.P. Dienes, R.M. Welsh, and L.K. Selin. 2013. Clonal exhaustion as a mechanism to protect against severe immunopathology and death from an overwhelming CD8 T cell response. *Front Immunol* 4:475.

Croce, M., V. Rigo, and S. Ferrini. 2015. IL-21: a pleiotropic cytokine with potential applications in oncology. *J Immunol Res* 2015:696578.

Cui, W., Y. Liu, J.S. Weinstein, J. Craft, and S.M. Kaech. 2011. An interleukin-21-interleukin-10-STAT3 pathway is critical for functional maturation of memory CD8+ T cells. *Immunity* 35:792-805.

D'Souza, W.N., and S.M. Hedrick. 2006. Cutting edge: latecomer CD8 T cells are imprinted with a unique differentiation program. *J Immunol* 177:777-781.

Danilo, M., V. Chennupati, J. Gomes Silva, S. Siegert, and W. Held. 2018. Suppression of Tcf1 by inflammatory cytokines facilitates effector CD8 T cell differentiation *Cell Reports* 22:2107-2117.

DeLong, J.H., A.O. Hall, C. Konradt, G.M. Coppock, J. Park, G. Harms Pritchard, and C.A. Hunter. 2018. Cytokine- and TCR-Mediated Regulation of T Cell Expression of Ly6C and Sca-1. *J Immunol* 200:1761-1770.

Delpoux, A., C.Y. Lai, S.M. Hedrick, and A.L. Doedens. 2017. FOXO1 opposition of CD8(+) T cell effector programming confers early memory properties and phenotypic diversity. *Proc Natl Acad Sci U S A* 114:E8865-E8874.

Dillon, S.R., S.C. Jameson, and P.J. Fink. 1994. V beta 5+ T cell receptors skew toward OVA+H-2Kb recognition. *J Immunol* 152:1790-1801.

Fearon, D.T., P. Manders, and S.D. Wagner. 2001. Arrested differentiation, the self-renewing memory lymphocyte, and vaccination. *Science* 293:248-250.

Frohlich, A., J. Kisielow, I. Schmitz, S. Freigang, A.T. Shamshiev, J. Weber, B.J. Marsland, A. Oxenius, and M. Kopf. 2009. IL-21R on T cells is critical for sustained functionality and control of chronic viral infection. *Science* 324:1576-1580.

Gaide, O., R.O. Emerson, X. Jiang, N. Gulati, S. Nizza, C. Desmarais, H. Robins, J.G. Krueger, R.A. Clark, and T.S. Kupper. 2015. Common clonal origin of central and resident memory T cells following skin immunization. *Nat Med* 21:647-653.

Gerlach, C., J.C. Rohr, L. Perie, N. van Rooij, J.W. van Heijst, A. Velds, J. Urbanus, S.H. Naik, H. Jacobs, J.B. Beltman, R.J. de Boer, and T.N. Schumacher. 2013. Heterogeneous differentiation patterns of individual CD8+ T cells. *Science* 340:635-639.

Gerlach, C., J.W. van Heijst, E. Swart, D. Sie, N. Armstrong, R.M. Kerkhoven, D. Zehn, M.J. Bevan, K. Schepers, and T.N. Schumacher. 2010. One naive T cell, multiple fates in CD8+ T cell differentiation. *J Exp Med* 207:1235-1246.

Gollob, J.A., E.A. Murphy, S. Mahajan, C.P. Schnipper, J. Ritz, and D.A. Frank. 1998. Altered interleukin-12 responsiveness in Th1 and Th2 cells is associated with the differential activation of STAT5 and STAT1. *Blood* 91:1341-1354.

Hand, T.W., W. Cui, Y.W. Jung, E. Sefik, N.S. Joshi, A. Chandele, Y. Liu, and S.M. Kaech. 2010. Differential effects of STAT5 and PI3K/AKT signaling on effector and memory CD8 T-cell survival. *Proc Natl Acad Sci U S A* 107:16601-16606.

Harker, J.A., K.A. Wong, S. Dallari, P. Bao, A. Dolgoter, Y. Jo, E.J. Wehrens, M. Macal, and E.I. Zuniga. 2018. Interleukin-27R Signaling Mediates Early Viral Containment and Impacts Innate and Adaptive Immunity after Chronic Lymphocytic Choriomeningitis Virus Infection. *J Virol* 92:

Held, W., B. Kunz, B. Lowin-Kropf, M. van de Wetering, and H. Clevers. 1999. Clonal acquisition of the Ly49A NK cell receptor is dependent on the trans-acting factor TCF-1. *Immunity* 11:433-442.

Henning, A.N., R. Roychoudhuri, and N.P. Restifo. 2018. Epigenetic control of CD8(+) T cell differentiation. *Nat Rev Immunol* 18:340-356.

Herndler-Brandstetter, D., H. Ishigame, R. Shinnakasu, V. Plajer, C. Stecher, J. Zhao, M. Lietzenmayer, L. Kroehling, A. Takumi, K. Kometani, T. Inoue, Y. Kluger, S.M. Kaech, T. Kurosaki, T. Okada, and R.A. Flavell. 2018. KLRG1(+) Effector CD8(+) T Cells Lose KLRG1, Differentiate into All Memory T Cell Lineages, and Convey Enhanced Protective Immunity. *Immunity* 48:716-729 e718.

Hess Michelini, R., A.L. Doedens, A.W. Goldrath, and S.M. Hedrick. 2013. Differentiation of CD8 memory T cells depends on Foxo1. *J Exp Med* 210:1189-1200.

Holmes, S., M. He, T. Xu, and P.P. Lee. 2005. Memory T cells have gene expression patterns intermediate between naive and effector. *Proc Natl Acad Sci U S A* 102:5519-5523.

Homann, D., L. Teyton, and M.B. Oldstone. 2001. Differential regulation of antiviral T-cell immunity results in stable CD8+ but declining CD4+ T-cell memory. *Nat Med* 7:913-919.

Hudson, W.H., J. Gensheimer, M. Hashimoto, A. Wieland, R.M. Valanparambil, P. Li, J.X. Lin, B.T. Konieczny, S.J. Im, G.J. Freeman, W.J. Leonard, H.T. Kissick, and R. Ahmed. 2019. Proliferating Transitory T Cells with an Effector-like Transcriptional Signature Emerge from PD-1(+) Stem-like CD8(+) T Cells during Chronic Infection. *Immunity* 51:1043-1058 e1044.

Ichii, H., A. Sakamoto, Y. Kuroda, and T. Tokuhisa. 2004. Bcl6 acts as an amplifier for the generation and proliferative capacity of central memory CD8+ T cells. *J Immunol* 173:883-891.

Im, S.J., M. Hashimoto, M.Y. Gerner, J. Lee, H.T. Kissick, M.C. Burger, Q. Shan, J.S. Hale, J. Lee, T.H. Nasti, A.H. Sharpe, G.J. Freeman, R.N. Germain, H.I. Nakaya, H.H. Xue, and R. Ahmed. 2016. Defining CD8+ T cells that provide the proliferative burst after PD-1 therapy. *Nature* 537:417-421.

Intlekofer, A.M., N. Takemoto, C. Kao, A. Banerjee, F. Schambach, J.K. Northrop, H. Shen, E.J. Wherry, and S.L. Reiner. 2007. Requirement for T-bet in the aberrant differentiation of unhelped memory CD8+ T cells. *J Exp Med* 204:2015-2021.

Intlekofer, A.M., N. Takemoto, E.J. Wherry, S.A. Longworth, J.T. Northrup, V.R. Palanivel, A.C. Mullen, C.R. Gasink, S.M. Kaech, J.D. Miller, L. Gapin, K. Ryan, A.P. Russ, T. Lindsten, J.S. Orange, A.W. Goldrath, R. Ahmed, and S.L. Reiner. 2005. Effector and memory CD8+ T cell fate coupled by T-bet and eomesodermin. *Nature Immunology* 6:1236-1244.

Ioannidis, V., F. Beermann, H. Clevers, and W. Held. 2001. The β-catenin-TCF-1 pathway ensures $CD4^+CD8^+$ thymocyte survival. *Nature Immunol.* 2:691-697.

Jandus, C., A.M. Usatorre, S. Vigano, L. Zhang, and P. Romero. 2017. The Vast Universe of T Cell Diversity: Subsets of Memory Cells and Their Differentiation. *Methods Mol Biol* 1514:1-17.

Janeway, C.A., Jr., and R. Medzhitov. 2002. Innate immune recognition. *Annu Rev Immunol* 20:197-216.

Jeannet, G., C. Boudousquie, N. Gardiol, J. Kang, J. Huelsken, and W. Held. 2010. Essential role of the Wnt pathway effector Tcf-1 for the establishment of functional CD8 T cell memory. *Proc Natl Acad Sci U S A* 107:9777-9782.

Ji, Y., Z. Pos, M. Rao, C.A. Klebanoff, Z. Yu, M. Sukumar, R.N. Reger, D.C. Palmer, Z.A. Borman, P. Muranski, E. Wang, D.S. Schrump, F.M. Marincola, N.P. Restifo, and L. Gattinoni. 2011. Repression of the DNA-binding inhibitor Id3 by Blimp-1 limits the formation of memory CD8+ T cells. *Nature immunology* 12:1230-1237.

Johnston, B., and E.C. Butcher. 2002. Chemokines in rapid leukocyte adhesion triggering and migration. *Semin Immunol* 14:83-92.

Joshi, N.S., W. Cui, A. Chandele, H.K. Lee, D.R. Urso, J. Hagman, L. Gapin, and S.M. Kaech. 2007. Inflammation directs memory precursor and short-lived effector CD8(+) T cell fates via the graded expression of T-bet transcription factor. *Immunity* 27:281-295.

Kaech, S.M., and R. Ahmed. 2001. Memory CD8+ T cell differentiation: initial antigen encounter triggers a developmental program in naive cells. *Nat Immunol* 2:415-422.

Kaech, S.M., and W. Cui. 2012. Transcriptional control of effector and memory CD8+ T cell differentiation. *Nat Rev Immunol* 12:749-761.

Kahan, S.M., E.J. Wherry, and A.J. Zajac. 2015. T cell exhaustion during persistent viral infections. *Virology* 479-480:180-193.

Kakaradov, B., J. Arsenio, C.E. Widjaja, Z. He, S. Aigner, P.J. Metz, B. Yu, E.J. Wehrens, J. Lopez, S.H. Kim, E.I. Zuniga, A.W. Goldrath, J.T. Chang, and G.W. Yeo. 2017. Early transcriptional and epigenetic regulation of CD8+ T cell differentiation revealed by single-cell RNA sequencing. *Nature immunology* 18:422-432.

Kalia, V., S. Sarkar, S. Subramaniam, W.N. Haining, K.A. Smith, and R. Ahmed. 2010. Prolonged interleukin-2Ralpha expression on virus-specific CD8+ T cells favors terminal-effector differentiation in vivo. *Immunity* 32:91-103.

Kallies, A., A. Xin, G.T. Belz, and S.L. Nutt. 2009. Blimp-1 transcription factor is required for the differentiation of effector CD8(+) T cells and memory responses. *Immunity* 31:283-295.

Kao, C., K.J. Oestreich, M.A. Paley, A. Crawford, J.M. Angelosanto, M.A. Ali, A.M. Intlekofer, J.M. Boss, S.L. Reiner, A.S. Weinmann, and E.J. Wherry. 2011. Transcription factor T-bet represses expression of the inhibitory receptor PD-1 and sustains virus-specific CD8+ T cell responses during chronic infection. *Nat Immunol* 12:663-671.

Kaplan, M.H., Y.L. Sun, T. Hoey, and M.J. Grusby. 1996. Impaired IL-12 responses and enhanced development of Th2 cells in Stat4-deficient mice. *Nature* 382:174-177.

Kehrl, J.H., L.M. Wakefield, A.B. Roberts, S. Jakowlew, M. Alvarez-Mon, R. Derynck, M.B. Sporn, and A.S. Fauci. 1986. Production of transforming growth factor beta by human T lymphocytes and its potential role in the regulation of T cell growth. *J Exp Med* 163:1037-1050.

Keppler, S.J., K. Theil, S. Vucikuja, and P. Aichele. 2009. Effector T-cell differentiation during viral and bacterial infections: Role of direct IL-12 signals for cell fate decision of CD8(+) T cells. *European journal of immunology* 39:1774-1783.

Kerdiles, Y.M., D.R. Beisner, R. Tinoco, A.S. Dejean, D.H. Castrillon, R.A. DePinho, and S.M. Hedrick. 2009. Foxo1 links homing and survival of naive T cells by regulating L-selectin, CCR7 and interleukin 7 receptor. *Nat Immunol* 10:176-184.

Khan, O., J.R. Giles, S. McDonald, S. Manne, S.F. Ngiow, K.P. Patel, M.T. Werner, A.C. Huang, K.A. Alexander, J.E. Wu, J. Attanasio, P. Yan, S.M. George, B. Bengsch, R.P. Staupe, G. Donahue, W. Xu, R.K. Amaravadi, X. Xu, G.C. Karakousis, T.C. Mitchell, L.M. Schuchter, J. Kaye, S.L. Berger, and E.J. Wherry. 2019. TOX transcriptionally and epigenetically programs CD8(+) T cell exhaustion. *Nature* 571:211-218.

Kim, M.T., and J.T. Harty. 2014. Impact of Inflammatory Cytokines on Effector and Memory CD8+ T Cells. *Frontiers in immunology* 5:295.

Kim, M.V., W. Ouyang, W. Liao, M.Q. Zhang, and M.O. Li. 2013. The transcription factor Foxo1 controls central-memory CD8+ T cell responses to infection. *Immunity* 39:286-297.

Klebanoff, C.A., L. Gattinoni, and N.P. Restifo. 2006. CD8+ T-cell memory in tumor immunology and immunotherapy. *Immunol Rev* 211:214-224.

Kolumam, G.A., S. Thomas, L.J. Thompson, J. Sprent, and K. Murali-Krishna. 2005. Type I interferons act directly on CD8 T cells to allow clonal expansion and memory formation in response to viral infection. *J Exp Med* 202:637-650.

Krishnamurty, A.T., and M. Pepper. 2014. Inflammatory interference of memory formation. *Trends Immunol* 35:355-357.

Kurachi, M., S.F. Ngiow, J. Kurachi, Z. Chen, and E.J. Wherry. 2019. Hidden Caveat of Inducible Cre Recombinase. *Immunity* 51:591-592.

Li, Q., C. Eppolito, K. Odunsi, and P.A. Shrikant. 2006. IL-12-programmed long-term CD8+ T cell responses require STAT4. *J Immunol* 177:7618-7625.

Lin, W.-H.W., S.A. Nish, B. Yen, Y.-H. Chen, W.C. Adams, R. Kratchmarov, N.J. Rothman, A. Bhandoola, H.-H. Xue, and S.L. Reiner. 2016. CD8(+) T Lymphocyte Self-Renewal during Effector Cell Determination. *Cell reports* 17:1773-1782.

Livet, J., T.A. Weissman, H. Kang, R.W. Draft, J. Lu, R.A. Bennis, J.R. Sanes, and J.W. Lichtman. 2007. Transgenic strategies for combinatorial expression of fluorescent proteins in the nervous system. *Nature* 450:56-62.

Lord, J.D., B.C. McIntosh, P.D. Greenberg, and B.H. Nelson. 2000. The IL-2 receptor promotes lymphocyte proliferation and induction of the c-myc, bcl-2, and bcl-x genes through the trans-activation domain of Stat5. *J Immunol* 164:2533-2541.

Lugli, E., G. Galletti, S.K. Boi, and B.A. Youngblood. 2020. Stem, Effector, and Hybrid States of Memory CD8(+) T Cells. *Trends Immunol* 41:17-28.

Mackay, L.K., A. Rahimpour, J.Z. Ma, N. Collins, A.T. Stock, M.-L. Hafon, J. Vega-Ramos, P. Lauzurica, S.N. Mueller, T. Stefanovic, D.C. Tscharke, W.R. Heath, M. Inouye, F.R. Carbone, and T. Gebhardt. 2013. The developmental pathway for CD103(+)CD8+ tissue-resident memory T cells of skin. *Nature immunology* 14:1294-1301.

Madisen, L., T.A. Zwingman, S.M. Sunkin, S.W. Oh, H.A. Zariwala, H. Gu, L.L. Ng, R.D. Palmiter, M.J. Hawrylycz, A.R. Jones, E.S. Lein, and H. Zeng. 2010. A robust and high-throughput Cre reporting and characterization system for the whole mouse brain. *Nat Neurosci* 13:133-140.

Maier, E., D. Hebenstreit, G. Posselt, P. Hammerl, A. Duschl, and J. Horejs-Hoeck. 2011. Inhibition of suppressive T cell factor 1 (TCF-1) isoforms in naive CD4+ T cells is mediated by IL-4/STAT6 signaling. *J Biol Chem* 286:919-928.

Martinez, G.J., R.M. Pereira, T. Aijo, E.Y. Kim, F. Marangoni, M.E. Pipkin, S. Togher, V. Heissmeyer, Y.C. Zhang, S. Crotty, E.D. Lamperti, K.M. Ansel, T.R. Mempel, H. Lahdesmaki, P.G. Hogan, and A. Rao. 2015. The transcription factor NFAT promotes exhaustion of activated $CD8^+$ T cells. *Immunity* 42:265-278.

Masopust, D., D. Choo, V. Vezys, E.J. Wherry, J. Duraiswamy, R. Akondy, J. Wang, K.A. Casey, D.L. Barber, K.S. Kawamura, K.A. Fraser, R.J. Webby, V. Brinkmann, E.C. Butcher, K.A. Newell, and R. Ahmed. 2010. Dynamic T cell migration program provides resident memory within intestinal epithelium. *J Exp Med* 207:553-564.

Masopust, D., and J.M. Schenkel. 2013. The integration of T cell migration, differentiation and function. *Nat Rev Immunol* 13:309-320.

Masopust, D., V. Vezys, A.L. Marzo, and L. Lefrancois. 2001. Preferential localization of effector memory cells in nonlymphoid tissue. *Science* 291:2413-2417.

Masopust, D., V. Vezys, E.J. Wherry, D.L. Barber, and R. Ahmed. 2006. Cutting edge: gut microenvironment promotes differentiation of a unique memory CD8 T cell population. *J Immunol* 176:2079-2083.

Matloubian, M., R.J. Concepcion, and R. Ahmed. 1994. CD4+ T cells are required to sustain CD8+ cytotoxic T-cell responses during chronic viral infection. *J Virol* 68:8056-8063.

Mercado, R., S. Vijh, S.E. Allen, K. Kerksiek, I.M. Pilip, and E.G. Pamer. 2000. Early programming of T cell populations responding to bacterial infection. *J Immunol* 165:6833-6839.

Mescher, M.F., J.M. Curtsinger, P. Agarwal, K.A. Casey, M. Gerner, C.D. Hammerbeck, F. Popescu, and Z. Xiao. 2006. Signals required for programming effector and memory development by CD8+ T cells. *Immunol Rev* 211:81-92.

Mollo, S.B., J.T. Ingram, R.L. Kress, A.J. Zajac, and L.E. Harrington. 2014. Virus-specific CD4 and CD8 T cell responses in the absence of Th1-associated transcription factors. *J Leukoc Biol* 95:705-713.

Moran, A.E., K.L. Holzapfel, Y. Xing, N.R. Cunningham, J.S. Maltzman, J. Punt, and K.A. Hogquist. 2011. T cell receptor signal strength in Treg and iNKT cell development demonstrated by a novel fluorescent reporter mouse. *J Exp Med* 208:1279-1289.

Morishima, N., T. Owaki, M. Asakawa, S. Kamiya, J. Mizuguchi, and T. Yoshimoto. 2005. Augmentation of effector CD8+ T cell generation with enhanced granzyme B expression by IL-27. *J Immunol* 175:1686-1693.

Muller, U., U. Steinhoff, L.F. Reis, S. Hemmi, J. Pavlovic, R.M. Zinkernagel, and M. Aguet. 1994. Functional role of type I and type II interferons in antiviral defense. *Science* 264:1918-1921.

Murali-Krishna, K., J.D. Altman, M. Suresh, D.J. Sourdive, A.J. Zajac, J.D. Miller, J. Slansky, and R. Ahmed. 1998. Counting antigen-specific CD8 T cells: a reevaluation of bystander activation during viral infection. *Immunity* 8:177-187.

Nguyen, K.B., W.T. Watford, R. Salomon, S.R. Hofmann, G.C. Pien, A. Morinobu, M. Gadina, J.J. O'Shea, and C.A. Biron. 2002. Critical role for STAT4 activation by type 1 interferons in the interferon-gamma response to viral infection. *Science (New York, N Y)* 297:2063-2066.

Nish, S.A., K.D. Zens, R. Kratchmarov, W.W. Lin, W.C. Adams, Y.H. Chen, B. Yen, N.J. Rothman, A. Bhandoola, H.H. Xue, D.L. Farber, and S.L. Reiner. 2017. CD4+ T cell effector commitment coupled to self-renewal by asymmetric cell divisions. *J Exp Med* 214:39-47.

Obar, J.J., E.R. Jellison, B.S. Sheridan, D.A. Blair, Q.M. Pham, J.M. Zickovich, and L. Lefrancois. 2011. Pathogen-induced inflammatory environment controls effector and memory CD8+ T cell differentiation. *J Immunol* 187:4967-4978.

Obar, J.J., K.M. Khanna, and L. Lefrancois. 2008. Endogenous naive CD8+ T cell precursor frequency regulates primary and memory responses to infection. *Immunity* 28:859-869.

Oliaro, J., V. Van Ham, F. Sacirbegovic, A. Pasam, Z. Bomzon, K. Pham, M.J. Ludford-Menting, N.J. Waterhouse, M. Bots, E.D. Hawkins, S.V. Watt, L.A. Cluse, C.J. Clarke, D.J. Izon, J.T. Chang, N. Thompson, M. Gu, R.W. Johnstone, M.J. Smyth, P.O. Humbert, S.L. Reiner, and S.M. Russell. 2010. Asymmetric cell division of T cells upon antigen presentation uses multiple conserved mechanisms. *J Immunol* 185:367-375.

Osborne, L.C., and N. Abraham. 2010. Regulation of memory T cells by gammac cytokines. *Cytokine* 50:105-113.

Pace, L., C. Goudot, E. Zueva, P. Gueguen, N. Burgdorf, J.J. Waterfall, J.P. Quivy, G. Almouzni, and S. Amigorena. 2018. The epigenetic control of stemness in CD8(+) T cell fate commitment. *Science* 359:177-186.

Pais Ferreira, D., J.G. Silva, T. Wyss, S.A. Fuertes Marraco, L. Scarpellino, M. Charmoy, R. Maas, I. Siddiqui, L. Tang, J.A. Joyce, M. Delorenzi, S.A. Luther, D.E. Speiser, and W. Held. 2020. Central memory CD8(+) T cells derive from stem-like Tcf7(hi) effector cells in the absence of cytotoxic differentiation. *Immunity* 53:985-1000 e1011.

Paley, M.A., D.C. Kroy, P.M. Odorizzi, J.B. Johnnidis, D.V. Dolfi, B.E. Barnett, E.K. Bikoff, E.J. Robertson, G.M. Lauer, S.L. Reiner, and E.J. Wherry. 2012. Progenitor and terminal subsets of CD8+ T cells cooperate to contain chronic viral infection. *Science* 338:1220-1225.

Pauken, K.E., M.A. Sammons, P.M. Odorizzi, S. Manne, J. Godec, O. Khan, A.M. Drake, Z. Chen, D.R. Sen, M. Kurachi, R.A. Barnitz, C. Bartman, B. Bengsch, A.C. Huang, J.M. Schenkel, G. Vahedi, W.N. Haining, S.L. Berger, and E.J. Wherry. 2016. Epigenetic stability of exhausted T cells limits durability of reinvigoration by PD-1 blockade. *Science (New York, N Y)* 354:1160-1165.

Pereira, R.M., P.G. Hogan, A. Rao, and G.J. Martinez. 2017. Transcriptional and epigenetic regulation of T cell hyporesponsiveness. *J Leukoc Biol* 102:601-615.

Perona-Wright, G., J.E. Kohlmeier, E. Bassity, T.C. Freitas, K. Mohrs, T. Cookenham, H. Situ, E.J. Pearce, D.L. Woodland, and M. Mohrs. 2012. Persistent loss of IL-27 responsiveness in CD8+ memory T cells abrogates IL-10 expression in a recall response. *Proc Natl Acad Sci U S A* 109:18535-18540.

Pham, N.L., V.P. Badovinac, and J.T. Harty. 2009. A default pathway of memory CD8 T cell differentiation after dendritic cell immunization is deflected by encounter with inflammatory cytokines during antigen-driven proliferation. *J Immunol* 183:2337-2348.

Pircher, H., K. Bürki, R. Lang, H. Hengartner, and R.M. Zinkernagel. 1989. Tolerance induction in double specific T-cell receptor transgenic mice varies with antigen. *Nature* 342:559-561.

Raghu, D., H.H. Xue, and L.A. Mielke. 2019. Control of Lymphocyte Fate, Infection, and Tumor Immunity by TCF-1. *Trends Immunol* 40:1149-1162.

Rao, R.R., Q. Li, M.R. Gubbels Bupp, and P.A. Shrikant. 2012. Transcription factor Foxo1 represses T-bet-mediated effector functions and promotes memory CD8(+) T cell differentiation. *Immunity* 36:374-387.

Rao, R.R., Q. Li, K. Odunsi, and P.A. Shrikant. 2010. The mTOR kinase determines effector versus memory CD8+ T cell fate by regulating the expression of transcription factors T-bet and Eomesodermin. *Immunity* 32:67-78.

Renkema, K.R., M.A. Huggins, H. Borges da Silva, T.P. Knutson, C.M. Henzler, and S.E. Hamilton. 2020. KLRG1(+) Memory CD8 T Cells Combine Properties of Short-Lived Effectors and Long-Lived Memory. *J Immunol* 205:1059-1069.

Restifo, N.P., and L. Gattinoni. 2013. Lineage relationship of effector and memory T cells. *Curr Opin Immunol* 25:556-563.

Rutishauser, R.L., G.A. Martins, S. Kalachikov, A. Chandele, I.A. Parish, E. Meffre, J. Jacob, K. Calame, and S.M. Kaech. 2009. Transcriptional repressor Blimp-1 promotes CD8(+) T cell terminal differentiation and represses the acquisition of central memory T cell properties. *Immunity* 31:296-308.

Sallusto, F., D. Lenig, R. Forster, M. Lipp, and A. Lanzavecchia. 1999. Two subsets of memory T lymphocytes with distinct homing potentials and effector functions. *Nature* 401:708-712.

Samji, T., and K.M. Khanna. 2017. Understanding memory CD8(+) T cells. *Immunol Lett* 185:32-39.

Sarkar, S., V. Kalia, W.N. Haining, B.T. Konieczny, S. Subramaniam, and R. Ahmed. 2008. Functional and genomic profiling of effector CD8 T cell subsets with distinct memory fates. *J Exp Med* 205:625-640.

Shin, H. 2018. Formation and function of tissue-resident memory T cells during viral infection. *Curr Opin Virol* 28:61-67.

Shin, H., S.D. Blackburn, A.M. Intlekofer, C. Kao, J.M. Angelosanto, S.L. Reiner, and E.J. Wherry. 2009. A role for the transcriptional repressor Blimp-1 in CD8(+) T cell exhaustion during chronic viral infection. *Immunity* 31:309-320.

Shin, K.S., I. Jeon, B.S. Kim, I.K. Kim, Y.J. Park, C.H. Koh, B. Song, J.M. Lee, J. Lim, E.A. Bae, H. Seo, Y.H. Ban, S.J. Ha, and C.Y. Kang. 2019. Monocyte-Derived Dendritic Cells Dictate the Memory Differentiation of CD8(+) T Cells During Acute Infection. *Front Immunol* 10:1887.

Shiow, L.R., D.B. Rosen, N. Brdickova, Y. Xu, J. An, L.L. Lanier, J.G. Cyster, and M. Matloubian. 2006. CD69 acts downstream of interferon-alpha/beta to inhibit S1P1 and lymphocyte egress from lymphoid organs. *Nature* 440:540-544.

Shipkova, M., and E. Wieland. 2012. Surface markers of lymphocyte activation and markers of cell proliferation. *Clin Chim Acta* 413:1338-1349.

Siddiqui, I., K. Schaeuble, V. Chennupati, S.A. Fuertes Marraco, S. Calderon-Copete, D. Pais Ferreira, S.J. Carmona, L. Scarpellino, D. Gfeller, S. Pradervand, S.A. Luther, D.E. Speiser, and W. Held. 2019. Intratumoral Tcf1(+)PD-1(+)CD8(+) T Cells with Stem-like Properties Promote Tumor

Control in Response to Vaccination and Checkpoint Blockade Immunotherapy. *Immunity* 50:195-211 e110.

Snippert, H.J., L.G. van der Flier, T. Sato, J.H. van Es, M. van den Born, C. Kroon-Veenboer, N. Barker, A.M. Klein, J. van Rheenen, B.D. Simons, and H. Clevers. 2010. Intestinal crypt homeostasis results from neutral competition between symmetrically dividing Lgr5 stem cells. *Cell* 143:134-144.

Stemberger, C., K.M. Huster, M. Koffler, F. Anderl, M. Schiemann, H. Wagner, and D.H. Busch. 2007. A single naive CD8+ T cell precursor can develop into diverse effector and memory subsets. *Immunity* 27:985-997.

Sun, J., A. Ramos, B. Chapman, J.B. Johnnidis, L. Le, Y.-J. Ho, A. Klein, O. Hofmann, and F.D. Camargo. 2014. Clonal dynamics of native haematopoiesis. *Nature* 514:322-327.

Surh, C.D., and J. Sprent. 2008. Homeostasis of naive and memory T cells. *Immunity* 29:848-862.

Sutherland, A.P., N. Joller, M. Michaud, S.M. Liu, V.K. Kuchroo, and M.J. Grusby. 2013. IL-21 promotes CD8+ CTL activity via the transcription factor T-bet. *J Immunol* 190:3977-3984.

Takemoto, N., A.M. Intlekofer, J.T. Northrup, E.J. Wherry, and S.L. Reiner. 2006. Cutting Edge: IL-12 inversely regulates T-bet and eomesodermin expression during pathogen-induced CD8+ T cell differentiation. *J Immunol* 177:7515-7519.

Teijaro, J.R., C. Ng, A.M. Lee, B.M. Sullivan, K.C. Sheehan, M. Welch, R.D. Schreiber, J.C. de la Torre, and M.B. Oldstone. 2013. Persistent LCMV infection is controlled by blockade of type I interferon signaling. *Science* 340:207-211.

Thomsen, A.R., J. Johansen, O. Marker, and J.P. Christensen. 1996. Exhaustion of CTL memory and recrudescence of viremia in lymphocytic choriomeningitis virus-infected MHC class II-deficient mice and B cell-deficient mice. *J Immunol* 157:3074-3080.

Tripathi, P., S. Kurtulus, S. Wojciechowski, A. Sholl, K. Hoebe, S.C. Morris, F.D. Finkelman, H.L. Grimes, and D.A. Hildeman. 2010. STAT5 is critical to maintain effector CD8+ T cell responses. *J Immunol* 185:2116-2124.

Utzschneider, D.T., F. Alfei, P. Roelli, D. Barras, V. Chennupati, S. Darbre, M. Delorenzi, D.D. Pinschewer, and D. Zehn. 2016a. High antigen levels induce an exhausted phenotype in a chronic infection without impairing T cell expansion and survival. *The Journal of experimental medicine* 213:1819-1834.

Utzschneider, D.T., M. Charmoy, V. Chennupati, L. Pousse, D.P. Ferreira, S. Calderon-Copete, M. Danilo, F. Alfei, M. Hofmann, D. Wieland, S. Pradervand, R. Thimme, D. Zehn, and W. Held. 2016b. T Cell Factor 1-Expressing Memory-like CD8(+) T Cells Sustain the Immune Response to Chronic Viral Infections. *Immunity* 45:415-427.

van den Broek, M.F., U. Muller, S. Huang, M. Aguet, and R.M. Zinkernagel. 1995. Antiviral defense in mice lacking both alpha/beta and gamma interferon receptors. *J Virol* 69:4792-4796.

van Stipdonk, M.J., E.E. Lemmens, and S.P. Schoenberger. 2001. Naive CTLs require a single brief period of antigenic stimulation for clonal expansion and differentiation. *Nat Immunol* 2:423-429.

Verbeek, S., D. Izon, F. Hofhuis, E. Robanus-Maandag, H. te Riele, M. van de Wetering, M. Oosterwegel, A. Wilson, H.R. MacDonald, and H. Clevers. 1995. An HMG-box-containing T-cell factor required for thymocyte differentiation. *Nature* 374:70-74.

Virgin, H.W., E.J. Wherry, and R. Ahmed. 2009. Redefining chronic viral infection. *Cell* 138:30-50.

Wang, Y., J. Hu, Y. Li, M. Xiao, H. Wang, Q. Tian, Z. Li, J. Tang, L. Hu, Y. Tan, X. Zhou, R. He, Y. Wu, L. Ye, Z. Yin, Q. Huang, and L. Xu. 2019. The Transcription Factor TCF1 Preserves the Effector Function of Exhausted CD8 T Cells During Chronic Viral Infection. *Front Immunol* 10:169.

Wherry, E.J., J.N. Blattman, K. Murali-Krishna, R. van der Most, and R. Ahmed. 2003. Viral persistence alters CD8 T-cell immunodominance and tissue distribution and results in distinct stages of functional impairment. *J Virol* 77:4911-4927.

Wherry, E.J., S.J. Ha, S.M. Kaech, W.N. Haining, S. Sarkar, V. Kalia, S. Subramaniam, J.N. Blattman, D.L. Barber, and R. Ahmed. 2007. Molecular signature of CD8+ T cell exhaustion during chronic viral infection. *Immunity* 27:670-684.

Whitmire, J.K. 2014. Editorial: Not all roads to T cell memory go through STAT4 and T-bet. *J Leukoc Biol* 95:699-701.

Whitmire, J.K., J.T. Tan, and J.L. Whitton. 2005. Interferon-gamma acts directly on CD8+ T cells to increase their abundance during virus infection. *J Exp Med* 201:1053-1059.

Wieland, D., and R. Thimme. 2016. Vaccine-induced hepatitis C virus-specific CD8+ T cells do not always help. *Hepatology* 63:1411-1414.

Wiesel, M., J. Crouse, G. Bedenikovic, A. Sutherland, N. Joller, and A. Oxenius. 2012. Type-I IFN drives the differentiation of short-lived effector CD8+ T cells in vivo. *Eur J Immunol* 42:320-329.

Williams, M.A., A.J. Tyznik, and M.J. Bevan. 2006. Interleukin-2 signals during priming are required for secondary expansion of CD8(+) memory T cells. *Nature* 441:890-893.

Wilson, C.H., I. Gamper, A. Perfetto, J. Auw, T.D. Littlewood, and G.I. Evan. 2014. The kinetics of ER fusion protein activation in vivo. *Oncogene* 33:4877-4880.

Wilson, E.B., D.H. Yamada, H. Elsaesser, J. Herskovitz, J. Deng, G. Cheng, B.J. Aronow, C.L. Karp, and D.G. Brooks. 2013. Blockade of chronic type I interferon signaling to control persistent LCMV infection. *Science* 340:202-207.

Wu, T., Y. Ji, E.A. Moseman, H.C. Xu, M. Manglani, M. Kirby, S.M. Anderson, R. Handon, E. Kenyon, A. Elkahloun, W. Wu, P.A. Lang, L. Gattinoni, D.B. McGavern, and P.L. Schwartzberg. 2016. The TCF1-Bcl6 axis counteracts type I interferon to repress exhaustion and maintain T cell stemness. *Sci Immunol* 1:

Wu, X., P. Wu, Y. Shen, X. Jiang, and F. Xu. 2018. CD8(+) Resident Memory T Cells and Viral Infection. *Front Immunol* 9:2093.

Xin, A., F. Masson, Y. Liao, S. Preston, T. Guan, R. Gloury, M. Olshansky, J.-X. Lin, P. Li, T.P. Speed, G.K. Smyth, M. Ernst, W.J. Leonard, M. Pellegrini, S.M. Kaech, S.L. Nutt, W. Shi, G.T. Belz, and A. Kallies. 2016. A molecular threshold for effector CD8(+) T cell differentiation controlled by transcription factors Blimp-1 and T-bet. *Nature immunology* 17:422-432.

Xing, S., F. Li, Z. Zeng, Y. Zhao, S. Yu, Q. Shan, Y. Li, F.C. Phillips, P.K. Maina, H.H. Qi, C. Liu, J. Zhu, R.M. Pope, C.A. Musselman, C. Zeng, W. Peng, and H.H. Xue. 2016. Tcf1 and Lef1 transcription factors establish CD8 T cell identity through intrinsic HDAC activity. *Nature Immunology* 17:695-703.

Xu, L., Y. Cao, Z. Xie, Q. Huang, Q. Bai, X. Yang, R. He, Y. Hao, H. Wang, T. Zhao, Z. Fan, A. Qin, J. Ye, X. Zhou, L. Ye, and Y. Wu. 2015. The transcription factor TCF-1 initiates the differentiation of T(FH) cells during acute viral infection. *Nat Immunol* 16:991-999.

Yang, C.Y., J.A. Best, J. Knell, E. Yang, A.D. Sheridan, A.K. Jesionek, H.S. Li, R.R. Rivera, K.C. Lind, L.M. D'Cruz, S.S. Watowich, C. Murre, and A.W. Goldrath. 2011. The transcriptional regulators Id2 and Id3 control the formation of distinct memory CD8+ T cell subsets. *Nature immunology* 12:1221-1229.

Yang, Q., F. Li, C. Harly, S. Xing, L. Ye, X. Xia, H. Wang, X. Wang, S. Yu, X. Zhou, M. Cam, H.H. Xue, and A. Bhandoola. 2015. TCF-1 upregulation identifies early innate lymphoid progenitors in the bone marrow. *Nature Immunology* 16:1044-1050.

Yao, C., H.W. Sun, N.E. Lacey, Y. Ji, E.A. Moseman, H.Y. Shih, E.F. Heuston, M. Kirby, S. Anderson, J. Cheng, O. Khan, R. Handon, J. Reilley, J. Fioravanti, J. Hu, S. Gossa, E.J. Wherry, L. Gattinoni, D.B. McGavern, J.J. O'Shea, P.L. Schwartzberg, and T. Wu. 2019. Single-cell RNA-seq reveals TOX as a key regulator of CD8(+) T cell persistence in chronic infection. *Nat Immunol* 20:890-901.

Yoshida, K., A. Sakamoto, K. Yamashita, E. Arguni, S. Horigome, M. Arima, M. Hatano, N. Seki, T. Ichikawa, and T. Tokuhisa. 2006. Bcl6 controls granzyme B expression in effector CD8+ T cells. *Eur J Immunol* 36:3146-3156.

Youngblood, B., J.S. Hale, and R. Ahmed. 2015. Memory CD8 T cell transcriptional plasticity. *F1000Prime Rep* 7:38.

Youngblood, B., J.S. Hale, H.T. Kissick, E. Ahn, X. Xu, A. Wieland, K. Araki, E.E. West, H.E. Ghoneim, Y. Fan, P. Dogra, C.W. Davis, B.T. Konieczny, R. Antia, X. Cheng, and R. Ahmed. 2017. Effector CD8 T cells dedifferentiate into long-lived memory cells. *Nature* 552:404-409.

Yu, Q., A. Sharma, S.Y. Oh, H.G. Moon, M.Z. Hossain, T.M. Salay, K.E. Leeds, H. Du, B. Wu, M.L. Waterman, Z. Zhu, and J.M. Sen. 2009. T cell factor 1 initiates the T helper type 2 fate by inducing the transcription factor GATA-3 and repressing interferon-gamma. *Nat Immunol* 10:992-999.

Zander, R., D. Schauder, G. Xin, C. Nguyen, X. Wu, A. Zajac, and W. Cui. 2019. CD4(+) T Cell Help Is Required for the Formation of a Cytolytic CD8(+) T Cell Subset that Protects against Chronic Infection and Cancer. *Immunity* 51:1028-1042 e1024.

Zehn, D., S.Y. Lee, and M.J. Bevan. 2009. Complete but curtailed T-cell response to very low-affinity antigen. *Nature* 458:211-214.

Zhao, D.M., S. Yu, X. Zhou, J.S. Haring, W. Held, V.P. Badovinac, J.T. Harty, and H.H. Xue. 2010. Constitutive activation of Wnt signaling favors generation of memory CD8 T cells. *J Immunol* 184:1191-1199.

Zhou, Q., A.D. Abraham, L. Li, A. Babalmorad, S. Bagby, J.J. Arcaroli, R.J. Hansen, F.A. Valeriote, D.L. Gustafson, J. Schaack, W.A. Messersmith, and D.V. LaBarbera. 2016. Topoisomerase IIalpha mediates TCF-dependent epithelial-mesenchymal transition in colon cancer. *Oncogene* 35:4990-4999.

Zhou, X., S. Ramachandran, M. Mann, and D.L. Popkin. 2012. Role of lymphocytic choriomeningitis virus (LCMV) in understanding viral immunology: past, present and future. *Viruses* 4:2650-2669.

Zhou, X., S. Yu, D.M. Zhao, J.T. Harty, V.P. Badovinac, and H.H. Xue. 2010. Differentiation and persistence of memory CD8(+) T cells depend on T cell factor 1. *Immunity* 33:229-240.